

Chapter 10

Grid Functions and Finite Difference Operators in 2D

This chapter is concerned with the extension of the difference operators introduced in Chapter 5 to two spatial dimensions. The 2D case is one of great interest in musical acoustics, given that many key components of musical instruments may be well described as such—for various percussion instruments such as drums, cymbals and gongs, a 2D structure serves as the main resonating element, whereas in keyboard instruments and some stringed instruments, it behaves as an auxiliary radiating element which imparts its own characteristic to the resulting sound. Perceptually speaking, the sound output from a 2D simulation is far richer than that of a 1D simulation. Part of this is due to the number of degrees of freedom, or modes which, in the linear case, is considerably larger, and of less regular a distribution than in 1D—sounds generated by 2D objects are generally inharmonic by nature. Beyond this, there are mechanisms at work, in particular in the nonlinear case, which lead to perceptual phenomena which have no real analogue in 1D; cymbal crashes are an excellent example of such behavior.

At the time of writing, there has been, so far, relatively little work on two-dimensional problems in sound synthesis (with some exceptions: [138, 46, 139, 384, 383]), partly because, until recently, real time synthesis from such systems on small computers was not possible. Another reason has been that percussion instruments have seen much less fundamental investigation from the point of view of musical acoustics than other instruments, though there is a growing body of work by Rossing and his collaborators (see [298, 135] for an overview), concerned mainly with experimental determination of modal frequencies, as well as considerable related work on time domain characterizations and nonlinear phenomena [282, 299]. On the other hand, such problems have a long research history in mainstream simulation, and, as a result, there is a wide expanse of literature and results which may be adapted to sound synthesis applications. Difference schemes are again a good choice for synthesis, and much of the material presented in Chapter 5 may be generalized in a natural way. The presentation here will be as brief as possible, except when it comes to certain features which are particular to 2D.

Partial differential operators in 2D, in both Cartesian and radial coordinates, are presented in §10.1, accompanied by frequency domain and energy analysis concepts and tools. Difference operators are then introduced in Cartesian coordinates in §10.2, and in radial coordinates in §10.3.

10.1 Partial Differential Operators and PDEs in Two Space Variables

The single largest headache in 2D, both at the algorithm design stage, and in programming a working synthesis routine is problem geometry. Whereas 1D problems are defined over a domain which may always be scaled to the unit interval, in 2D, no such simplification is possible. As such, the choice of coordinates becomes important. Here, to keep the emphasis on basic principles, only two such choices, namely Cartesian and radial coordinates (certainly the most useful in musical acoustics) will be discussed. Despite this, it is worth keeping in mind that numerical simulation methods are by no means limited to such coordinate choices, though as the choice of coordinate system (generally governed by geometry) becomes more complex, finite difference methods lose a good deal of their appeal, and finite element methods (see page 390) become an attractive option.

10.1.1 Cartesian and Radial Coordinates

Certainly the simplest coordinate system, and one which is ideal for working with problems defined over square or rectangular regions, is the Cartesian coordinate system, where a position is defined by the pair (x, y) . For problems defined over circles, radial coordinates (r, θ) , defined in terms of Cartesian coordinates by

$$r = \sqrt{x^2 + y^2} \quad \theta = \arctan(y/x) \quad (10.1)$$

may be more appropriate. See Figure 10.1 for an illustration of such coordinate systems.

In finite difference applications, Cartesian coordinates are undeniably much simpler to deal with, due to the symmetry between the x and y coordinate directions. Radial coordinates are trickier in some respects, especially due to the existence of a coordinate center, and also because differential operators exhibit a dependence on radius r .

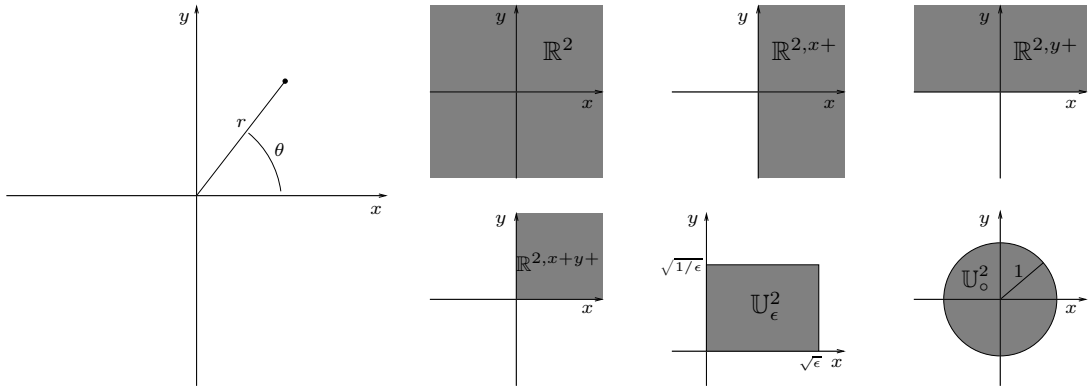


Figure 10.1: *Coordinates (x, y) , and (r, θ) , and various regions of interest in Cartesian and radial coordinates.*

10.1.2 Spatial Domains

As in 1D, a 2D problem is defined over a given domain \mathcal{D} , a subset of the plane \mathbb{R}^2 —see Figure 10.1 for an illustration of some of the regions to be discussed here. For analysis purposes, it is often convenient to work over the entire plane, or with $\mathcal{D} = \mathbb{R}^2$. In Cartesian coordinates, sometimes, for the analysis of boundary conditions, it is useful to examine a semi-infinite domain, or half plane, of the form $\mathbb{R}^{2,x+} = \{(x, y) \in \mathbb{R}^2, x \geq 0\}$, or $\mathbb{R}^{2,y+} = \{(x, y) \in \mathbb{R}^2, y \geq 0\}$, and in order to deal with corner conditions, the quarter plane $\mathbb{R}^{2,x+y+} = \{(x, y) \in \mathbb{R}^2, x \geq 0, y \geq 0\}$.

In practice, however, at least in Cartesian coordinates, it is the $L_x \times L_y$ rectangular region, of the form $\{(x, y) \in \mathbb{R}^2, 0 \leq x \leq L_x, 0 \leq y \leq L_y\}$ which is of most interest. Through scaling of spatial variables, i.e., setting coordinates

$$x' = x/\sqrt{L_x L_y} \quad y' = y/\sqrt{L_x L_y}$$

this region may always be reduced to the unit area rectangle of dimensions $\sqrt{\epsilon} \times \sqrt{1/\epsilon}$, where $\epsilon = L_x/L_y$ is the aspect ratio for the rectangle. This region will henceforth be called \mathbb{U}_ϵ^2 , and scaled coordinates will always be assumed (with the primed notation dropped). When $\epsilon = 1$ (i.e., the region is a square), the symbol \mathbb{U}^2 will be used.

In radial coordinates, the main region of interest is the circle of radius R , i.e., $\{(r, \theta) \in \mathbb{R}^2, 0 \leq r \leq R\}$. Again, through the introduction of a scaled coordinate this region may be reduced to the circle of radius 1, \mathbb{U}_\circ^2 .

10.1.3 Partial Differential Operators

In Cartesian coordinates, the differential operators which appear, beyond partial time derivatives, which have already been discussed in Chapter 5, are of the form $\frac{\partial}{\partial x}$, $\frac{\partial}{\partial y}$, $\frac{\partial^2 u}{\partial x^2}$, $\frac{\partial^2 u}{\partial y^2}$, $\frac{\partial^2 u}{\partial x \partial y}$, etc. When applied to a function $u(x, y, t)$, the following notation will be used:

$$\frac{\partial u}{\partial x} = u_x, \quad \frac{\partial u}{\partial y} = u_y, \quad \frac{\partial^2 u}{\partial x^2} = u_{xx}, \quad \frac{\partial^2 u}{\partial y^2} = u_{yy}, \quad \frac{\partial^2 u}{\partial x \partial y} = u_{xy}, \quad \text{etc.}$$

Technical considerations having to do with interchanging the order of derivatives will be neglected here, so it may be assumed, e.g., that $u_{xy} = u_{yx}$.

In radial coordinates, similar operators and accompanying notation are used, i.e.,

$$\frac{\partial u}{\partial r} = u_r, \quad \frac{\partial u}{\partial \theta} = u_\theta, \quad \frac{\partial^2 u}{\partial r^2} = u_{rr}, \quad \frac{\partial^2 u}{\partial \theta^2} = u_{\theta\theta}, \quad \frac{\partial^2 u}{\partial r \partial \theta} = u_{r\theta}, \quad \text{etc.}$$

For isotropic systems in musical acoustics, the most commonly occurring differential operator is not any of the above operators in isolation, but rather the 2D Laplacian Δ , defined in terms of its action on a function u as

$$\Delta u = u_{xx} + u_{yy} \quad \Delta u = \frac{1}{r} (ru_r)_r + \frac{1}{r^2} u_{\theta\theta} \quad (10.2)$$

in Cartesian and radial coordinates, respectively. Also important, especially in problems in plate dynamics, is the fourth-order operator known as bi-Laplacian, or biharmonic operator $\Delta\Delta$, a double application of the Laplacian operator. In Cartesian coordinates, for example, when applied to a function u , it behaves as

$$\Delta\Delta u = u_{xxxx} + 2u_{xxyy} + u_{yyyy} \quad (10.3)$$

10.1.4 Differential Operators in the Spatial Frequency Domain

Just as in 1D, it is possible to view differential operators in terms of their behavior in the spatial frequency domain—in general, this is only simple in Cartesian coordinates, where differential operators remain shift-invariant. (Notice that in radial coordinates, operators such as the Laplacian show an explicit dependence on the coordinate r .)

In 2D, the frequency domain ansatz (5.4) is generalized to

$$u(x, y, t) = e^{st+j\beta_x x+j\beta_y y}$$

When $s = j\omega$, this corresponds to a wave traveling in direction $\beta = (\beta_x, \beta_y)$ in the Cartesian plane, of wavelength $2\pi/|\beta|$, where $|\beta| = \sqrt{\beta_x^2 + \beta_y^2}$ is the wavenumber magnitude, and where β_x and β_y are the individual components. For such a test function, the various differential operators above act as

$$\frac{\partial u}{\partial x} = j\beta_x u \quad \frac{\partial u}{\partial y} = j\beta_y u \quad \frac{\partial^2 u}{\partial x^2} = -\beta_x^2 u \quad \frac{\partial^2 u}{\partial y^2} = -\beta_y^2 u \quad \frac{\partial^2 u}{\partial x \partial y} = -\beta_y \beta_x u$$

and

$$\Delta u = -(\beta_x^2 + \beta_y^2)u = -|\beta|^2 u \quad \Delta \Delta u = |\beta|^4 u$$

Notice in particular that the operators Δ and $\Delta \Delta$ lead to multiplicative factors which depend only on the wavenumber magnitude $|\beta|$, and not on the individual components β_x and β_y —this is a reflection of the isotropic character of such operations, which occur naturally in problems which do not exhibit any directional dependence. The same is not true, however, of the discrete operators which approximate them; see §10.2.2.

10.1.5 Inner Products

The definition of the L_2 inner product in 2D is a natural extension of that in 1D. For two functions f and g , dependent on two spatial coordinates, and possibly time as well, one may write

$$\langle f, g \rangle_{\mathcal{D}} = \iint_{\mathcal{D}} f g dx dy \quad \langle f, g \rangle_{\mathcal{D}} = \iint_{\mathcal{D}} f g r dr d\theta \quad (10.4)$$

in Cartesian and radial coordinates, respectively; the same notation will be used for both coordinate systems, though one should note the presence of the factor r implicit in the definition in the radial case. The norm of a function f may be defined, as in the 1D case, as $\|f\|_{\mathcal{D}} = \langle f, f \rangle_{\mathcal{D}}$.

Integration by parts follows; in Cartesian coordinates, for example, over $\mathcal{D} = \mathbb{R}^2$,

$$\langle f, g_x \rangle_{\mathbb{R}^2} = -\langle f_x, g \rangle_{\mathbb{R}^2} \quad \langle f, g_y \rangle_{\mathbb{R}^2} = -\langle f_y, g \rangle_{\mathbb{R}^2} \quad (10.5)$$

The following identity also holds for inner products involving the Laplacian:

$$\langle f, \Delta g \rangle_{\mathbb{R}^2} = \langle \Delta f, g \rangle_{\mathbb{R}^2} \quad (10.6)$$

This holds in Cartesian coordinates, and in radial coordinates, provided that f and g and their radial derivatives are bounded near the origin.

The Cauchy-Schwartz inequality (5.7a) and triangle inequality (5.7b) hold as in 1D, over any domain \mathcal{D} .

Edges

As in 1D, when the domain \mathcal{D} possesses a boundary, or, in this case, and edge, extra terms appear in above identities. Consider first the half plane $\mathcal{D} = \mathbb{R}^{2,x+}$. Now, the first of the integration by

parts identities (10.5) becomes

$$\langle f, g_x \rangle_{\mathbb{R}^{2,x+}} = -\langle f_x, g \rangle_{\mathbb{R}^{2,x+}} - \{f, g\}_{(0,\mathbb{R})}$$

where $\{f, g\}_{(0,\mathbb{R})}$ indicates a 1D inner product over the domain boundary at $x = 0$, i.e.,

$$\{f, g\}_{(0,\mathbb{R})} = \int_{y=-\infty}^{\infty} f(0, y)g(0, y)dy \quad (10.7)$$

This special notation for the 1D inner product used to indicate boundary terms arising in 2D problems is distinct from that employed in previous chapters—see §5.1.3.

Additional terms appear when higher derivatives are involved. For the case of the Laplacian, over the same domain, (10.6) becomes

$$\langle f, \Delta g \rangle_{\mathbb{R}^{2,x+}} = \langle \Delta f, g \rangle_{\mathbb{R}^{2,x+}} - \{f, g_x\}_{(0,\mathbb{R})} + \{f_x, g\}_{(0,\mathbb{R})}$$

The case of the quarter plane, $\mathcal{D} = \mathbb{R}^{2,x+y+}$ is of particular interest in problems defined over rectangular regions. Now, in the case of the Laplacian, boundary terms appear along both edges:

$$\langle f, \Delta g \rangle_{\mathbb{R}^{2,x+y+}} = \langle \Delta f, g \rangle_{\mathbb{R}^{2,x+y+}} - \{f, g_x\}_{(0,\mathbb{R}^+)} + \{f_x, g\}_{(0,\mathbb{R}^+)} - \{f, g_y\}_{(\mathbb{R}^+, 0)} + \{f_y, g\}_{(\mathbb{R}^+, 0)}$$

Circular Domains

The circular domain $\mathcal{D} = \mathbb{U}_o^2$ is of great practical utility in sound synthesis applications for certain percussion instruments, such as cymbals and gongs. There is only a single edge, at $r = 1$, though, in difference approximations, an artificial “edge” appears at $r = 0$, which must be treated carefully—see the discussion of the discrete Laplacian beginning on page 304. In order to examine boundary conditions, integration by parts is again a necessary tool. Here is an identity of great utility:

$$\langle f, \Delta g \rangle_{\mathbb{U}_o^2} = -\langle f_r, g_r \rangle_{\mathbb{U}_o^2} - \left\langle \frac{1}{r} f_\theta, \frac{1}{r} g_\theta \right\rangle_{\mathbb{U}_o^2} + \{f, g_r\}_{(1,[0,2\pi))} \quad (10.8a)$$

$$= \langle \Delta f, g \rangle_{\mathbb{U}_o^2} + \{f, g_r\}_{(1,[0,2\pi))} - \{f_r, g\}_{(1,[0,2\pi))} \quad (10.8b)$$

of slight concern are the factors of $1/r$ which appear the inner products above; it must further be assumed that f and g are bounded and single-valued at $r = 0$.

10.2 Grid Functions and Difference Operators: Cartesian Coordinates

The extension of the definitions in §5.2.2 to two spatial coordinates is, in the Cartesian case, immediate. A grid function $u_{l,m}^n$, for $(l, m) \in \mathcal{D}$, and $n \geq 0$, represents an approximation to a continuous function $u(x, y, t)$, at coordinates $x = lh_x$, $y = mh_y$, $t = nk$. Here, \mathcal{D} is a subset of the set of pairs of integers, \mathbb{Z}^2 , and h_x and h_y are the grid spacings in the x and y directions. The semi infinite domains, or half planes corresponding to $\mathbb{R}^{2,x+}$ and $\mathbb{R}^{2,y+}$ are $\mathbb{Z}^{2,x+} = \{(l, m) \in \mathbb{Z}^2, l \geq 0\}$ and $\mathbb{Z}^{2,y+} = \{(l, m) \in \mathbb{Z}^2, m \geq 0\}$. For the quarter plane, one can define $\mathbb{Z}^{2,x+y+} = \{(l, m) \in \mathbb{Z}^2, l, m \geq 0\}$. Most important, in real-world simulation, is the rectangular region $\mathbb{U}_{N_x, N_y}^2 = \{(l, m) \in \mathbb{Z}^2, 0 \leq l \leq N_x, 0 \leq m \leq N_y\}$.

Temporal operators behave exactly as those defined in 1D, in §5.2.1, and it is not worth repeating these definitions here. Spatial shift operators, in the x and y directions may be defined as

$$e_{x+} u_{l,m}^n = u_{l+1,m}^n \quad e_{x-} u_{l,m}^n = u_{l-1,m}^n \quad e_{y+} u_{l,m}^n = u_{l,m+1}^n \quad e_{y-} u_{l,m}^n = u_{l,m-1}^n$$

and forward, backward and centered difference operators as

$$\begin{aligned}\delta_{x+} &\triangleq \frac{1}{h_x}(e_{x+} - 1) \approx \frac{\partial}{\partial x} & \delta_{x-} &\triangleq \frac{1}{h_x}(1 - e_{x-}) \approx \frac{\partial}{\partial x} & \delta_{x\cdot} &\triangleq \frac{1}{2h_x}(e_{x+} - e_{x-}) \approx \frac{\partial}{\partial x} \\ \delta_{y+} &\triangleq \frac{1}{h_y}(e_{y+} - 1) \approx \frac{\partial}{\partial y} & \delta_{y-} &\triangleq \frac{1}{h_y}(1 - e_{y-}) \approx \frac{\partial}{\partial y} & \delta_{y\cdot} &\triangleq \frac{1}{2h_y}(e_{y+} - e_{y-}) \approx \frac{\partial}{\partial y}\end{aligned}$$

Centered second derivative approximations follow immediately as

$$\delta_{xx} = \delta_{x+}\delta_{x-} \approx \frac{\partial^2}{\partial x^2} \quad \delta_{yy} = \delta_{y+}\delta_{y-} \approx \frac{\partial^2}{\partial y^2}$$

and various mixed derivative approximations, such as $\delta_{x+}\delta_{y-}$ approximating $\partial^2/\partial x\partial y$ may be arrived at through composition. It is also possible to define averaging operators in the x and y directions, such as μ_{x+} , μ_{y-} etc., generalizing those presented in §5.2.2. See Figure 10.2, and Problem 10.1.

Equal Grid Spacings

Though, in general, one can choose unequal grid spacings h_x and h_y in the two Cartesian coordinates x and y , for simplicity of analysis and programming, it is often easier set them equal to a single constant, i.e., $h_x = h_y = h$. This is natural for problems which are isotropic (i.e., for which wave propagation is independent of direction). This simplification is employed in much of the remainder of this book. There are cases, though, for which such a choice can lead to errors which can become perceptually important when a very coarse grid is used (i.e., typically in simulating musical systems of high pitch). For some examples relating to the 2D wave equation, see Problem 11.7 and Programming Exercise 11.1 in the following chapter. When the system itself exhibits significant anisotropy, however (such as, e.g., in the case of certain plates used as soundboards—see §12.5), this simplification must be revisited.

The Discrete Laplacian and Biharmonic Operators

Quite important in musical sound synthesis applications is the approximation to the Laplacian operator, as given in (10.2)—there are clearly many ways of doing this. The simplest, by far, is to make use of what is known as the five-point Laplacian. Here are two possible forms of this operator, one making use of points adjacent to the center point, and another employing points diagonally adjacent:

$$\delta_{\Delta\boxplus} = \delta_{xx} + \delta_{yy} = \Delta + O(h^2) \quad \delta_{\Delta\boxtimes} = \delta_{xx} + \delta_{yy} + \frac{h^2}{2}\delta_{xx}\delta_{yy} = \Delta + O(h^2) \quad (10.9)$$

These two operators may be combined in a standard way (see §2.2.2) to yield a so-called nine-point Laplacian, depending on a free parameter α :

$$\delta_{\Delta\alpha} \triangleq \alpha\delta_{\Delta\boxplus} + (1 - \alpha)\delta_{\Delta\boxtimes} = \Delta + O(h^2) \quad (10.10)$$

Though it involves more grid points, it may be used in order to render an approximation more isotropic—see §11.3 for an application of this in the case of the 2D wave equation.

Also important, in the case of the vibrating stiff plate, is the discrete biharmonic operator, or bi-Laplacian, which consists of the composition of the Laplacian with itself, or $\Delta\Delta$. A simple approximation may be given as

$$\delta_{\Delta\boxplus,\Delta\boxplus} \triangleq \delta_{\Delta\boxplus}\delta_{\Delta\boxplus} = \Delta\Delta + O(h^2)$$

One could go further here and develop a family of approximations using a parameterized combination of the operators $\delta_{\Delta\boxplus}$ and $\delta_{\Delta\boxtimes}$ —see [48] for more on this topic, and the text of Szilard [347], which

covers difference approximations to the biharmonic operator in great detail.

The stencils or footprints of the above spatial difference operators are illustrated in Figure 10.2. The precise coefficients to be applied at the various points are not indicated, but easily determined—see Problem 10.1.

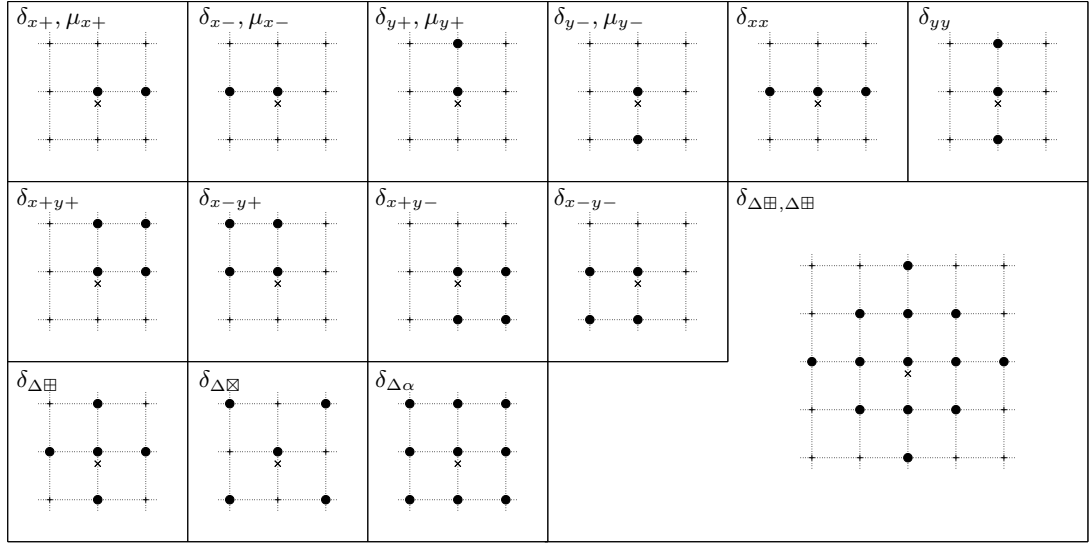


Figure 10.2: Stencils, or footprints for various 2D spatial difference operators, in Cartesian coordinates, as indicated. In each case, the point at which operator acts is indicated by a \times symbol.

10.2.1 2D Interpolation and Spreading Operators

Interpolation, necessary for reading out a waveform from a discrete grid, and spreading, necessary when one is interested in exciting such a grid, or coupling it to another object, are direct extensions of their 1D counterparts, as described in §5.2.4.

For a grid function $u_{l,m}$, defined for integer l and m , with grid spacings h_x and h_y , a zeroth-order (westward/southward) interpolant $I_0(x_o, y_o)$ operating at position (x_o, y_o) is defined by

$$I_0(x_o, y_o)u = u_{l_o, m_o} \quad \text{where} \quad l_o = \text{floor}(x_o/h_x), \quad m_o = \text{floor}(y_o/h_y) \quad (10.11)$$

Such an interpolant corresponds to a crude “staircase” approximation, as illustrated in Figure 10.3(b). It is particularly useful in cases in which the interpolation point is static, and when there is good grid resolution.

Another choice which is appealing, due to its simplicity, is the bilinear interpolant, $I_1(x_o, y_o)$. If the grid indices l_o and m_o are as given in (10.11), and furthermore the remainders by $\alpha_{x,o} = x_o/h_x - l_o$ and $\alpha_{y,o} = y_o/h_y - m_o$, it is defined as

$$\begin{aligned} I_1(x_o, y_o)u &= (1 - \alpha_{x,o})(1 - \alpha_{y,o})u_{l_o, m_o} + (1 - \alpha_{x,o})\alpha_{y,o}u_{l_o, m_o+1} \\ &\quad + \alpha_{x,o}(1 - \alpha_{y,o})u_{l_o+1, m_o} + \alpha_{x,o}\alpha_{y,o}u_{l_o+1, m_o+1} \end{aligned}$$

This interpolant makes use of the four grid points neighboring the interpolation point, using a bilinear function of these values—see Figure 10.3(c). It is more accurate than I_0 , and the simplest interpolant

one could realistically use in situations where the readout point is moving. See Programming Exercise 10.1.

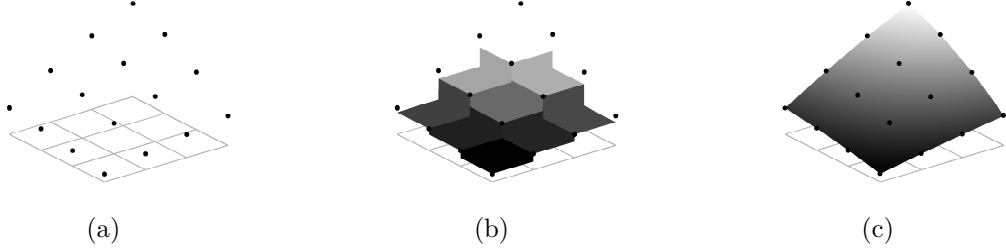


Figure 10.3: *2D Interpolation.* (a) *Values of a grid function,* (b) *the simple truncating interpolant I_0 ,* and (c) *a bilinear interpolant I_1 .* The interpolants are viewed as “reconstructing” a 2D function underlying the grid function shown in (a), from which interpolated values may then be drawn.

Spreading grid functions $J_0(x_i, y_i)$ and $J_1(x_i, y_i)$, operating at position (x_i, y_i) may be similarly defined as the duals to these interpolants, i.e.,

$$J_{l,m,0}(x_i, y_i) = \frac{1}{h_x h_y} \begin{cases} 1 & l = l_i, m = m_i \\ 0 & \text{else} \end{cases}$$

$$J_{l,m,1}(x_i, y_i) = \frac{1}{h_x h_y} \begin{cases} (1 - \alpha_{x,i})(1 - \alpha_{y,i}) & l = l_i, m = m_i \\ (1 - \alpha_{x,i})\alpha_{y,i} & l = l_i, m = m_i + 1 \\ \alpha_{x,i}(1 - \alpha_{y,i}) & l = l_i + 1, m = m_i \\ \alpha_{x,i}\alpha_{y,i} & l = l_i + 1, m = m_i + 1 \\ 0 & \text{else} \end{cases}$$

where $l_i = \text{floor}(x_i/h_x)$, $m_i = \text{floor}(y_i/h_y)$, $\alpha_{x,i} = x_i/h_x - l_i$ and $\alpha_{y,i} = y_i/h_y - m_i$. Either approximates a two-dimensional Dirac delta function $\delta(x - x_i, y - y_i)$.

One could go further here, and develop higher-order interpolants—as those with a background in image processing may know, this is a much more complex matter in 2D than in the 1D case [305], and the matter is not pursued further here. See also Programming Exercise 11.2 for some exploration of the perceptual effects of the choice of a bilinear interpolant in audio applications.

10.2.2 Frequency Domain Analysis

Frequency domain analysis of difference operators in the Cartesian case is a straightforward generalization from 1D. Skipping over the definition of Fourier and z transforms, the ansatz is now

$$u_{l,m}^n = z^n e^{j h(l\beta_x + m\beta_y)} \quad (10.12)$$

where again, β_x and β_y are components of a vector wavenumber $\beta = (\beta_x, \beta_y)$ of magnitude $|\beta| = \sqrt{\beta_x^2 + \beta_y^2}$. The frequency domain behavior of temporal operators is unchanged from the 1D case.

Defining the variables p_x and p_y by

$$p_x = \sin^2(\beta_x h/2) \quad p_y = \sin^2(\beta_y h/2) \quad (10.13)$$

it is true for a single component of the form (10.12), that

$$\delta_{xx} u = -\frac{4}{h^2} p_x u \quad \delta_{yy} u = -\frac{4}{h^2} p_y u$$

$$\delta_{\Delta \boxplus} u = -\frac{4}{h^2} (p_x + p_y) u \quad \delta_{\Delta \boxtimes} u = -\frac{4}{h^2} (p_x + p_y - 2p_x p_y) u \quad \delta_{\Delta \boxplus, \Delta \boxtimes} u = \frac{16}{h^4} (p_x + p_y)^2 u \quad (10.14)$$

Notice in particular that the frequency domain multiplication factors for the approximations to the Laplacian are bilinear functions of p_x and p_y defined over the unit square—one may use properties of such functions in order to simplify stability analysis. See Problem 10.2.

Anisotropic Behavior

One new facet of finite difference schemes in 2D is numerical anisotropy—waves travel at different speeds in different directions, even when the underlying problem is isotropic. This is wholly due to the directional asymmetry imposed on a problem by introducing a grid and is a phenomenon which shows itself most prominently at high frequencies (or short wavelengths)—in the long-wavelength limit, the numerical behavior of operators which approximate isotropic differential operators becomes approximately isotropic.

As a simple example of this, consider the operator $\delta_{\Delta \boxplus}$, as defined in (10.9). It is perhaps easiest to examine the anisotropy in the frequency domain representation. Expanding from (10.14) in powers of the wavenumber components β_x and β_y , gives

$$\delta_{\Delta \boxplus} \implies -\frac{4}{h^2} (p_x + p_y) = -|\boldsymbol{\beta}|^2 + \frac{h^2}{12} (\beta_x^4 + \beta_y^4) + O(h^4)$$

Thus, as expected, the operator $\delta_{\Delta \boxplus}$ approximates the Laplacian Δ to second-order accuracy in the grid spacing h , but the higher-order terms can not be grouped in terms of the wavenumber magnitude alone. Such numerical anisotropy, and ways of reducing it, will be discussed with regard to the 2D wave equation in §11.3. See also Problem 10.3, and Programming Exercise 10.2.

Amplification Polynomials

Just as in the lumped and 1D cases, for LSI problems in 2D, in the analysis of difference schemes, one often arrives at amplification polynomials of the following form:

$$P(z) = \sum_{l=0}^N a_l(\beta_x, \beta_y) z^l = 0 \quad (10.15)$$

and as before, a stability condition is arrived at by finding conditions such that the roots are bounded by 1 in magnitude, now for all values of β_x and β_y supported on the grid.

10.2.3 A Discrete Inner Product

The discrete inner product and norm over a Cartesian grid in 2D are a direct extension of those given in §5.2.9, in the 1D case. For an arbitrary domain \mathcal{D} , the simplest definition, for two grid functions $f_{l,m}, g_{l,m}$ defined over a grid of uniform spacing h in the x and y directions, is:

$$\langle f, g \rangle_{\mathcal{D}} = \sum_{(l,m) \in \mathcal{D}} h^2 f_{l,m} g_{l,m} \quad \|f\|_{\mathcal{D}} = \langle f, f \rangle_{\mathcal{D}}$$

The Cauchy-Schwartz and triangle inequalities again hold, as in 1D.

Summation by Parts and Inequalities

Summation by parts extends naturally to 2D. Consider, in the first instance, grid functions f and g defined over the domain $\mathcal{D} = \mathbb{Z}^2$. It is direct to show that

$$\langle f, \delta_{x-} g \rangle_{\mathbb{Z}^2} = -\langle \delta_{x+} f, g \rangle_{\mathbb{Z}^2} \quad \langle f, \delta_{y-} g \rangle_{\mathbb{Z}^2} = -\langle \delta_{y+} f, g \rangle_{\mathbb{Z}^2} \quad (10.16)$$

From these identities, one may go further and show, for the five-point Laplacian that

$$\langle f, \delta_{\Delta \boxplus} g \rangle_{\mathbb{Z}^2} = -\langle \delta_{x-} f, \delta_{x-} g \rangle_{\mathbb{Z}^2} - \langle \delta_{y-} f, \delta_{y-} g \rangle_{\mathbb{Z}^2} = \langle \delta_{\Delta \boxplus} f, g \rangle_{\mathbb{Z}^2} \quad (10.17)$$

Inequalities relating norms of grid functions under difference operators to norms of the grid functions themselves also follow:

$$\|\delta_{x+} u\|_{\mathbb{Z}^2} \leq \frac{2}{h} \|u\|_{\mathbb{Z}^2} \quad \|\delta_{y+} u\|_{\mathbb{Z}^2} \leq \frac{2}{h} \|u\|_{\mathbb{Z}^2} \quad \|\delta_{xx} u\|_{\mathbb{Z}^2} \leq \frac{4}{h^2} \|u\|_{\mathbb{Z}^2} \quad \|\delta_{yy} u\|_{\mathbb{Z}^2} \leq \frac{4}{h^2} \|u\|_{\mathbb{Z}^2} \quad (10.18)$$

from which it may be deduced that

$$\|\delta_{\Delta \boxplus} u\|_{\mathbb{Z}^2} = \|(\delta_{xx} + \delta_{yy}) u\|_{\mathbb{Z}^2} \leq \|\delta_{xx} u\|_{\mathbb{Z}^2} + \|\delta_{yy} u\|_{\mathbb{Z}^2} \leq \frac{8}{h^2} \|u\|_{\mathbb{Z}^2}$$

Boundary Terms

When the domain has an edge, boundary terms appear in the summation by parts identities above. Consider, for example, the half plane $\mathcal{D} = \mathbb{Z}^{2,x+}$. Now, instead of the first of (10.16), one has

$$\langle f, \delta_{x-} g \rangle_{\mathbb{Z}^{2,x+}} = -\langle \delta_{x+} f, g \rangle_{\mathbb{Z}^{2,x+}} - \{f, e_{x-} g\}_{(0,\mathbb{Z})} \quad (10.19)$$

Here, the $\{\cdot, \cdot\}$ notation indicates a 1D inner product over the boundary of the region $\mathbb{Z}^{2,x+}$, i.e.,

$$\{f, e_{x-} g\}_{(0,\mathbb{Z})} = \sum_{m=-\infty}^{\infty} h f_{0,m} g_{-1,m}$$

Notice the appearance here of values of the grid function at virtual locations with $l = -1$; such values may be set once boundary conditions have been specified.

Similarly, over the domain $\mathcal{D} = \mathbb{Z}^{2,y+}$, summation by parts becomes

$$\langle f, \delta_{y-} g \rangle_{\mathbb{Z}^{2,y+}} = -\langle \delta_{y+} f, g \rangle_{\mathbb{Z}^{2,y+}} - \{f, e_{y-} g\}_{(\mathbb{Z},0)}$$

The above identities allow the determination of numerical boundary conditions when energy methods are employed. For examples, see the case of the 2D wave equation, in §11.2.2, and linear plate vibration, on page 341.

10.2.4 Matrix Interpretation of Difference Operators

As in 1D, it is sometimes useful to represent difference operators in matrix form, especially in the case of implicit schemes which require linear system solution techniques. As a first step, the grid function to be operated on should be “flattened” to a vector. For a grid function $u_{l,m}$, for instance, defined over $\mathcal{D} = \mathbb{Z}^2$, one can stack the columns to create a vector \mathbf{u} , as

$$\mathbf{u} = [\dots, \mathbf{u}_{l-1}^T, \mathbf{u}_l^T, \mathbf{u}_{l+1}^T \dots]^T$$

where $\mathbf{u}_l = [\dots, u_{l,m-1}, u_{l,m}, u_{l,m+1}, \dots]^T$. (In other words, consecutive vertical strips of the 2D grid function u are lined up end to end in a single column vector.) Matrix forms of difference operators, then, have a particularly sparse form. Consider, for example, the operators δ_{xx} and δ_{yy} , corresponding to second derivatives in the x and y directions, respectively. In matrix form, and

assuming equal grid spacings $h_x = h_y = h$, these look like:

$$\mathbf{D}_{xx}^{(2)} = \frac{1}{h^2} \begin{bmatrix} \ddots & \ddots & & \mathbf{0} \\ \ddots & -2\mathbf{I} & \mathbf{I} & \\ & \mathbf{I} & -2\mathbf{I} & \mathbf{I} \\ \mathbf{0} & & \mathbf{I} & -2\mathbf{I} \\ & & & \ddots & \ddots \end{bmatrix} \quad \mathbf{D}_{yy}^{(2)} = \begin{bmatrix} \ddots & & & & \\ & \mathbf{D}_{yy}^{(1)} & & & \\ & & \mathbf{D}_{yy}^{(1)} & & \\ & & & \mathbf{D}_{yy}^{(1)} & \\ & & & & \ddots \end{bmatrix}$$

where the ⁽²⁾ indicates that the matrix operators are not to be confused with their 1D counterparts. Here, \mathbf{I} is again the identity matrix, and $\mathbf{D}_{yy}^{(1)}$ is a 1D difference matrix, identical in form to that of \mathbf{D}_{xx} given in (5.17).

Matrix forms of other difference operators follow immediately. The difference operators $\delta_{\Delta\boxplus}$ and $\delta_{\Delta\boxplus,\Delta\boxplus}$, discrete approximations to the Laplacian and biharmonic operators, have the following forms, at interior points in the domain:

$$\mathbf{D}_{\Delta\boxplus} = \mathbf{D}_{xx}^{(2)} + \mathbf{D}_{yy}^{(2)} \quad \mathbf{D}_{\Delta\boxplus,\Delta\boxplus} = \mathbf{D}_{\Delta\boxplus} \mathbf{D}_{\Delta\boxplus}$$

It is probably easiest to understand the action of these operators by examining sparsity plots, indicating where non-zero entries occur, as shown in Figure 10.4.

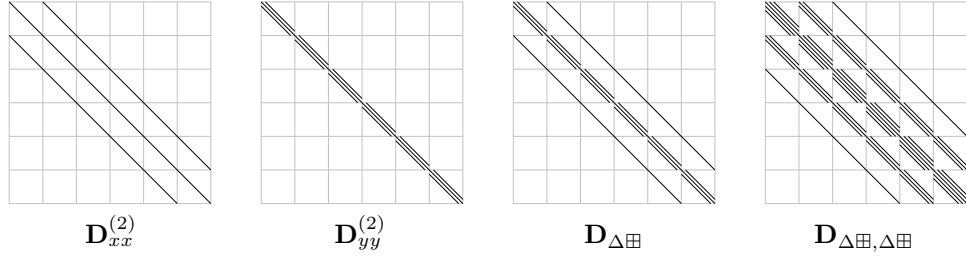


Figure 10.4: Sparsity patterns for various 2D difference operators written in matrix form, in Cartesian coordinates.

Boundary Conditions

As in 1D, when boundary conditions are taken into account, the matrices are of finite size, though values in the extreme blocks, and also in extreme rows and columns of other blocks, must be modified. From an implementation point of view, it is useful to examine the form of such modifications.

As an example, consider the operator $\delta_{\Delta\boxplus}$, operating on a grid function $u_{l,m}$ defined over the finite rectangular domain $\mathcal{D} = \mathbb{U}_{N_x,N_y}^2$, or, in other words, the set of values of $u_{l,m}$ defined for $0 \leq l \leq N_x$, $0 \leq m \leq N_y$. A particularly simple case is that of Dirichlet, or fixed termination, in which case the values of $u_{l,m}$ are set permanently to zero at the domain boundary. The total grid consists of $N_x - 1$ vertical strips of length $N_y - 1$, leaving out the values on the boundary. Thus, if the state vector \mathbf{u} is defined as the concatenation of these vertical strips, the matrix operator $\mathbf{D}_{\Delta\boxplus}$ is as shown in Figure 10.5(a); it consists of $(N_y - 1) \times (N_y - 1)$ blocks. See also Problem 10.4.

As another example, consider the same operator acting on a grid function over the same domain,

but under Neumann type, or zero normal derivative conditions on all sides:

$$\delta_{x-} u_{0,m} = 0 \quad , \quad m = 0, \dots, N_y \quad (10.20a)$$

$$\delta_{x+} u_{N_x,m} = 0 \quad , \quad m = 0, \dots, N_y \quad (10.20b)$$

$$\delta_{y-} u_{l,0} = 0 \quad , \quad l = 0, \dots, N_x \quad (10.20c)$$

$$\delta_{y+} u_{l,N_y} = 0 \quad , \quad l = 0, \dots, N_x \quad (10.20d)$$

Now, when operating at a boundary point, the operator makes use of virtual grid points outside the domain. Consider the condition $\delta_{x-} u_{0,m} = 0$, for $0 < m < N_y$ (i.e., excluding the corner points at $l = 0, m = 0$ and $l = 0, m = N_y$). This implies that, in terms of virtual grid points, one may write $u_{-1,m} = u_{0,m}$. Thus in order to evaluate the discrete Laplacian $\delta_{\Delta\boxplus}$ at such a point in terms of values over the grid interior, one has

$$\delta_{\Delta\boxplus} u_{0,m} = \frac{1}{h^2} (u_{0,m+1} + u_{0,m-1} + u_{-1,m} + u_{1,m} - 4u_{0,m}) = \frac{1}{h^2} (u_{0,m+1} + u_{0,m-1} + u_{1,m} - 3u_{0,m}) \quad (10.21)$$

A similar evaluation may be written for points with $0 < l < N_x$, and $m = 0$. At a domain corner, such as $l = 0, m = 0$, when Neumann conditions are employed along both edges, one has $\delta_{x-} u_{0,0} = \delta_{y-} u_{0,0} = 0$, and thus, for the Laplacian,

$$\delta_{\Delta\boxplus} u_{0,0} = \frac{1}{h^2} (u_{0,1} + u_{1,0} - 2u_{0,0}) \quad (10.22)$$

The matrix operator $\mathbf{D}_{\Delta\boxplus}$ operates over the full grid, which when written as a vector, consists of $N_x + 1$ concatenated vertical strips of length $N_y + 1$ (i.e., the points on the boundary now form part of the state). The matrix operator appears in Figure 10.5(b), where it is to be noted that the top left-hand block, and the top row entries of the other central blocks have slightly modified values. For different approximations to the Neumann condition, the modifications are distinct. See Problem 10.5 and Programming Exercise 10.3. Both the Dirichlet and Neumann conditions presented here arise naturally in the analysis of finite difference schemes for the 2D wave equation—see §11.2.2.

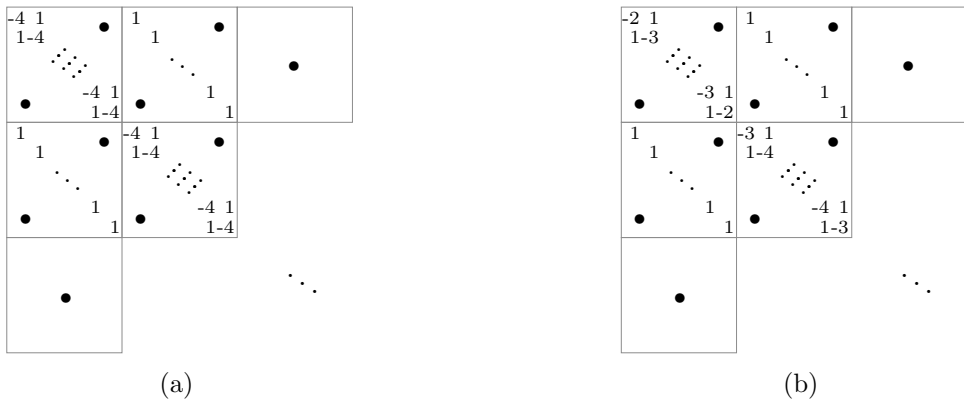


Figure 10.5: *Upper left-hand corners of the matrix representation $\mathbf{D}_{\Delta\boxplus}$ of the discrete Laplacian operator $\delta_{\Delta\boxplus}$ under (a) Dirichlet conditions, and (b) Neumann conditions. Values are to be scaled by $1/h^2$, and • indicates zero entries.*

As one can imagine, for operators of wider stencil, such as, e.g., $\mathbf{D}_{\Delta\boxplus,\Delta\boxplus}$, more boundary conditions are required, and thus more values in the resulting matrix form must be modified. See Problem

10.6 and Programming Exercise 10.5.

10.3 Grid Functions and Difference Operators: Radial Coordinates

Problems defined over a circular geometry play a large role in musical acoustics, in particular when it comes to the modeling of percussion instruments such as drums and gongs. Though finite element models are often used under such conditions, a finite difference approach is still viable, and can lead to very efficient, and easily programmed sound synthesis algorithm designs. A grid function $u_{l,m}^n$, for $(l, m) \in \mathcal{D}$, and $n \geq 0$, represents an approximation to a continuous function $u(r, \theta, t)$, at coordinates $r = lh_r$, $\theta = mh_\theta$ and $t = nk$. In general, the grid spacings h_r and h_θ will not be the same. See Figure 10.6(a). Here, the main domain of interest will be the unit area circle $\mathcal{D} = \mathbb{U}_{\circ, N_r, N_\theta}^2$, the set of points l, m with $0 \leq l \leq N_r$, and $0 \leq m \leq N_\theta - 1$, where $h_r = 1/N_r$, and $h_\theta = 2\pi/N_\theta$. Also useful is the domain $\overline{\mathbb{U}}_{\circ, N_r, N_\theta}^2$ which is the same as $\mathbb{U}_{\circ, N_r, N_\theta}^2$ without the central grid location at $l = 0$. At the central grid point, at $l = 0$, for any m , any grid function u is assumed to be single-valued, and its value here will be called $u_{0,0}$. A special grid function of interest is $r_l = lh_r$.

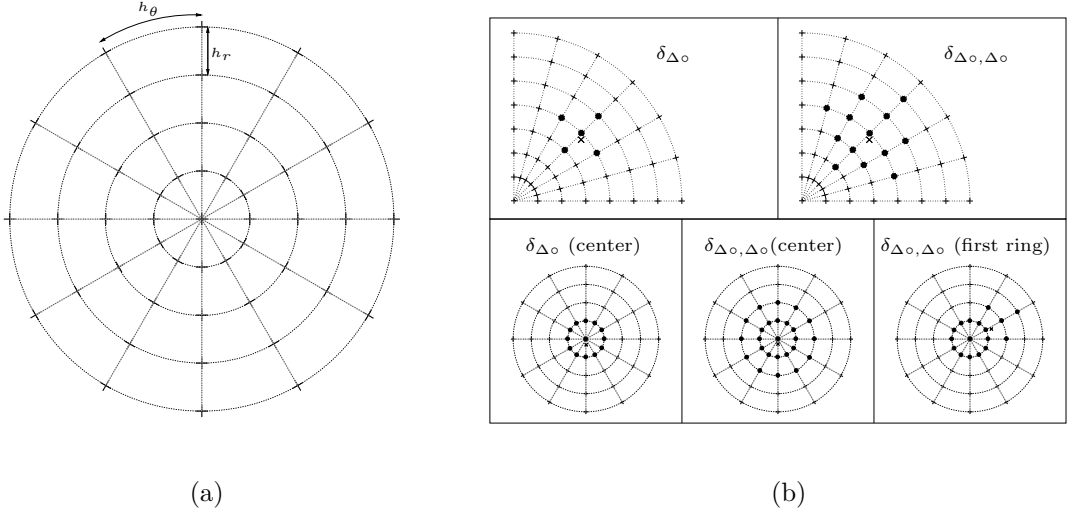


Figure 10.6: (a) Grid in radial coordinates, with radial spacing h_r , and angular spacing h_θ . (b) Stencils of the discrete Laplacian δ_{Δ_0} and biharmonic operator $\delta_{\Delta_0, \Delta_0}$, with specialized forms near the grid center. In each case, the point at which the operator acts is indicated by a \times symbol.

Spatial shift operators, in the r and θ directions may be defined as

$$e_{r+} u_{l,m}^n = u_{l+1,m}^n \quad e_{r-} u_{l,m}^n = u_{l-1,m}^n \quad e_{\theta+} u_{l,m}^n = u_{l,m+1}^n \quad e_{\theta-} u_{l,m}^n = u_{l,m-1}^n$$

and forward, backward and centered difference operators as

$$\begin{aligned} \delta_{r+} &\triangleq \frac{1}{h_r} (e_{r+} - 1) \approx \frac{\partial}{\partial r} & \delta_{r-} &\triangleq \frac{1}{h_r} (1 - e_{r-}) \approx \frac{\partial}{\partial r} & \delta_{x.} &\triangleq \frac{1}{2h_r} (e_{r+} - e_{r-}) \approx \frac{\partial}{\partial r} \\ \delta_{\theta+} &\triangleq \frac{1}{h_\theta} (e_{\theta+} - 1) \approx \frac{\partial}{\partial \theta} & \delta_{\theta-} &\triangleq \frac{1}{h_\theta} (1 - e_{\theta-}) \approx \frac{\partial}{\partial \theta} & \delta_{\theta.} &\triangleq \frac{1}{2h_\theta} (e_{\theta+} - e_{\theta-}) \approx \frac{\partial}{\partial \theta} \end{aligned}$$

The operators e_{r-} , δ_{r-} and $\delta_{r.}$ above are only well-defined at grid locations with $l \geq 1$. The

operators in θ act on grid points with index m modulo N_θ , e.g., $\delta_{\theta-}u_{l,0} = (u_{l,0} - u_{l,N_\theta-1})/h_\theta$.

In analogy with the second form in (10.4), one may define a discrete inner product, over the domain $\mathcal{D} = \overline{\mathbb{U}}_{\circ, N_r, N_\theta}^2$, as

$$\langle f, g \rangle_{\overline{\mathbb{U}}_{\circ, N_r, N_\theta}}^2 = \sum_{l=1}^{N_r} \sum_{m=0}^{N_\theta-1} h_\theta h_r r_l f_{l,m} g_{l,m}$$

The Discrete Laplacian and Biharmonic Operators in Radial Coordinates

The main operator of interest is, as in Cartesian coordinates, the Laplacian, defined in radial coordinates in (10.2). Here is a second-order accurate approximation, as applied to a grid function u :

$$\delta_{\Delta\circ} u = \frac{1}{r} \delta_{r+} ((\mu_r - r) \delta_{r-} u) + \frac{1}{r^2} \delta_{\theta\theta} u \quad (10.23)$$

where $\delta_{\theta\theta} = \delta_{\theta+} \delta_{\theta-}$. When expanded, this reads as

$$\delta_{\Delta\circ} u_{l,m} = \frac{1}{lh_r^2} ((l + 1/2)u_{l+1,m} - 2lu_{l,m} + (l - 1/2)u_{l-1,m}) + \frac{1}{l^2 h_r^2 h_\theta^2} (u_{l,m+1} - 2u_{l,m} + u_{l,m-1})$$

The above difference operation holds at grid points $u_{l,m}$ with $l > 0$. At the center point, a special form is necessary [120]:

$$\delta_{\Delta\circ} u_{0,0} = \frac{4}{N_\theta h_r^2} \sum_{m=0}^{N_\theta-1} (u_{1,m} - u_{0,0}) \quad (10.24)$$

It is not difficult to show that this operator indeed approximates the Laplacian to second-order accuracy at the domain center—see Problem 10.7. The matrix form of this operator may be constructed without much difficulty—see Programming Exercise 10.6.

The biharmonic operator in radial coordinates $\delta_{\Delta\circ, \Delta\circ}$, may be defined, at interior points in a domain, as

$$\delta_{\Delta\circ, \Delta\circ} u_{l,m} = \delta_{\Delta\circ} \delta_{\Delta\circ} u_{l,m} \quad 2 \leq l \leq N_r - 2 \quad (10.25)$$

At grid points near the boundary, the form of the operator must be specialized to include boundary conditions. As for the case of the Laplacian, however, in the neighborhood of the center, at grid locations l, m , with $l = 0, 1$, special forms are necessary:

$$\begin{aligned} \delta_{\Delta\circ, \Delta\circ} u_{0,0} &= \frac{16}{3N_\theta h_r^4} \sum_{m=0}^{N_\theta-1} (u_{2,m} - 4u_{1,m} + 3u_{0,0}) \\ \delta_{\Delta\circ, \Delta\circ} u_{1,m} &= \frac{4}{N_\theta h_r^2} \sum_{m=0}^{N_\theta-1} \delta_{\Delta\circ} u_{1,m} - \delta_{\Delta\circ} u_{0,0} \end{aligned}$$

Slightly different settings have been proposed—see [12]. See also Programming Exercise 10.7.

Summation by Parts

For circular domains, identities analogous to integration by parts are available, but one must pay special attention to the definition of the Laplacian at the center point. As a practically important example, consider the inner product of a grid function f and the discrete Laplacian applied to a grid function g , over the domain $\overline{\mathbb{U}}_{\circ, N_r, N_\theta}^2$, the unit circle without its center grid point. In this case, the definition (10.23) holds at all points in the domain, and one has

$$\langle f, \delta_{\Delta\circ} g \rangle_{\overline{\mathbb{U}}_{\circ, N_r, N_\theta}^2} = -\langle \delta_{r-} f, \frac{\mu_r - r}{r} \delta_{r-} g \rangle_{\overline{\mathbb{U}}_{\circ, N_r, N_\theta}^2} - \langle \delta_{\theta-} f, \frac{1}{r^2} \delta_{\theta-} g \rangle_{\overline{\mathbb{U}}_{\circ, N_r, N_\theta}^2} + b_{\text{outer}} - b_{\text{inner}}$$

where

$$\begin{aligned}\mathfrak{b}_{\text{outer}} &= \{f, \mu_{r+r} \delta_{r+g}\}_{(N_r, [0, N_\theta-1])} \triangleq \sum_{m=0}^{N_\theta-1} h_\theta f_{N_r, m} \mu_{r+r} \delta_{r+g} g_{N_r, m} \\ \mathfrak{b}_{\text{inner}} &= \{e_{r-f}, \mu_{r-r} \delta_{r-g}\}_{(1, [0, N_\theta-1])} \triangleq \sum_{m=0}^{N_\theta-1} h_\theta f_{0,0} \mu_{r-r} \delta_{r-g} e_{1,m}\end{aligned}$$

The term $\mathfrak{b}_{\text{outer}}$ clearly corresponds to the boundary term at the domain edge in (10.8a). But the term $\mathfrak{b}_{\text{inner}}$ results purely from the choice of the domain of summation. But it may be rewritten as follows, using single-valuedness of f and g at the grid location $l = 0, m$, and the definition of the discrete Laplacian at the central grid point, from (10.24):

$$\mathfrak{b}_{\text{inner}} = \frac{f_{0,0} h_\theta}{2} \sum_{m=0}^{N_\theta-1} (g_{1,m} - g_{0,0}) = \frac{\pi h_r^2}{4} f_{0,0} \delta_{\Delta \circ} g_{0,0}$$

Thus, finally, one has

$$\langle f, \delta_{\Delta \circ} g \rangle_{\overline{\mathbb{U}}_{\circ, N_r, N_\theta}^2} + \frac{\pi h_r^2}{4} f_{0,0} \delta_{\Delta \circ} g_{0,0} = -\langle \delta_{r-f}, \frac{\mu_{r-r}}{r} \delta_{r-g} \rangle_{\overline{\mathbb{U}}_{\circ, N_r, N_\theta}^2} - \langle \delta_{\theta-f}, \frac{1}{r^2} \delta_{\theta-g} \rangle_{\overline{\mathbb{U}}_{\circ, N_r, N_\theta}^2} + \mathfrak{b}_{\text{outer}} \quad (10.27)$$

Bounds

As before, bounds are available relating the norms of grid functions under difference operators to norms of the grid functions themselves. Here are two of interest in the analysis of schemes involving the discrete Laplacian:

$$\|\delta_{\theta-f}\|_{\overline{\mathbb{U}}_{\circ, N_r, N_\theta}^2} \leq \frac{2}{h_\theta} \|f\|_{\overline{\mathbb{U}}_{\circ, N_r, N_\theta}^2} \quad \|\sqrt{\frac{\mu_{r-r}}{r}} \delta_{r-f}\|_{\overline{\mathbb{U}}_{\circ, N_r, N_\theta}^2} \leq \frac{4}{h_r^2} \|f\|_{\overline{\mathbb{U}}_{\circ, N_r, N_\theta}^2} + 2\pi f_{0,0}^2 \quad (10.28)$$

10.4 Problems

Problem 10.1 *The stencils of various 2D difference operators are shown in Figure 10.2. Not shown, however, are the coefficients to be applied at each point included in the stencil. Determine these for all the operators shown in the figure, assuming equal grid spacings $h_x = h_y = h$. (For the operator $\delta_{\Delta \boxplus}$, for example, the coefficients from left to right, and top to bottom, are: $1/h^2$, $1/h^2$, $-4/h^2$, $1/h^2$ and $1/h^2$.)*

There are certain operators which appear in the figure which are not defined in the main body of the text, namely averaging and mixed derivative operators:

$$\begin{aligned}\mu_{x+} &= \frac{1}{2} (e_{x+} + 1) & \mu_{x-} &= \frac{1}{2} (1 + e_{x-}) & \mu_{y+} &= \frac{1}{2} (e_{y+} + 1) & \mu_{y-} &= \frac{1}{2} (1 + e_{y-}) \\ \delta_{x+y+} &= \delta_{x+} \delta_{y+} & \delta_{x+y-} &= \delta_{x+} \delta_{y-} & \delta_{x-y+} &= \delta_{x-} \delta_{y+} & \delta_{x-y-} &= \delta_{x-} \delta_{y-}\end{aligned}$$

Problem 10.2 *Given a general bilinear function $f(p, q)$ in the variables p and q*

$$f(p, q) = a + bp + cq + dpq$$

defined over the square region $0 \leq p, q \leq 1$, for constants a, b, c and d , show that f takes on its maximum and minimum values at the corners of the domain.

Problem 10.3 *Recalling the analysis of the anisotropy of the operator $\delta_{\Delta \boxplus}$ in §10.2.2, consider the nine-point Laplacian operator as given in (10.10), which depends on the free parameter α , and show*

that its expansion, in terms of wavenumber components β_x and β_y is

$$\delta_{\Delta\alpha} \triangleq \alpha\delta_{\Delta\square} + (1-\alpha)\delta_{\Delta\boxtimes} \implies -(\beta_x^2 + \beta_y^2) + \frac{h^2}{12}(\beta_x^4 + 6(1-\alpha)\beta_x^2\beta_y^2 + \beta_y^4) + O(h^4)$$

For an arbitrary choice of α , can the $O(h^2)$ term be written in terms of the wavenumber magnitude $|\beta| = \sqrt{\beta_x^2 + \beta_y^2}$ alone? If not, is there a value (or values) of α such that it can be? If you can find such a value of α , then the anisotropic behavior of the parameterized operator will exhibit itself only at fourth order (though the operator remains a second-order accurate approximation to the Laplacian).

Problem 10.4 Find the matrix form $\mathbf{D}_{\Delta\alpha}$ of the operator $\delta_{\Delta\alpha}$, assuming that it acts on a grid function defined over \mathbb{U}_{N_x, N_y}^2 , under Dirichlet conditions.

Problem 10.5 Consider the operator $\delta_{\Delta\square}$, operating over the rectangular domain \mathbb{U}_{N_x, N_y}^2 , which is of size $(N_x + 1) \times (N_y + 1)$ points. A centered zero derivative, or Neumann condition may be written as

$$\begin{aligned}\delta_x \cdot u_{0,m} &= 0 & m = 0, \dots, N_y \\ \delta_x \cdot u_{N_x,m} &= 0 & m = 0, \dots, N_y \\ \delta_y \cdot u_{l,0} &= 0 & l = 0, \dots, N_x \\ \delta_y \cdot u_{l,N_y} &= 0 & l = 0, \dots, N_x\end{aligned}$$

Supposing that the state vector is defined as the concatenation of $N_x + 1$ vertical strips of length $N_y + 1$, write the matrix form of the operator under the conditions above. Assume that $h_x = h_y = h$. Again, as in the case of the non-centered condition discussed beginning on page 300, your matrix will consist of $(N_y + 1) \times (N_y + 1)$ blocks, each of which is Toeplitz except for in the extreme rows and columns. See also Programming Exercise 10.3.

Problem 10.6 Consider the discrete biharmonic operator $\delta_{\Delta\square, \Delta\square}$, operating over the rectangular domain \mathbb{U}_{N_x, N_y}^2 , which is of size $(N_x + 1) \times (N_y + 1)$ points. Consider the following two sets of boundary conditions:

Clamped:

$$\begin{aligned}\delta_x \cdot u_{0,m} &= 0 & u_{0,m} = 0 & m = 0, \dots, N_y \\ \delta_x \cdot u_{N_x,m} &= 0 & u_{N_x,m} = 0 & m = 0, \dots, N_y \\ \delta_y \cdot u_{l,0} &= 0 & u_{l,0} = 0 & l = 0, \dots, N_x \\ \delta_y \cdot u_{l,N_y} &= 0 & u_{l,N_y} = 0 & l = 0, \dots, N_x\end{aligned}$$

Simply supported:

$$\begin{aligned}\delta_{xx} u_{0,m} &= 0 & u_{0,m} = 0 & m = 0, \dots, N_y \\ \delta_{xx} u_{N_x,m} &= 0 & u_{N_x,m} = 0 & m = 0, \dots, N_y \\ \delta_{yy} u_{l,0} &= 0 & u_{l,0} = 0 & l = 0, \dots, N_x \\ \delta_{yy} u_{l,N_y} &= 0 & u_{l,N_y} = 0 & l = 0, \dots, N_x\end{aligned}$$

First, find the explicit form of the stencil of the operator, including all coefficients, when applied at any point directly adjacent to the boundary—take special care when near corners! Then, write the matrix form $\mathbf{D}_{\Delta\square, \Delta\square}$ of the operator, assuming that it acts on a vector consisting of concatenated vertical strips of the grid function $u_{l,m}$. You may leave out values on the boundary itself (which are constrained to be zero in either case), so your matrix will be square and of size $(N_x - 1)(N_y - 1) \times (N_x - 1)(N_y - 1)$.

Problem 10.7 Consider the discrete Laplacian operator, in radial coordinates, acting on a grid function $u_{l,m}$ at the central grid point $l = 0, m = 0$. Given the definition of this operator, from (10.24), prove that it is indeed a second-order accurate approximation to the Laplacian. In order to do this, consider the values of the grid function $u_{1,m}$ which appear in the definition to be values

of a continuous function at the location $x = h_r \cos(mh_\theta)$, $y = h_r \sin(mh_\theta)$, and perform Taylor expansions about the point $x = 0$, $y = 0$.

10.5 Programming Exercises

Programming Exercise 10.1 Create a Matlab function which, for a given rectangular grid function, calculates an interpolated value at coordinates x_o , y_o , using either truncation or bilinear interpolation, as described in §10.2.1. Assume equal grid spacings in the x and y directions, and thus that the aspect ratio may be determined from the dimensions of the input grid function. Make sure that your code takes account of whether the input grid function includes values on its boundary—this must also be specified as an input parameter.

Programming Exercise 10.2 Consider the parameterized nine-point approximation $\delta_{\Delta\alpha}$ to the Laplacian, as defined in (10.10). When applied to a test function of the form $u_{l,m} = e^{jh(\beta_x l + \beta_y m)}$, it behaves as

$$\delta_{\Delta\alpha} u = \frac{-4}{h^2} (\sin^2(\beta_x h/2) + \sin^2(\beta_y h/2) - 2(1-\alpha) \sin^2(\beta_x h/2) \sin^2(\beta_y h/2)) u = F_\alpha(\beta_x, \beta_y) u$$

Create a Matlab script which plots the function $-F_\alpha(\beta_x, \beta_y)/|\beta|^2$ as a function of $\beta_x h$ and $\beta_y h$, for $-\pi \leq \beta_x h, \beta_y h \leq \pi$ as a surface, for various values of the free parameter α . (This function is a comparison of the dispersive behavior of the difference operator with the continuous operator Δ as a function of wavenumber.) Verify that the difference operator is approximately isotropic when $\alpha \approx 2/3$.

Programming Exercise 10.3 Create a Matlab function which generates difference matrices $\mathbf{D}_{\Delta\boxplus}$ corresponding to the discrete Laplacian operator $\delta_{\Delta\boxplus}$, operating over the rectangular domain \mathbb{U}_{N_x, N_y}^2 . Suppose also that the aspect ratio is $\epsilon = N_x/N_y$, and that the grid spacing is $h = \sqrt{\epsilon}/N_x$. Your code thus depends only on N_x and N_y , and should generate matrices corresponding to fixed, or Dirichlet conditions, non-centered Neumann conditions, and centered Neumann conditions—the first two cases are discussed in §10.2.4, and the third in Problem 10.5. Note that your output matrix will be square, and of size $(N_x-1)(N_y-1) \times (N_x-1)(N_y-1)$ in the first case, and $(N_x+1)(N_y+1) \times (N_x+1)(N_y+1)$ in the latter two. Be sure that the matrix is generated in sparse form—make use of the function `sparse` for this purpose.

Programming Exercise 10.4 Create a Matlab function which generates a difference matrix $\mathbf{D}_{\Delta\alpha}$ corresponding to the parameterized nine-point discrete Laplacian operator $\delta_{\Delta\alpha}$, operating over the rectangular domain \mathbb{U}_{N_x, N_y}^2 , under Dirichlet conditions. Your code will necessarily depend on the free parameter α .

Programming Exercise 10.5 Create a Matlab function which generates difference matrices $\mathbf{D}_{\Delta\boxplus, \Delta\boxplus}$ corresponding to the discrete biharmonic operator $\delta_{\Delta\boxplus, \Delta\boxplus}$, operating over the rectangular domain \mathbb{U}_{N_x, N_y}^2 . As above, suppose also that the aspect ratio is $\epsilon = N_x/N_y$, and that the grid spacing is $h = \sqrt{\epsilon}/N_x$. Your code should generate matrices corresponding to clamped and simply supported conditions, as described in Problem 10.6. Your output matrix will be square, and of size $(N_x-1)(N_y-1) \times (N_x-1)(N_y-1)$.

Programming Exercise 10.6 Consider the discrete Laplacian operator $\delta_{\Delta\circ}$ in radial coordinates, operating over the domain $\mathbb{U}_{\circ, N_r, N_\theta}^2$, which is defined by (10.23) at grid points $l > 0$, and by (10.24) at $l = 0$. Create a Matlab function which generates, for a given N_r and N_θ , the matrix form \mathbf{D}_\circ of the operator, under fixed conditions at the outer edge of the domain, at $l = N_r$.

In preparation for this, suppose that the values of the grid function $u_{l,m}$ on which $\mathbf{D}_{\Delta\circ}$ operates are written as a vector \mathbf{u} consisting of the central value $u_{0,0}$, followed by concatenated concentric rings of the grid function, or as:

$$\mathbf{u} = [u_{0,0}, u_{1,0}, \dots, u_{1,N_\theta}, \dots, u_{N_r-1,0}, \dots, u_{N_r-1,N_\theta-1}]^T$$

As such, the matrix $\mathbf{D}_{\Delta\circ}$ will be of size $(N_\theta(N_r-1)+1) \times (N_\theta(N_r-1)+1)$.

Programming Exercise 10.7 Consider the discrete biharmonic operator $\delta_{\Delta\circ,\Delta\circ}$ in radial coordinates, operating over the domain $\mathbb{U}_{\circ,N_r,N_\theta}^2$, which is defined by (10.25) at grid points $l > 1$, and by (10.26) at $l = 0$ and $l = 1$. Create a Matlab function which generates, for a given N_r and N_θ , the matrix form $\mathbf{D}_{\Delta\circ,\Delta\circ}$ of the operator.

Assume clamped boundary conditions at the domain edge, i.e., $u_{N_r,m} = \delta_r u_{N_r,m} = 0$, so that as in the case of the Laplacian in the previous exercise, the matrix operates only over values of the grid function for $l < N_r$.

Chapter 11

The 2D Wave Equation

A good starting point in the investigation of 2D synthesis is, as in 1D, the wave equation, introduced in §11.1, which serves as a useful test problem for the vibration of membranes as well as room acoustics, and also as another good point of comparison for the various physical modeling synthesis techniques, including finite difference schemes (§11.2 and §11.3), digital waveguide meshes (§11.4), lumped networks (§11.5), and modal methods (§11.6). Finally, finite difference schemes are developed in radial coordinates in §11.7. The previous chapter serves as a reference for the techniques to be discussed here and in the following two chapters.

11.1 Definition and Properties

The wave equation in one spatial dimension (6.1) may be directly generalized to two dimensions as

$$u_{tt} = c^2 \Delta u \quad (11.1)$$

Here, u is the dependent variable of interest, c is a wave speed, and Δ is the 2D Laplacian operator as discussed in Chapter 10. The problem is assumed defined over some 2D domain \mathcal{D} . When the spatial coordinates are scaled using a characteristic length L , the 2D wave equation is of the form

$$u_{tt} = \gamma^2 \Delta u \quad (11.2)$$

where again, $\gamma = c/L$ is a parameter with units of frequency. In some cases, a good choice of the scaling parameter L for problems defined over a finite region \mathcal{D} is $L = \sqrt{|\mathcal{D}|}$, so that (11.2) is then defined over a region of unit area. For other domains, such as the circle of radius R , it may be more convenient to choose $L = R$, so that the problem is then defined over a unit circle.

The 2D wave equation, as given above, is a simple approximation to the behavior of a vibrating membrane; indeed, a lumped model of membrane is often employed in order to derive the 2D wave equation itself—see §11.5. It also can serve as a preliminary step towards the treatment of room acoustics problems (where, in general, a 3D wave equation would be employed); direct solution of the 2D and 3D wave equations for room modeling has been employed for some time [56], and artificial reverberation applications are currently an active research topic [248, 249, 28, 207]. Other applications include articulatory vocal tract modeling [245, 246], and detailed studies of wind instrument bores [257, 253, 254]. It will be assumed, for the moment, that the 2D wave equation is defined over \mathbb{R}^2 , so that a discussion of boundary conditions may be postponed.

The wave equation, like all second order in time PDEs, must be initialized with two functions (see §6.1.3); in Cartesian coordinates, for example, one would set, normally, $u(x, y, 0) = u_0(x, y)$ and $\frac{\partial u}{\partial t}(x, y, 0) = v_0(x, y)$. In the case of a membrane, as for the string, the first condition corresponds

to a pluck, and the second to a strike. A useful all-purpose initializing distribution is a 2D raised cosine, of the form

$$c_{\text{rc}}(x, y) = \begin{cases} \frac{c_0}{2} \left(1 + \cos(\pi \sqrt{(x - x_0)^2 + (y - y_0)^2} / r_{\text{hw}}) \right), & \sqrt{(x - x_0)^2 + (y - y_0)^2} \leq r_{\text{hw}} \\ 0, & \sqrt{(x - x_0)^2 + (y - y_0)^2} > r_{\text{hw}} \end{cases} \quad (11.3)$$

which has amplitude c_0 , half-width r_{hw} , and is centered at coordinates (x_0, y_0) . Such a distribution can be used in order to model both plucks and strikes. Of course, in full models of percussion instruments, a model of the excitation mechanism, such as a mallet, should be included as well—see §12.3 where this topic is taken up in the more musically interesting setting of plate vibration.

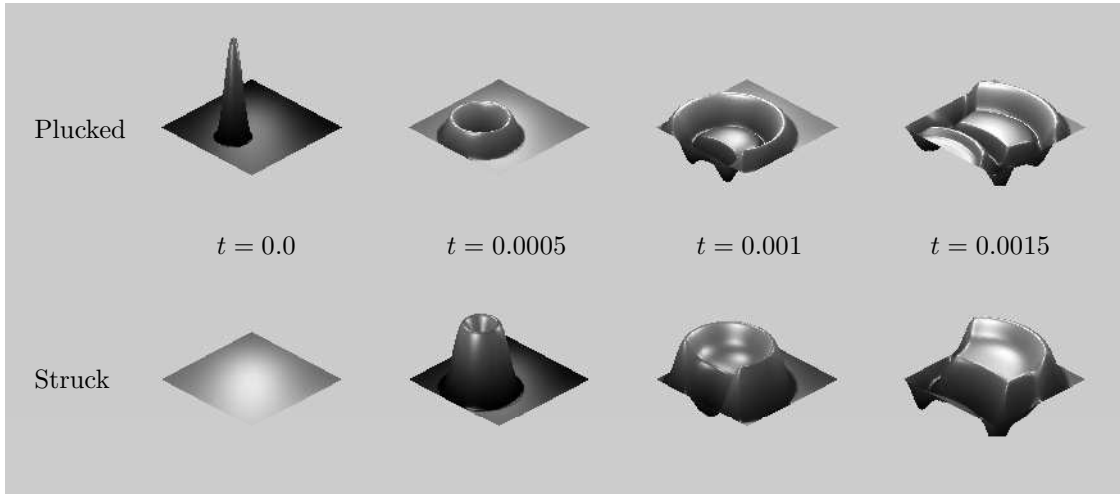


Figure 11.1: *Time evolution of solutions to the 2D wave equation, defined over a unit square, with fixed boundary conditions. In this case, $\gamma = 400$, and snapshots of the displacement are shown at times as indicated, under plucked conditions (top row) and struck conditions (bottom row). In the first case, the initial displacement condition is a raised cosine of half-width 0.15, centered at coordinates $x = 0.3$, $y = 0.5$, and in the second, the initial velocity profile is a raised cosine of half-width 0.15, centered at the same location.*

A pair of simulation results, under plucked and struck conditions, is illustrated in Figure 11.1. The main feature which distinguishes the behavior of solutions to the 2D wave equation from the 1D case is the reduction in amplitude of the wave as it evolves, due to spreading effects—related to this is the presence of a “wake” behind the wavefront, which is absent in the 1D case, as well as the fact that, even when simple boundary conditions are employed, the solution is not periodic—reflections from domain boundaries occur with increasing frequency, as illustrated in Figure 11.2(a). One might guess, from these observations alone, that the efficiency of the digital waveguide formulation for the 1D case, built around waves which travel without distortion, will disappear in this case—this is in fact true, as will be discussed in §11.4.

11.1.1 Phase and Group Velocity

Assuming, in Cartesian coordinates, a plane wave solution of the form

$$u(x, y, t) = e^{st+j(\beta_x x + \beta_y y)}$$

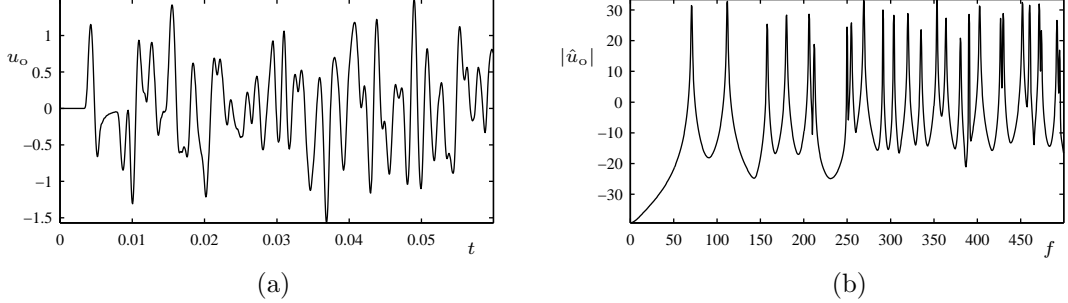


Figure 11.2: *Solution of the 2D wave equation, with $\gamma = 100$, defined over a unit square, in response to a plucked excitation, in the form of a raised cosine, centered at $x = 0.7$, $y = 0.5$, of amplitude 10, and of half-width 0.2. (a) Time response, at location $x = 0.3$, $y = 0.7$, and (b) its frequency spectrum.*

leads to the characteristic equation and dispersion relation

$$s^2 = -\gamma^2 |\beta|^2 \quad \rightarrow \quad \omega = \pm \gamma |\beta|$$

and, thus, to expressions for the phase and group velocity,

$$v_\phi = \gamma \quad v_g = \gamma$$

Thus, just as in 1D, all wave-like components travel at the same speed. Note that as the Laplacian operator is isotropic, wave speed is independent not only of frequency or wavenumber, but also of direction.

In 1D, for LSI systems, it is often possible to rewrite the phase and group velocities as functions of frequency alone. While this continues to be possible for isotropic systems in 2D, it is not possible when the system exhibits anisotropy. Furthermore, most numerical methods exhibit spurious anisotropy, and thus the only way to analyze such behavior is through expressions of wavenumber.

11.1.2 Energy and Boundary Conditions

The 2D wave equation, like its 1D counterpart, is lossless. This can be seen, as usual, by writing the energy for the system, which is conserved. Assuming (11.1) to be defined over the infinite plane $\mathcal{D} = \mathbb{R}^2$, taking an inner product with u_t in Cartesian coordinates followed by integration by parts leads to

$$\langle u_t, u_{tt} \rangle_{\mathcal{D}} = \gamma^2 \langle u_t, \Delta u \rangle_{\mathcal{D}} = \gamma^2 \langle u_t, u_{xx} \rangle_{\mathcal{D}} + \gamma^2 \langle u_t, u_{yy} \rangle_{\mathcal{D}} = -\gamma^2 \langle u_{xt}, u_x \rangle_{\mathcal{D}} - \gamma^2 \langle u_{yt}, u_y \rangle_{\mathcal{D}}$$

or,

$$\frac{d\mathfrak{H}}{dt} = 0 \quad \text{with} \quad \mathfrak{H} = \mathfrak{T} + \mathfrak{V}$$

and

$$\mathfrak{T} = \frac{1}{2} \|u_t\|_{\mathcal{D}}^2 \quad \mathfrak{V} = \frac{\gamma^2}{2} (\|u_x\|_{\mathcal{D}}^2 + \|u_y\|_{\mathcal{D}}^2) = \frac{\gamma^2}{2} \|\nabla u\|_{\mathcal{D}}^2 \quad (11.4)$$

where ∇ signifies the gradient operation. Such a result is obviously independent of the chosen coordinate system. The expression is, again, non-negative, and leads immediately to bounds on the growth of the norm of the solution, by exactly the same methods as discussed in §6.1.8.

Edges

In order to examine boundary conditions at, e.g., a straight edge, consider (11.1) defined over the semi-infinite region $\mathcal{D} = \mathbb{R}^{2,x+}$, as discussed in §10.1.2. Through the same manipulations above, one arrives at the energy balance

$$\frac{d\mathfrak{H}}{dt} = \mathfrak{B} \quad \text{with} \quad \mathfrak{H} = \mathfrak{T} + \mathfrak{V} \quad (11.5)$$

where \mathfrak{T} and \mathfrak{V} are as defined in (11.4) above. The boundary term \mathfrak{B} , depending only on values of the solution at $x = 0$, is

$$\mathfrak{B} = -\gamma^2 \{u_x, u_t\}_{(0,\mathbb{R})} \triangleq -\gamma^2 \int_{-\infty}^{\infty} u_x(0, y', t) u_t(0, y', t) dy' \quad (11.6)$$

Thus, the natural extensions of the lossless Dirichlet and Neumann conditions (6.18) and (6.19) for the 1D wave equation are

$$u(0, y, t) = 0 \quad \text{or} \quad u_x(0, y, t) = 0 \quad \text{at } x = 0$$

in which case \mathfrak{B} vanishes. In the case of the membrane, where u is a displacement, these correspond to fixed and free conditions, respectively. For room acoustics problems, in which case u is a pressure, the Neumann condition corresponds to a rigid wall termination. As in the case of the 1D wave equation, it should be obvious that many other terminations, including those of lossless energy-storing type and lossy conditions, possibly nonlinear, and combinations of these can be arrived at through the above analysis. One particularly interesting family of conditions, useful in modeling terminations in this setting of room acoustics [207], appears in Problem 11.1.

Corners

An extra concern, especially when working in Cartesian coordinates in 2D, is the domain corner. Though it is not particularly problematic in the case of the wave equation, for more complex systems, such as the stiff plate, one must be very careful with such points, especially in the discrete setting. To this end, consider the wave equation defined over the quarter-plane $\mathcal{D} = \mathbb{R}^{2,x+y+}$. The energy balance is again as in (11.5), but the boundary term is now

$$\begin{aligned} \mathfrak{B} &= -\gamma^2 \int_0^{\infty} u_x(0, y', t) u_t(0, y', t) dy' - \gamma^2 \int_0^{\infty} u_y(x', 0, t) u_t(x', 0, t) dx' \\ &= -\gamma^2 \{u_x, u_t\}_{(0,\mathbb{R}^+)} - \gamma^2 \{u_y, u_t\}_{(\mathbb{R}^+, 0)} \end{aligned}$$

The system is lossless under a combination of the conditions

$$u_x(0, y, t) = 0 \quad \text{or} \quad u_t(0, y, t) = 0 \quad \text{at } x = 0 \quad (11.7a)$$

$$u_y(x, 0, t) = 0 \quad \text{or} \quad u_t(x, 0, t) = 0 \quad \text{at } y = 0 \quad (11.7b)$$

It is thus possible to choose distinct conditions over each edge of the domain; notice, however, that if free or Neumann conditions are chosen on both edges, then at the domain corner $x = y = 0$, both such conditions must be enforced.

Though only a quarter plane has been analyzed here, it should be clear that such results extend to the case of a rectangular domain—see Problem 11.2.

11.1.3 Modes

The modal decomposition of solutions to the 2D wave equation under certain simple geometries and boundary conditions is heavily covered in the musical acoustics literature—see, e.g., standard texts

such as [135, 243]. It is useful, however, to at least briefly review such a decomposition in the case of the rectangular domain.

As in the case of the 1D wave equation (see §6.1.11) and the ideal bar equation (see §7.1.3), one may assume an oscillatory solution to the 2D wave equation of the form $u(x, y, t) = e^{j\omega t}U(x, y)$, leading to

$$-\omega^2 U = \gamma^2 \Delta U$$

The wave equation defined over a unit area rectangle \mathbb{U}_ϵ^2 of aspect ratio ϵ , and under fixed boundary conditions is separable, and the Fourier series solution to the above equation are

$$U_{p,q}(x, y) = \sin(p\pi x/\sqrt{\epsilon}) \sin(q\pi\sqrt{\epsilon}y) \quad \omega_{p,q} = \pi\gamma\sqrt{p^2/\epsilon + q^2} \quad (11.8)$$

The modal functions are illustrated in Figure 11.3, in the case of a square domain. (It is worth pointing out that, under some choices of the aspect ratio ϵ , it is possible for modal frequencies corresponding to distinct modes to coincide or become degenerate.)

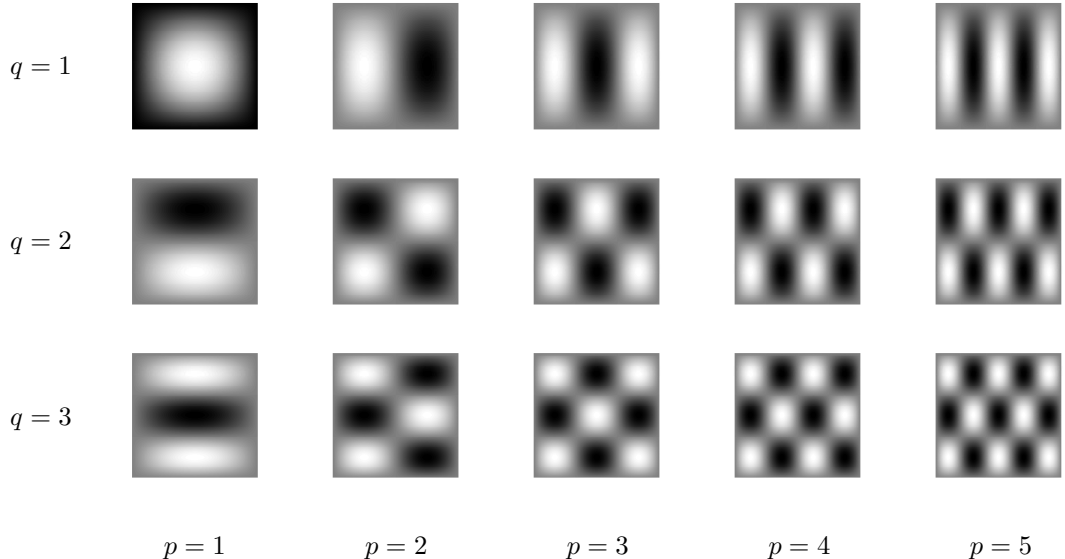


Figure 11.3: *Modal shapes $U_{p,q}(x, y)$ for a square membrane, under fixed boundary conditions. In all cases, dark and light areas correspond to modal maxima and minima.*

Given the above expression for the modal frequencies $f_{p,q}$, it is not difficult to show that the number of degrees of freedom, for frequencies less than or equal to $f_s/2$ will be¹

$$N_m(f_s/2) = \frac{\pi f_s^2}{2\gamma^2} \quad (11.9)$$

See Problem 11.3. Twice this number is, as before, the number of degrees of freedom of the system when it is simulated at a sample rate f_s . This indicates that the density of modes increases strongly with frequency, which is easily visible in a spectral plot of output taken from the solution to the 2D wave equation, as shown in Figure 11.2(b). This is to be compared with the situation for the 1D

¹This expression is approximate, and does not take into account modal degeneracy. It is correct in the limit of high f_s . See [242] for exact expressions for the numbers of modes in 3D.

wave equation, where modal density is roughly constant—see §6.1.11. Serious (and not unexpected) ramifications in terms of computational complexity result, as will be discussed shortly. For more on synthesis for the 2D wave equation using modal methods, see §11.6.

It is direct to extend this modal analysis to the case of the wave equation in 3D, defined over a suitable region such as a cube; such analysis yields useful information about modal densities in the context of room acoustics. See Problem 11.4. Another system which may be analyzed in this way is the case of the membrane coupled to a cavity, which serves as a simple model of a drum-like instrument—see Problem 11.5.

11.2 A Simple Finite Difference Scheme

Consider the wave equation in Cartesian coordinates. The simplest possible finite difference scheme employs a second difference in time, and a five-point Laplacian approximation $\delta_{\Delta \boxplus}$, as defined in §10.2:

$$\delta_{tt} u = \gamma^2 \delta_{\Delta \boxplus} u \quad (11.10)$$

where $u = u_{l,m}^n$ is a 2D grid function representing an approximation to the continuous solution $u(x, y, t)$ at $x = lh_x$, $y = mh_y$, $t = nk$, for integer l , m and n .

The case of equal grid spacings $h_x = h_y = h$ is the most straightforward in terms of analysis and implementation; expanding out the operator notation above leads to

$$u_{l,m}^{n+1} = \lambda^2 (u_{l+1,m}^n + u_{l-1,m}^n + u_{l,m+1}^n + u_{l,m-1}^n) + 2(1 - 2\lambda^2) u_{l,m}^n - u_{l,m}^{n-1} \quad (11.11)$$

where again, as in 1D, the Courant number λ is defined as

$$\lambda = \frac{k\gamma}{h}$$

Notice that under the special choice of $\lambda = 1/\sqrt{2}$ (this case is of particular relevance to the so-called digital waveguide mesh, to be discussed in §11.4), the recursion above may be simplified to

$$u_{l,m}^{n+1} = \frac{1}{2} (u_{l+1,m}^n + u_{l-1,m}^n + u_{l,m+1}^n + u_{l,m-1}^n) - u_{l,m}^{n-1} \quad (11.12)$$

which requires only a single multiplication by the factor $1/2$, and one fewer addition than the general form (11.11). Again, as in the case of the special difference scheme for the 1D wave equation (6.54), the value at the central grid point at l, n is no longer employed. Related to this is the interesting observation that the scheme may be decomposed into two independent schemes operating over the black and white squares on a “checkerboard” grid. See Problem 11.6.

Scheme (11.10) continues to hold if the grid spacings are not the same, though the stability condition (discussed below) must be altered, and computational complexity increases. See Problem 11.7. There is a slight advantage if such a scheme is to be used for non-square regions, but perhaps not enough to warrant its use in synthesis applications, except for high values of γ , where the grid is necessarily coarse, and truncation becomes an issue. See Programming Exercise 11.1.

Output may be drawn from the scheme using 2D interpolation operators—see §10.2.1. For example, one may take output from a position x_o, y_o as $u_o = I(x_o, y_o)u$. For a static output location, a simple truncated interpolant is probably sufficient, but for moving output locations, a bilinear interpolant is a better choice—see Programming Exercise 11.2.

Beyond being a synthesis algorithm for a simple percussion instrument, such a scheme can be modified to behave as an artificial reverberation algorithm through the insertion of an input signal—see Programming Exercise 11.4.

It is direct to develop schemes for the 3D wave equation in a similar manner (see Problem 11.8),

as well as for the case of the membrane coupled to a cavity (see Problem 11.9 and Programming Exercise 11.5).

11.2.1 von Neumann analysis

Use of the ansatz $u_{l,m}^n = z^n e^{jh(l\beta_x + m\beta_y)}$ leads to the characteristic equation

$$z - 2 + 4\lambda^2(p_x + p_y) + z^{-1} = 0$$

in the two variables $p_x = \sin^2(\beta_x h/2)$ and $p_y = \sin^2(\beta_y h/2)$, as defined in §10.2.2. This equation is again of the form (2.13), and the solutions in z will be of unit modulus when

$$0 \leq \lambda^2(p_x + p_y) \leq 1$$

The left-hand inequality is clearly satisfied. Given that the variables p_x and p_y take on values between 0 and 1, the right hand inequality is satisfied for

$$\lambda \leq \frac{1}{\sqrt{2}} \quad (11.13)$$

which is the stability condition for scheme (11.10). Notice that just as in the case of scheme (6.34) for the 1D wave equation, at the stability limit (i.e., when $\lambda = 1/\sqrt{2}$), a simplified scheme results, namely (11.12).

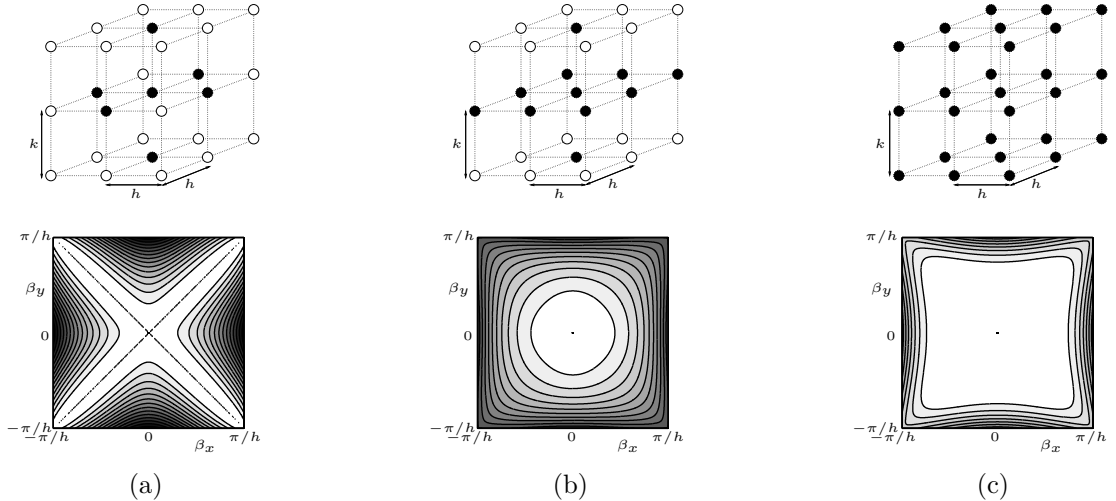


Figure 11.4: Computational stencil (top) and relative numerical phase velocity v_ϕ/γ (bottom) for (a) The explicit scheme (11.10), with $\lambda = 1/\sqrt{2}$, (b) the parameterized scheme (11.16) with the special choice of $\alpha = 2/\pi$, and λ chosen to satisfy bound (11.17) with equality, and (c) the implicit scheme (11.18), with $\alpha = 2/\pi$, $\theta = 1.2$, and λ chosen to satisfy bound (11.19) with equality. Relative phase velocity deviations of 2% are plotted as contours in the wavenumber plane $-\frac{\pi}{h} \leq \beta_x, \beta_y \leq \frac{\pi}{h}$.

11.2.2 Energy Analysis and Numerical Boundary Conditions

In order to arrive at stable numerical boundary conditions for scheme (11.10), it is again of great use to derive an expression for the numerical energy. Considering first the case of the scheme defined

over the infinite region $\mathcal{D} = \mathbb{Z}^2$, taking an inner product with $\delta_t \cdot u$, and using summation by parts (10.17) leads to:

$$\begin{aligned}\langle \delta_t \cdot u, \delta_{tt} u \rangle_{\mathbb{Z}^2} &= \gamma^2 \langle \delta_t \cdot u, \delta_{\Delta \boxplus} u \rangle_{\mathbb{Z}^2} = \gamma^2 (\langle \delta_t \cdot u, \delta_{xx} u \rangle_{\mathbb{Z}^2} + \langle \delta_t \cdot u, \delta_{yy} u \rangle_{\mathbb{Z}^2}) \\ &= -\gamma^2 (\langle \delta_t \cdot \delta_{x+} u, \delta_{x+} u \rangle_{\mathbb{Z}^2} + \langle \delta_t \cdot \delta_{y+} u, \delta_{y+} u \rangle_{\mathbb{Z}^2})\end{aligned}$$

and, finally, to energy conservation:

$$\delta_{t+} \mathfrak{h} = 0 \quad \text{with} \quad \mathfrak{h} = \mathfrak{t} + \mathfrak{v}$$

and

$$\mathfrak{t} = \frac{1}{2} \|\delta_{t-} u\|_{\mathbb{Z}^2} \quad \mathfrak{v} = \frac{\gamma^2}{2} (\langle \delta_{x+} u, e_{t-} \delta_{x+} u \rangle_{\mathbb{Z}^2} + \langle \delta_{y+} u, e_{t-} \delta_{y+} u \rangle_{\mathbb{Z}^2}) \quad (11.14)$$

The basic steps in the stability analysis are the same as in the 1D case: Beginning from the expression above for the numerical potential energy \mathfrak{v} , and assuming, for simplicity, $h_x = h_y = h$, one may bound it, using inequalities of the form (10.18), as

$$\mathfrak{v} \geq -\frac{\gamma^2 k^2}{8} (\|\delta_{x+} \delta_{t-} u\|_{\mathbb{Z}^2} + \|\delta_{y+} \delta_{t-} u\|_{\mathbb{Z}^2}) \geq -\frac{\gamma^2 k^2}{2h^2} (\|\delta_{t-} u\|_{\mathbb{Z}^2} + \|\delta_{t-} u\|_{\mathbb{Z}^2})$$

and thus

$$\mathfrak{h} \geq \frac{1}{2} \left(1 - \frac{2\gamma^2 k^2}{h^2} \right) \|\delta_{t-} u\|_{\mathbb{Z}^2}^2$$

the energy is non-negative under condition (11.13), obtained through von Neumann analysis.

To arrive at stable numerical boundary conditions, one may proceed as in the continuous case; jumping directly to the case of a discrete quarter plane $\mathcal{D} = \mathbb{Z}^{2,x+y+}$, the energy balance above becomes

$$\delta_{t+} \mathfrak{h} = \mathfrak{b}$$

where

$$\begin{aligned}\mathfrak{b} &= -\gamma^2 \left(\sum_{m=0}^{\infty} h \delta_{t-} u_{0,m} \delta_{x-} u_{0,m} + \sum_{l=0}^{\infty} h \delta_{t-} u_{l,0} \delta_{y-} u_{l,0} \right) \\ &= -\gamma^2 (\{\delta_{t-} u, \delta_{x-} u\}_{(0,\mathbb{Z}^+)} + \{\delta_{t-} u, \delta_{y-} u\}_{(\mathbb{Z}^+, 0)})\end{aligned}$$

For more on these boundary terms, see the discussion on page 300. The lossless numerical conditions which then follow are:

$$u_{0,m \geq 0} = 0 \quad \text{or} \quad \delta_{x-} u_{0,m \geq 0} = 0 \quad \text{and} \quad u_{l \geq 0,0} = 0 \quad \text{or} \quad \delta_{y-} u_{l \geq 0,0} = 0 \quad (11.15)$$

The first in each pair corresponds, naturally, to a Dirichlet condition, and the second to a Neumann condition, as in the continuous case as per (11.7). Given losslessness of the boundary condition (i.e., $\mathfrak{b} = 0$), stability analysis follows as for the case of the scheme defined over \mathbb{Z}^2 . Implementation details of these conditions, as well as the matrix form of the discrete Laplacian have been discussed in §10.2.4. Such conditions are first-order accurate, and so there will be some distorting effect on modal frequencies—through the use of a different inner product, it is possible to arrive at second-order (or centered) boundary conditions which are provably stable—see Problem 11.10, and Programming Exercise 11.6 for some investigation of this.

11.3 Other Finite Difference Schemes

In the case of the 1D wave equation, certain parameterized finite difference schemes have been examined in §6.3, but given the good behavior of the simplest explicit scheme, these variations are of virtually no use—the power of such parameterized methods has been seen to some extent in the

case of bar and stiff string simulation, in §7.1.5 and §7.2.3, and is even more useful in the present case of multidimensional systems such as the 2D wave equation (among others). The chief interest is in reducing numerical dispersion. The 2D wave equation, like its 1D counterpart, is a standard numerical test problem, and, as such, finite difference schemes have seen extensive investigation—see, e.g., [365, 49, 40].

11.3.1 A Parameterized Explicit Scheme

Instead of a five-point Laplacian approximation, as employed in scheme (11.10), one might try a nine-point approximation, of the type discussed in §10.2. This leads to

$$\delta_{tt}u = \gamma^2 \delta_{\Delta\alpha}u = \gamma^2 (\alpha \delta_{\Delta\boxplus}u + (1 - \alpha) \delta_{\Delta\boxtimes}u) \quad (11.16)$$

which reduces to scheme (11.10) when $\alpha = 1$. The computational stencil is, obviously, more dense in this case than for the simple scheme (11.10)—see Figure 11.4(b). Simplified forms are possible involving less computation, as in the case of scheme (11.10), as has been observed in relation to the so-called interpolated waveguide mesh [311, 41]. See Problem 11.11.

Using von Neumann analysis, it is straightforward to show that the stability conditions for this scheme are

$$\alpha \geq 0 \quad \lambda \leq \min(1, \frac{1}{\sqrt{2\alpha}}) \quad (11.17)$$

See Problem 11.12. The dispersion characteristics of this scheme depend quite heavily on the choice of α , and, as one might expect, for intermediate values of this parameter over the allowable range $\alpha \in [0, 1]$, the dispersion is far closer to isotropic—a desirable characteristic, given that the wave equation itself exhibits such behavior. Through trial and error, optimization strategies, or Taylor series analysis (see Problem 10.3) one may find particularly good behavior when α is between 0.6 and 0.8, as illustrated in the plot of relative phase velocity in Figure 11.4(b). The behavior of this scheme is clearly more isotropic than that of (11.10), but numerical dispersion still persists. See also the comparison among modal frequencies generated by the various schemes discussed here in Table 11.1.

Such a choice may be justified, again, by looking at computational complexity (see §7.1.5 for similar analysis in the case of the ideal bar). For a surface of unit area, and when the stability bound above is satisfied with equality, the number of degrees of freedom will be

$$N_{fd} = \frac{2}{h^2} = \frac{2f_s^2}{\gamma^2 \min(1, 1/2\alpha)}$$

and equating this with the number of degrees of freedom in a modal representation, one arrives at a choice of $\alpha = 2/\pi = 0.637$.

11.3.2 A Compact Implicit Scheme

A family of compact implicit schemes for the 2D wave equation is given by

$$\delta_{tt}u = \gamma^2 \left(1 + \frac{k^2(1 - \theta)}{2} \delta_{tt} \right) \delta_{\Delta\alpha}u \quad (11.18)$$

This scheme depends on the free parameters θ , as well as α through the use of the nine-point discrete Laplacian operator $\delta_{\Delta\alpha}$.

von Neumann analysis, though now somewhat more involved, again allows fairly simple stability

Table 11.1: Comparison among modal frequencies of the 2D wave equation, defined over a square, under fixed conditions, with $\gamma = 1000$, and modal frequencies (as well as their cent deviations from the exact frequencies) of the simple explicit scheme (11.10), the parameterized explicit scheme (11.16) with $\alpha = 2/\pi$, and the implicit scheme (11.18), with $\alpha = 2/\pi$ and $\theta = 1.2$, with a sample rate $f_s = 16000$ Hz, and where λ is chosen so as to satisfy the stability condition in each case as close to equality as possible.

Mode number	Exact Freq.	Explicit		Nine-pt. Explicit		Implicit	
		Freq.	Cent Dev.	Freq.	Cent Dev.	Freq.	Cent Dev.
(1,1)	707.1	707.0	-0.3	706.3	-2.0	707.1	-0.1
(1,2)	1118.0	1114.0	-6.2	1114.9	-4.8	1118.0	0.0
(2,2)	1414.2	1413.1	-1.3	1407.6	-8.1	1413.4	-1.0
(1,4)	2061.6	2009.2	-44.5	2042.7	-15.9	2058.8	-2.2
(3,3)	2121.3	2117.5	-3.1	2098.7	-18.5	2115.7	-4.6

conditions on the free parameters and λ :

$$\alpha \geq 0 \quad \theta \text{ unconstrained} \quad \begin{cases} \lambda \leq \sqrt{\frac{\min(1,1/(2\alpha))}{\sqrt{(2\theta-1)}}}, & \theta > \frac{1}{2} \\ \lambda \text{ unconstrained} & \theta \leq \frac{1}{2} \end{cases} \quad (11.19)$$

See Problem 11.13. Under judicious choices of α and θ , an excellent match to the ideal phase velocity may be obtained over nearly the entire range of wavenumbers—see Figure 11.4(c). This good behavior can also be seen in the numerical modal frequencies of this scheme, which are very close to exact values—see Table 11.1. Such is the interest in compact implicit schemes—very good over-all behavior, at the additional cost of sparse linear system solutions, without unpleasant side-effects such as complex boundary termination. An even more general compact family of schemes is possible—see Problem 11.14.

In this case, as in 1D, a vector-matrix representation is necessary. Supposing that the problem is defined over the finite rectangular domain $\mathcal{D} = \mathbb{U}_{N_x, N_y}^2$, and referring to the discussion in §10.2.4, scheme (11.18) may be written as

$$\mathbf{A}\mathbf{u}^{n+1} + \mathbf{B}\mathbf{u}^n + \mathbf{A}\mathbf{u}^{n-1} = 0 \quad (11.20)$$

where here, \mathbf{u}^n is a vector consisting of the consecutive vertical strips of the 2D grid function $u_{l,m}^n$ laid end-to-end (each such strip will consist of $N_y - 1$ values in the case of Dirichlet conditions, and $N_y + 1$ values for Neumann conditions). The matrices \mathbf{A} and \mathbf{B} may be written as

$$\mathbf{A} = \mathbf{I} - \frac{\gamma^2 k^2 (1 - \theta)}{2} \mathbf{D}_{\Delta\alpha} \quad \mathbf{B} = -2\mathbf{I} - \gamma^2 k^2 \theta \mathbf{D}_{\Delta\alpha}$$

where $\mathbf{D}_{\Delta\alpha}$ is a matrix operator corresponding to $\delta_{\Delta\alpha}$. See Programming Exercise 11.7.

11.3.3 Further Varieties

Beyond the two families of schemes presented here, there are of course many other varieties—further properties of parameterized schemes for the 2D wave equation are detailed elsewhere [40, 207], and other schemes are discussed in standard texts [341]. In musical acoustics, finite difference schemes for the wave equation in 2D and 3D have also been employed in detailed studies of wind instrument bores, sometimes involving more complex coordinate systems—see, e.g., [253, 254, 257].

11.4 Digital Waveguide Meshes

The extension of digital waveguides to multiple dimensions for sound synthesis applications was first undertaken by van Duyne and Smith in the mid 1990s [383, 384, 385]. It has continued to see a fair amount of activity in sound synthesis and artificial reverberation applications—see the comments and references in §1.2.3. Most interesting was the realization by van Duyne and others of the association with finite difference schemes [383, 41]. Waveguide meshes may be viewed as acoustic analogues to similar scattering structures which appear in electromagnetic simulation, such as the transmission line matrix method (TLM) [181, 83, 173].

A regular Cartesian mesh is shown in Figure 11.5(a). Here, each box labelled **S** represents a four-port parallel scattering junction. A scattering junction at location $x = lh, y = mh$ is connected to its four neighbors on the grid by four bidirectional delay lines, or waveguides, each of a single sample delay (of k seconds, where $f_s = 1/k$ is the sample rate). The signals, or wave variables impinging on a given scattering junction at grid location l, m at time step n from a waveguide from the north, south, east and west are written as $u_{l,m}^{n,(+),N}$, $u_{l,m}^{n,(+),S}$, $u_{l,m}^{n,(+),E}$, and $u_{l,m}^{n,(+),W}$, respectively, and those exiting as $u_{l,m}^{n,(-),N}$, $u_{l,m}^{n,(-),S}$, $u_{l,m}^{n,(-),E}$ and $u_{l,m}^{n,(-),W}$. The scattering operation at a given junction may be written as

$$u_{l,m}^n = \frac{1}{2} \left(u_{l,m}^{n,(+),N} + u_{l,m}^{n,(+),S} + u_{l,m}^{n,(+),E} + u_{l,m}^{n,(+),W} \right) \quad (11.21)$$

$$u_{l,m}^{n,(-),\bullet} = -u_{l,m}^{n,(+),\bullet} + u_{l,m}^n \quad (11.22)$$

Here, $u_{l,m}^n$ is the junction variable (often referred to as a junction pressure, and written as p in room acoustics applications). Shifting in digital waveguides themselves can be written as

$$u_{l,m}^{n,(+),N} = u_{l,m+1}^{n-1,(-),S} \quad u_{l,m}^{n,(+),S} = u_{l,m-1}^{n-1,(-),N} \quad u_{l,m}^{n,(+),E} = u_{l+1,m}^{n-1,(-),W} \quad u_{l,m}^{n,(+),W} = u_{l-1,m}^{n-1,(-),E} \quad (11.23)$$

The scattering and shifting operations are the basis of all wave-based numerical methods, including, in addition to digital waveguides, wave digital filter methods, as well as the transmission line matrix method mentioned above. Numerical stability for an algorithm such as the above is obvious: the shifting operations clearly cannot increase any norm of the state, in terms of wave variables, and the scattering operation corresponds to an orthogonal (i.e., l_2 norm-preserving) matrix multiplication.

On the other hand, by applying the scattering and shifting rules above, one may arrive at a recursion in the junction variables $u_{l,m}^n$, which is none other than scheme (11.10), with $\lambda = \gamma k/h = 1/\sqrt{2}$ —see Problem 11.15. Notice, however, that the finite difference scheme requires two units of memory per grid point, whereas in the wave implementation, five are necessary (i.e., in order to hold the waves impinging on a junction at a given time step, as well as the junction variable itself). Furthermore, the mesh requires eight arithmetic operations (four in order to form the junction variable, and four in order to perform scattering), whereas the finite difference scheme requires five. Thus the efficiency advantage of the waveguide in 1D, based around the use of delay lines, does not carry over to the multidimensional case. Indeed, the finite difference scheme computes an identical solution, at roughly half the cost. Still, the structural robustness of the waveguide mesh is a very desirable property—termination of a mesh structure using passive filtering blocks (thus ensuring stability) can be a nice alternative to the more involved energy analysis tools described here, though one must beware the temptation to extend such results to more complex systems. This mesh structure may be extended, through the addition of an extra “self-loop” at each junction, in order

to correspond directly to scheme (11.10), for any allowable value of λ [41]. Other more commonly-seen extensions include different tilings of 2D and 3D space, involving, e.g., hexagonal, triangular or tetrahedral grids [385, 28], which also correspond to well-known finite difference schemes [41]. Such non-Cartesian grids have also, of course, been examined in the mainstream simulation literature [419, 362].

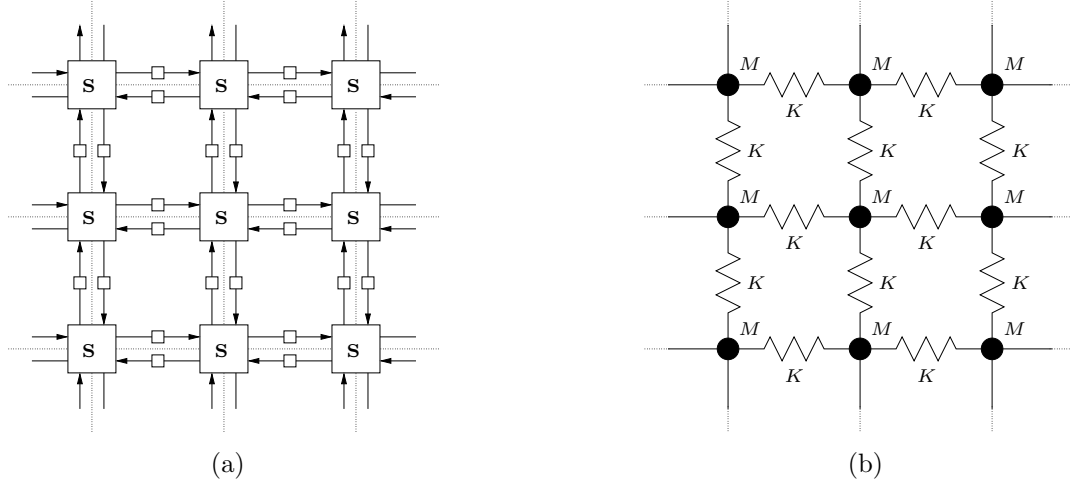


Figure 11.5: (a) A digital waveguide network corresponding to scheme (11.10) for the wave equation, under the special choice of $\lambda = 1/\sqrt{2}$, and (b), a lumped network corresponding to the same scheme, for any value of λ .

11.5 Lumped Mass-spring Networks

A regular lumped network of masses and springs also, not surprisingly, may be viewed in terms of the same underlying finite difference scheme; the manipulations are very similar to the case of the 1D wave equation, as discussed in §6.1.1. It may also, of course, be used as a starting point for a derivation of the 2D wave equation—see, e.g., [114]. 2D lumped structures simulating membranes appear as components in, e.g., the TAO synth environment [266].

Suppose that, as shown in Figure 11.5(b), the network consists of a regularly spaced array of masses M , located at positions $x = lh, y = mh$, and constrained to move vertically (i.e., in and out of the plane array), with displacement indicated by $u_{l,m}(t)$. Each is connected to neighboring masses by springs of stiffness K , and the force exerted on the mass l, m by its neighbors to the north and east are indicated by $f_{l,m+1/2}$ and $f_{l+1/2,m}$, respectively.

The equation of motion for a single mass will be

$$M \frac{d^2 u_{l,m}}{dt^2} = f_{l,m+1/2} - f_{l,m-1/2} + f_{l+1/2,m} - f_{l-1/2,m}$$

with

$$f_{l,m+1/2} \approx K(u_{l,m+1} - u_{l,m}) \quad f_{l+1/2,m} \approx K(u_{l+1,m} - u_{l,m})$$

Just as in 1D, these two definitions coalesce as

$$M \frac{d^2 u_{l,m}}{dt^2} = K(u_{l,m+1} + u_{l,m-1} + u_{l+1,m} + u_{l-1,m} - 4u_{l,m})$$

Discretizing the above system of ODEs with a second time difference δ_{tt} leads immediately to scheme (11.10) for the 2D wave equation, with $\gamma = h\sqrt{K/M}$.

11.6 Modal Synthesis

One of the interesting (and attractive) things about modal synthesis is that, once one has determined the modal frequencies, and the weighting coefficients, the form of the algorithm is completely insensitive to problem dimensionality—all one is doing is summing sine waves, or, more generally, damped sine waves. Modal synthesis for 2D objects such as plates has been developed by various researchers, and membrane- and plate-like objects are components within the Modalys/MOSAIC synthesis environment developed at IRCAM [241].

Consider the case of the 2D wave equation, defined over the unit area rectangle of aspect ratio ϵ , $\mathcal{D} = \mathbb{U}_\epsilon^2$. Again, just as in 1D (see §6.1.11), once one has derived a set of modal functions $U_m(x, y)$ ordered according to some index m , where the m th modal frequency is ω_m , the modal decomposition is of the form:

$$u(x, y, t) = \sum_m U_m(x, y)\Phi_m(t) \quad \text{with} \quad \frac{d^2\Phi_m(t)}{dt^2} = -\omega_m^2 \Phi_m(t)$$

It is useful to order the modes such that $\omega_m \geq \omega_{m'}$ when $m \geq m'$. (In general, the 2D modal functions cannot be consistently ordered according to two indices except for in regular geometries such as the rectangle and circle, and under particular boundary conditions; for the rectangle, Dirichlet or Neumann conditions at all edges are among these, and one may instead use functions $U_{p,q}(x, y)$ indexed according to p and q as described in §11.1.3.)

This form is now suitable for discretization along the lines presented in Chapter 3. For each SHO in the set above, one could use a simple scheme such as (3.12), but there is no reason not to use the exact scheme (3.39) at sample rate $f_s = 1/k$, for some time step k :

$$u^n(x_o, y_o) = \sum_{m=1}^{N_m/2} U_m(x_o, y_o)\Phi_m^n \quad \Phi_m^{n+1} = 2\cos(\omega_m k)\Phi_m^n - \Phi_m^{n-1} \quad \text{for } m = 1, \dots, N_m/2 \quad (11.24)$$

Here x_o, y_o are the readout coordinates, and N_m , the number of degrees of freedom should be chosen such that $\omega_{N_m/2} \leq \pi f_s$, to avoid aliasing. For an initial value problem, the variables Φ_m must be initialized using Fourier expansion coefficients of the initializing distribution—see Programming Exercise 11.8 for more details.

It is instructive to compare the output of this modal method with that of a finite difference scheme, such as (11.10)—see Figure 11.6, in which time responses for the two methods are plotted together, in the cases of plucked initial conditions of (a) wide and (b) narrow spatial extent. For the wide excitation, which excites mainly the lower modes, the two responses are nearly identical; but in the case of the narrow excitation, numerical dispersion effects of the finite difference scheme, leading to “ringing” of sharp transients (due to reflections) in the signal are clearly in evidence. For the modal method, no such dispersion is evident, and transients remain well-localized. On the other hand, as this dispersion is only an issue at high frequencies, it is questionable whether it is in fact audible—the reader may wish to experiment with the two methods to this end.

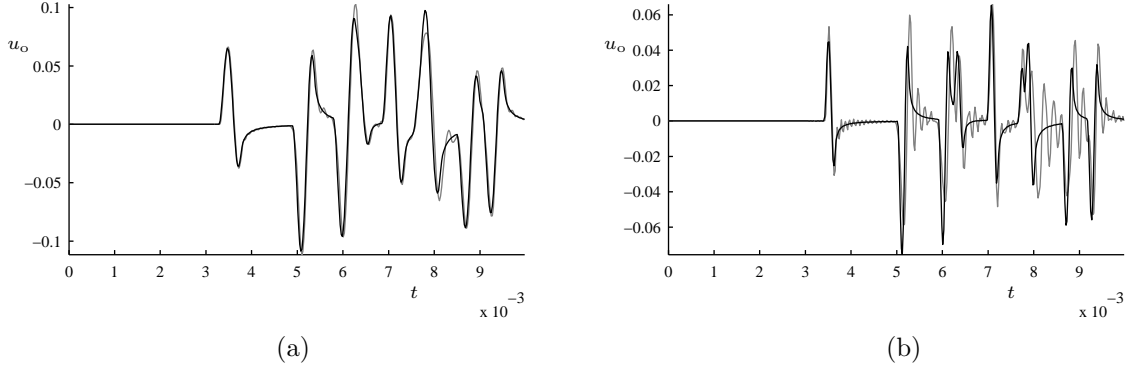


Figure 11.6: Comparison between modal synthesis output (in black), using scheme (11.24) and that of finite difference scheme (11.10) (in grey), for the 2D wave equation, with $\gamma = 200$, and aspect ratio $\epsilon = 1$. The system is subjected to a “plucked” initial condition of the form of a raised 2D cosine, of amplitude 1, centered at $x = 0.3$, $y = 0.3$, of half-width 0.1 in (a), and a narrower distribution of half-width 0.05, in (b). In both cases, output is produced at 44.1 kHz, and read from the position $x_o = 0.8$, $y_o = 0.8$.

11.7 Finite Difference Schemes in Radial Coordinates

The 2D wave equation defined over a circular region is a good starting point for drum models. Here, due to the geometry, if one is interested in pursuing a finite difference synthesis approach, radial coordinates are convenient. The wave equation in radial coordinates, using the form of the Laplacian given at right in (10.2), is as follows:

$$u_{tt} = \gamma^2 \left(\frac{1}{r} (ru_r)_r + \frac{1}{r^2} u_{\theta\theta} \right)$$

The equation is assumed defined over the unit circle $\mathcal{D} = \mathbb{U}_o^2$, and scaled such that, if the physical wave speed is c , and the radius is R , $\gamma = c/R$. Energy analysis leads to the usual expression for energy conservation, i.e.,

$$\frac{d\mathfrak{H}}{dt} = \mathfrak{B}$$

with

$$\mathfrak{T} = \frac{1}{2} \|u_t\|_{\mathbb{U}_o^2}^2 \quad \mathfrak{V} = \frac{\gamma^2}{2} \left(\|u_r\|_{\mathbb{U}_o^2}^2 + \|u_\theta/r\|_{\mathbb{U}_o^2}^2 \right) \quad \mathfrak{B} = \gamma^2 \{u_t, u_r\}_{(1,[0,2\pi))}$$

(See §10.1.5 for information on integration by parts in radial coordinates.) Clearly, the conditions $u = 0$ or $u_r = 0$ at the outer rim of the circle lead to losslessness.

11.7.1 An Explicit Finite Difference Scheme

An obvious choice of explicit difference scheme (and one the reader is advised against using—read on) is the following:

$$\delta_{tt} u = \gamma^2 \delta_{\Delta_o} u \tag{11.25}$$

where the discrete Laplacian $\delta_{\Delta\circ}$ is as defined in (10.23), with the exception of at the center point, where the definition (10.24) is used. The update form of this scheme, when $l > 0$, is

$$\begin{aligned} u_{l,m}^{n+1} = & 2u_{l,m}^n - u_{l,m}^{n-1} + \frac{\gamma^2 k^2 \mu_r + r_l}{r_l h_r^2} u_{l+1,m}^n - \frac{2\gamma^2 k^2}{h_r^2} u_{l,m}^n + \frac{\gamma^2 k^2 \mu_r - r_l}{r_l h_r^2} u_{l-1,m}^n \\ & + \frac{\gamma^2 k^2}{r_l^2 h_\theta^2} (u_{l,m+1}^n - 2u_{l,m}^n + u_{l,m-1}^n) \end{aligned}$$

Here, the subscripts l and m refer to grid points, of spacing h_r and h_θ , in the radial and angular coordinate, respectively; the index m is taken modulo N_θ , where $h_\theta = 2\pi/N_\theta$. At the central grid point $l = 0$, the update is

$$u_{0,0}^{n+1} = 2u_{0,0}^n - u_{0,0}^{n-1} + \frac{4\gamma^2 k^2}{N_\theta h_r^2} \sum_{m=0}^{N_\theta-1} (u_{1,m}^n - u_{0,0}^n)$$

Energy Analysis and Numerical Boundary Conditions

von Neumann analysis is not available in a direct form in order to determine stability conditions in radial coordinates, but energy methods remain viable. One must, however, take special care with regard to the center point. To this end, take the inner product with $\delta_t \cdot u$ over the region $\overline{\mathbb{U}}_{\circ, N_r, N_\theta}^2$, consisting of the grid locations $l = 1, \dots, N_r$, $m = 0, \dots, N_\theta - 1$, and employ the summation by parts identity (10.27):

$$\begin{aligned} \langle \delta_t \cdot u, \delta_{tt} u \rangle_{\overline{\mathbb{U}}_{\circ, N_r, N_\theta}^2} &= \gamma^2 \langle \delta_t \cdot u, \delta_{\Delta\circ} u \rangle_{\overline{\mathbb{U}}_{\circ, N_r, N_\theta}^2} \\ &= -\gamma^2 \langle \delta_t \cdot \delta_r \cdot u, \frac{\mu_r - r}{r} \delta_r \cdot u \rangle_{\overline{\mathbb{U}}_{\circ, N_r, N_\theta}^2} - \gamma^2 \langle \delta_t \cdot \delta_\theta \cdot u, \frac{1}{r^2} \delta_\theta \cdot u \rangle_{\overline{\mathbb{U}}_{\circ, N_r, N_\theta}^2} \\ &\quad + \mathfrak{b} - \frac{\gamma^2 \pi h_r^2}{4} \delta_t \cdot u_{0,0} \delta_{\Delta\circ} u_{0,0} \end{aligned}$$

This may be written, as usual, as $\delta_{t+}\mathfrak{h} = \mathfrak{b}$, where $\mathfrak{h} = \mathfrak{t} + \mathfrak{v}$, and

$$\begin{aligned} \mathfrak{t} &= \frac{1}{2} \|\delta_t \cdot u\|_{\overline{\mathbb{U}}_{\circ, N_r, N_\theta}^2}^2 + \frac{\pi h_r^2}{8} (\delta_t \cdot u_{0,0})^2 \\ \mathfrak{v} &= \frac{\gamma^2}{2} \langle \delta_r \cdot u, \frac{\mu_r - r}{r} e_t \cdot \delta_r \cdot u \rangle_{\overline{\mathbb{U}}_{\circ, N_r, N_\theta}^2} + \frac{\gamma^2}{2} \langle \delta_\theta \cdot u, \frac{1}{r^2} e_t \cdot \delta_\theta \cdot u \rangle_{\overline{\mathbb{U}}_{\circ, N_r, N_\theta}^2} \\ \mathfrak{b} &= \gamma^2 \{ \delta_t \cdot u, \mu_r + r \delta_r \cdot u \}_{(N_r, [0, N_\theta - 1])} \end{aligned}$$

Notice in particular the appearance of a component of the kinetic energy at the central grid location. Clearly, \mathfrak{t} is non-negative, and for stability it suffices to bound \mathfrak{v} in terms of it. To this end, one may write, using the bounds (10.28),

$$\begin{aligned} \mathfrak{v} &\geq -\frac{\gamma^2 k^2}{8} \left\| \sqrt{\frac{\mu_r - r}{r}} \delta_r \cdot \delta_t \cdot u \right\|_{\overline{\mathbb{U}}_{\circ, N_r, N_\theta}^2}^2 - \frac{\gamma^2 k^2}{8} \left\| \frac{1}{r} \delta_\theta \cdot \delta_t \cdot u \right\|_{\overline{\mathbb{U}}_{\circ, N_r, N_\theta}^2}^2 \\ &\geq -\frac{\gamma^2 k^2}{2h_r^2} \|\delta_t \cdot u\|_{\overline{\mathbb{U}}_{\circ, N_r, N_\theta}^2}^2 - \frac{\pi \gamma^2 k^2}{4} (\delta_t \cdot u_{0,0})^2 - \frac{\gamma^2 k^2}{2h_\theta^2} \left\| \frac{1}{r} \delta_t \cdot u \right\|_{\overline{\mathbb{U}}_{\circ, N_r, N_\theta}^2}^2 \end{aligned}$$

Now that \mathfrak{v} has been bounded in terms of the grid function $\delta_t \cdot u$, it is possible to extract the following conditions for non-negativity of \mathfrak{h} :

$$\frac{\gamma^2 k^2}{h_r^2} \left(1 + \frac{1}{h_\theta^2} \right) \leq 1 \quad h_r \geq \sqrt{2} \gamma k \quad (11.26)$$

The first condition arises from examination of the grid function over interior points, and the second for the central point; normally, the first condition above is much stronger than the second. These

serve as stability conditions for scheme (11.25), as long as lossless or dissipative boundary conditions are applied; notice that \mathfrak{b} vanishes when

$$u_{N_r,m} = 0 \quad \text{or} \quad \delta_r + u_{N_r,m} = 0$$

These conditions correspond to Dirichlet and Neumann conditions at the outer edge of the circle.

In general, h_r and h_θ are independent in the above scheme, and there is thus an extra degree of freedom when these quantities are subject to the stability condition (11.26). For some guidance as to how to proceed in choosing these, see Problem 11.16.

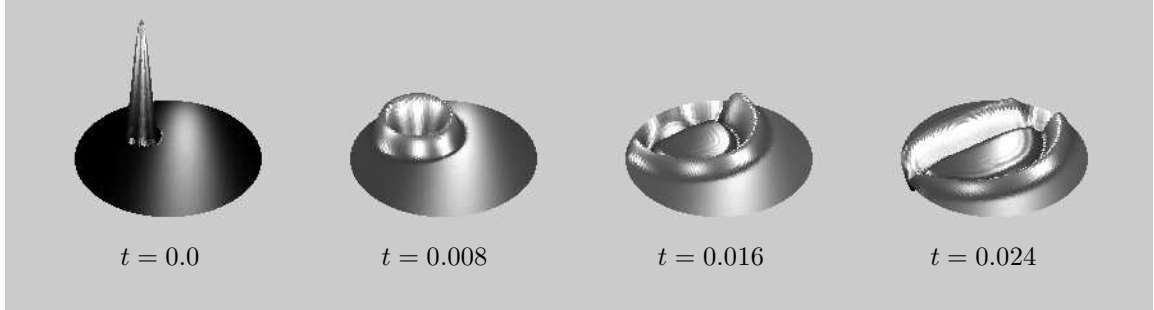


Figure 11.7: Snapshots of the time evolution of the solution to the 2D wave equation, with $\gamma = 40$, defined over a unit circle with fixed boundary conditions, at times as indicated. Scheme (11.25) is employed, at a sample rate of 44100 Hz, and is initialized with a raised cosine distribution.

Numerical Bandwidth

The behavior of this scheme is, at first sight, as expected—see Figure 11.7, which illustrates the time evolution of a plucked initial condition. Upon inspection of a typical spectral output, however, it is clear that all is not well, as in Figure 11.8(a). The output is severely bandlimited, in some cases to as low as 1/8 the sample rate. Furthermore, the components which do appear suffer from extreme numerical dispersion. This scheme, though it has been employed by various authors in an analysis setting, is probably not suitable for synthesis, except at extremely high sample rates—clearly, more work at the stage of scheme design is necessary.

11.7.2 A Parameterized Scheme

Given the difficulties mentioned above, one might wonder whether one can do better with a parameterized implicit scheme—and indeed one can. Here is a simple form:

$$(1 + \gamma^2 k^2 \alpha \delta_{\Delta_0}) \delta_{tt} u = \gamma^2 \delta_{\Delta_0} u \quad (11.27)$$

The new free parameter is α , and the scheme reduces to (11.25) when $\alpha = 0$. In vector-matrix form, the scheme update looks like

$$\mathbf{A}\mathbf{u}^{n+1} + \mathbf{B}\mathbf{u}^n + \mathbf{A}\mathbf{u}^{n-1} = \mathbf{0}$$

where

$$\mathbf{A} = \mathbf{I} + \gamma^2 k^2 \alpha \mathbf{D}_{\Delta_0} \quad \mathbf{B} = -2\mathbf{I} - (2\alpha + 1)\gamma^2 k^2 \mathbf{D}_{\Delta_0}$$

Here, \mathbf{u}^n is a vector consisting of the value $u_{0,0}^n$ followed by a concatenation of the successive concentric rings of the grid function $u_{l,m}^n$ for $l = 1, 2, \dots$, and \mathbf{D}_{Δ_0} is the Laplacian operator in matrix form.

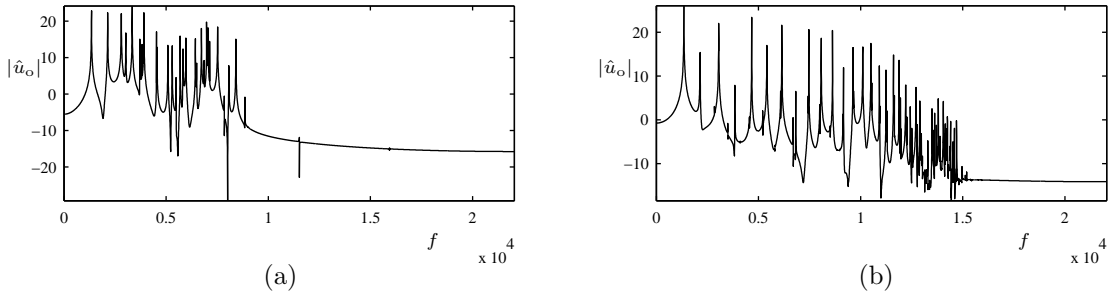


Figure 11.8: *Typical output spectra for radial finite difference schemes for the 2D wave equation defined over the unit area circle, with $\gamma = 2000$, under fixed boundary conditions at the outer edge. In (a), scheme (11.25) is employed, and in (b), the parameterized scheme (11.27), with $\alpha = -0.248$. In both cases, the sample rate is 44100 Hz, and $h_\theta/h_r \approx 6$.*

The stability condition for scheme (11.27) must be adjusted from (11.26) to

$$\frac{4(\alpha + 1/4)\gamma^2 k^2}{h_r^2} \left(1 + \frac{1}{h_\theta^2}\right) \leq 1 \quad (11.28)$$

when $\alpha \geq -1/4$ (otherwise the scheme is unconditionally stable).

For certain ranges of the parameter α , particularly when α is slightly above $-1/4$, this scheme exhibits markedly better performance, in terms of bandwidth, and numerical dispersion, though even under optimal conditions, it performs less well than schemes in Cartesian coordinates—see Figure 11.8(b). For some exploration of this family of difference schemes, see Programming Exercise 11.9.

11.8 Comparative Study II

The case of the 2D wave equation is somewhat more representative of the relative merits of the various synthesis methods than its counterpart in 1D. This section continues the previous discussion of computational issues associated with various different synthesis methods with regard to the 1D wave equation in §6.6.

The most important observation that one can make is that the efficiency advantage of digital waveguides does not extend to 2D—indeed, any solution produced by a digital waveguide mesh structure can always be more efficiently calculated using an associated finite difference scheme. Similarly, lumped network representations also can be viewed, as in 1D, as finite difference schemes². Thus the main comparison here will be between difference schemes, and modal methods, which remain distinct in the 2D case.

With regard to accuracy, modal methods are, under fairly strict conditions on problem geometry and boundary conditions, and if properly employed, extremely accurate. Finite difference methods suffer from a greater degree of numerical dispersion (and thus mode detuning) than in the 1D case, where an exact FD solution is available. In addition, there is the added issue of numerical anisotropy. A more interesting question, and one which is too involved to address here, is the perceptual relevance

²In fact, it is generally only easy to associate mesh structures and lumped networks with simple explicit schemes such as (11.10); making this association with more refined designs, such as implicit schemes is very strenuous, and thus there is a real advantage to a finite difference framework, from a design perspective.

of such dispersion effects. More elaborate schemes may be designed which minimize such dispersive effects, at the expense of higher computational cost and algorithm complexity.

In terms of memory use, modal methods and difference schemes are roughly comparable. For a unit area domain, and for a given wave speed γ , and sampling rate f_s , the number of memory locations necessary to store state in a modal method will be twice the number of modes in the range $[0, f_s/2]$, or, from (11.9), $\pi f_s^2 / 2\gamma^2$. For a typical difference scheme, the stability condition leads to a minimum grid spacing which again determines the number of memory locations. For scheme (11.10), for example, which is a two-step scheme, the memory requirement will be f_s^2 / γ^2 , which is of the same order as for a modal method (less, in fact, though this apparent advantage is illusory once numerical dispersion effects are taken into account). As in 1D, however, if the modal shapes are not expressible in closed form, then one is again faced with the extra tasks of (a) computing the mode shapes, through the solution of a potentially large eigenvalue problem and reintroducing numerical inaccuracy, and possibly (b) storing them. For even moderately low values of γ , and at audio sample rates, this is, in 2D, a daunting task, as full storage of $\pi f_s^2 / 2\gamma^2$ modal shapes, with sufficient spatial resolution amounts to storage on the order of f_s^4 / γ^4 units, which can be very large indeed. On the other hand, in a modal approach, it is relatively easy to discard higher modal frequencies and thus reduce computational cost; in an FD schemes, this can be done by increasing the grid spacing away from that prescribed by the stability bound, at the expense of introducing serious dispersion effects. In either case, however, the best way to reduce computational complexity is to simply work at a reduced sample rate, in which case the two methods are again on an equal footing in terms of computational cost.

The operation count/time step scales, as in 1D, with the number of degrees of freedom for a given γ and f_s . Calling this number N (as mentioned above, it is comparable for FD schemes and modal methods). A modal method requires, in the lossless case, $2N$ additions/multiplications/time step, whereas for a finite difference scheme, the number of operations depends on the sparsity of the scheme, as αN , for some (low) scheme-dependent parameter α . For the scheme (11.10), $\alpha = 7$, but it will be larger for interpolated explicit schemes such as (11.16), and even larger if an implicit method such as (11.18) is used.

The issues of precomputation, stability and generating output may be addressed in a manner similar to those of the 1D case.

For more general comments on the relative merits of these methods, see the closing remarks in §14.1.

11.9 Problems

Problem 11.1 Consider the 2D wave equation, defined over the half-plane $\mathbb{R}^{2,x+}$, and recall the expression for the energy balance given in (11.5) and (11.6):

$$\frac{d\mathfrak{H}}{dt} = -\gamma^2 \{u_x, u_t\}_{(0,\mathbb{R})}$$

Suppose the boundary condition, at $x = 0$, is given as follows:

$$u_t = \alpha u_x + \phi u_{xt} + \epsilon m \quad \text{with} \quad m_t = u_x(0, y, t)$$

and where the constants α , ϕ and ϵ are non-negative. Such an energy-storing condition may be used in order to model effects of mass, stiffness, and loss at a wall in the context of room acoustics [207]. Show that the above condition implies that the energy balance becomes:

$$\frac{d}{dt} (\mathfrak{H} + \mathfrak{H}_b) = -\mathfrak{Q}$$

where $\mathfrak{H}_b \geq 0$ and $\mathfrak{Q} \geq 0$. Thus the total energy $\mathfrak{H} + \mathfrak{H}_b$ remains non-negative, and monotonically decreasing.

Problem 11.2 Extend the energy analysis of the 2D wave equation to the case for which the domain \mathcal{D} is a unit area rectangle $\mathbb{U}_\epsilon^2 = [0, \sqrt{\epsilon}] \times [0, 1/\sqrt{\epsilon}]$. Show that the energy balance (11.5) holds as before, where the boundary term \mathfrak{B} is given by

$$\mathfrak{B} = \gamma^2 (\{u_x, u_t\}_{(\sqrt{\epsilon}, [0, 1/\sqrt{\epsilon}])} - \{u_x, u_t\}_{(0, [0, 1/\sqrt{\epsilon}])} + \{u_y, u_t\}_{([0, \sqrt{\epsilon}], 1/\sqrt{\epsilon})} - \{u_y, u_t\}_{([0, \sqrt{\epsilon}], 0)})$$

Problem 11.3 Considering the 2D wave equation defined over a square of unit area, under fixed boundary conditions, the frequency of mode (p, q) is given by (11.8), or, in Hertz,

$$f_{p,q} = \frac{\gamma}{2} \sqrt{p^2 + q^2}$$

for $p, q > 0$.

(a) Show that $f_{p,q}$ corresponds to the distance between the origin and the point of coordinates $(p\gamma/2, q\gamma/2)$ in a plane.

(b) Find the density (per unit area) of such points in the plane.

(c) The total number of modes of frequency less than or equal to $f_s/2$ may be represented as the number of modal points contained within a quarter circle of radius $f_s/2$ in the plane. Given the expression obtained above for the density of such points, find the approximate value for $N_m(f_s/2)$ given in (11.9). (N_m is twice the number of modes over this band.)

(d) Show that this expression remains unchanged, in the limit of high f_s , if the 2D wave equation is defined instead over a arbitrary rectangle of unit area, i.e., over \mathbb{U}_ϵ^2 .

(e) Show that this expression remains unchanged, in the limit of high f_s , in the case of free boundary conditions at all edges of the rectangular domain.

Problem 11.4 (3D Wave Equation I.) Most key components of musical instruments, such as strings, bars, plates, membranes, and acoustic tubes are well-modeled in 1D or 2D. There are, however, occasions when one might be interested in full 3D modeling—this comes up when one is faced with, say, the interior of an instrument body, such as an acoustic guitar or kettle drum, whose dimensions are not small in any coordinate direction. Another application, slightly removed from synthesis, is room acoustics simulation, of interest in developing physical artificial reverberation algorithms. The equation to be solved in these cases is invariably the 3D wave equation, written in terms of time t , coordinates x, y and z and wave speed c as

$$u_{tt} = c^2 \Delta u = c^2 (u_{xx} + u_{yy} + u_{zz})$$

or, when spatially scaled with reference to a characteristic length L ,

$$u_{tt} = \gamma^2 \Delta u \quad (11.29)$$

with $\gamma = c/L$.

(a) Supposing that the 3D wave equation is defined over a unit cube, under fixed boundary conditions, show that the modal frequencies $\omega_{p,q,r}$ are given by

$$\omega_{p,q,r} = \pi \gamma \sqrt{p^2 + q^2 + r^2}$$

(b) Extend the analysis of Problem 11.3, and show that an expression for the number of degrees of freedom (or twice the number of modes of frequency less than $f_s/2$) is given by

$$N_m(f_s/2) = \frac{\pi f_s^3}{3\gamma^3}$$

(c) Given a typical audio range (i.e., choose $f_s = 44100$ Hz), and for a wave speed $c = 340$ m/s, determine the number of modes necessary to describe the behavior of an object such as a violin, a kettle drum or a large concert hall. (For each, estimate a characteristic length as $L = V^{1/3}$, where V is the total volume enclosed, and thus obtain a rough estimate of $\gamma = c/L$.) Comment on the feasibility of performing simulations using modal methods for each of these cases, keeping in mind the memory available in RAM on typical computers (look this up for your own machine).

Problem 11.5 (Kettledrum I.) Drum modeling always takes as its starting point a membrane model, described by a variant of the 2D wave equation (perhaps involving stiffness—see the next chapter), coupled to a resonator, which is effectively a closed cavity. A detailed model necessarily requires the solution of the 3D wave equation in the body of the resonator, either through a time domain method, or a modal decomposition. (One such study has been carried out, in the case of the kettledrum, by Rhaouti et al. [282].)

Here is a very crude model, proposed early on by Morse [242]. For simplicity, assume an $L \times L$ square membrane, with wave speed c_M , under fixed boundary conditions, coupled to an enclosed volume of air, of density ρ , volume V_0 with wave speed c_0 , and under tension T_0 per unit length applied at the edge. In scaled form, the equation of motion of the membrane is

$$u_{tt} = \gamma^2 \Delta u - \gamma^2 d^2 \int_0^1 \int_0^1 u dx dy \quad \text{for } (x, y) \in \mathbb{U}^2$$

where $\gamma = c_M/L$, and where $d^2 = \rho c_0^2 L^4 / (T_0 V_0)$ is a dimensionless parameter. Such a model, in that the effect of the cavity is averaged over the membrane, is reminiscent of the Kirchhoff-Carrier string model (see §8.1), though here the averaging is linear. One should only expect it to hold for low frequencies.

(a) Assuming a modal solution of the form $u(x, y, t) = e^{j\omega t} \sin(p\pi x) \sin(q\pi y)$, show that the modal frequencies $\omega_{p,q}$ are given by

$$\omega_{p,q}^2 = \gamma^2 \pi^2 (p^2 + q^2) + \frac{\gamma^2 d^2}{pq\pi^2} ((-1)^p - 1)((-1)^q - 1), \quad p, q \geq 1 \quad (11.30)$$

Which modal frequencies are altered with respect to those of the uncoupled wave equation (i.e., when $d = 0$)? Are they raised or lowered?

(b) Show that an expression for the total energy of the membrane coupled to the cavity is given by

$$\mathfrak{H} = \frac{1}{2} \|u_t\|_{\mathbb{U}^2}^2 + \frac{\gamma^2}{2} (\|u_x\|_{\mathbb{U}^2}^2 + \|u_y\|_{\mathbb{U}^2}^2) + \frac{\gamma^2 d^2}{2} (\langle u, 1 \rangle_{\mathbb{U}^2})^2 \quad (11.31)$$

which remains non-negative.

Problem 11.6 Show that scheme (11.10), operating over the infinite domain $\mathcal{D} = \mathbb{Z}^2$, and at the stability limit $\lambda = 1/\sqrt{2}$, may be decomposed into two separate schemes, one operating over values of the grid function $u_{l,m}^n$ for even values of $n + l + m$, and one for odd values. If the scheme is restricted to operate over a finite domain, discuss the effects of various boundary conditions on the ability to obtain such a decomposition.

Problem 11.7 Consider scheme (11.10), but with h_x and h_y not, in general, equal.

(a) Show, from von Neumann analysis, that the stability condition relating k , h_x and h_y becomes

$$\gamma^2 k^2 \leq \frac{h_x^2 h_y^2}{h_x^2 + h_y^2} \quad (11.32)$$

(b) Write the update explicitly in terms of the grid function $u_{l,m}^n$, in a manner similar to that shown in (11.11). How many additions/multiplications are necessary in order to perform the update at a given grid point? Is there a particular choice of k , h_x , and h_y such that computational complexity may be reduced?

Problem 11.8 (3D Wave Equation II.) The direct extension of scheme (11.10) for the 2D wave equation to the 3D wave equation (11.29) is of the following form:

$$\delta_{tt} u = \gamma^2 (\delta_{xx} u + \delta_{yy} u + \delta_{zz} u)$$

Here, $u = u_{l,m,p}^n$ is a 3D grid function representing an approximation to $u(x, y, z, t)$ at $x = lh, y = mh, z = ph, t = nk$. for a time step t and a grid spacing h (assumed uniform in all directions). The spatial difference operators δ_{xx} and δ_{yy} are as in the 2D case, and δ_{zz} is defined, in terms of its action on the grid function u , as $\delta_{zz} u_{l,m,p}^n = \frac{1}{h^2} (u_{l,m,p+1}^n - 2u_{l,m,p}^n + u_{l,m,p-1}^n)$.

(a) Using an extension of either von Neumann analysis or energy methods, show that the stability condition for the scheme will be

$$\frac{\gamma k}{h} \leq \frac{1}{\sqrt{3}}$$

(b) Assuming that the 3D wave equation is defined over a unit volume, and that the stability condition above is satisfied with equality, how does the number of degrees of freedom (twice the number of grid points necessary to fill the domain) depend on γ and the sample rate $f_s = 1/k$? Compare your answer with your calculation of the number of modes in Problem 11.4.

Problem 11.9 (Kettledrum II.)

Consider the following explicit finite difference scheme for the coupled membrane/cavity system given in Problem 11.5:

$$\delta_{tt}u = \gamma^2 \delta_{\Delta} u - \gamma^2 d^2 \langle u, 1 \rangle_{\mathbb{U}_{N,N}^2} \quad \text{over } \mathbb{U}_{N,N}^2$$

where “1” refers to a grid function taking the value unity over the entire domain. Assume fixed boundary conditions, i.e., the grid function u takes on the value zero at the edges of the domain $\mathbb{U}_{N,N}^2$.

(a) Find an expression for the conserved energy of this scheme, by taking an inner product of the scheme with $\delta_t u$ over $\mathbb{U}_{N,N}^2$. It should correspond to (11.31) for the model system.

(b) By ensuring non-negativity of this expression, show that the CFL condition becomes

$$h \geq \gamma k \sqrt{\frac{2}{1 - d^2 \gamma^2 k^2 / 4}} \quad (11.33)$$

For what values of d will this scheme allow such a stability condition? How does the number of degrees of freedom (i.e., the grid size for a given γ and time step k) change with d ? Does this coincide with your analysis of the deviation in modal frequencies with d , in Problem 11.5?

Problem 11.10 Consider scheme (11.10) for the 2D wave equation, defined over the quarter space $\mathcal{D} = \mathbb{Z}^{2,x+y+}$. Assume $h_x = h_y = h$. Instead of the first-order Neumann boundary conditions given as the second of each pair in (11.15), consider the following centered (second-order) conditions:

$$\delta_x \cdot u_{0,m} \geq 0 \quad \delta_y \cdot u_{l,0} \geq 0$$

Such conditions have been introduced earlier in Problem 10.5. Show numerical stability, using energy methods. Recall the use of the primed inner product in the analogous case in 1D, as described on page 143. Here, consider an inner product of the form:

$$\langle f, g \rangle'_{\mathbb{Z}^{2,x+y+}} = \sum_{l=1}^{\infty} \sum_{m=1}^{\infty} h^2 f_{l,m} g_{l,m} + \frac{h^2}{2} \sum_{l=1}^{\infty} f_{l,0} g_{l,0} + \frac{h^2}{2} \sum_{m=1}^{\infty} f_{0,m} g_{0,m} + \frac{h^2}{4} f_{0,0} g_{0,0}$$

Problem 11.11 For the parameterized explicit scheme (11.16) for the 2D wave equation,

(a) Write the update explicitly in terms of the grid function $u_{l,m}^n$, in a manner similar to that shown in (11.11).

(b) For a given value of α , the scheme free parameter, what is the condition on λ such that the scheme update no longer depends on the value of the grid function $u_{l,m}^n$ at the “center point.” Does this condition conflict with the stability condition (11.17) for the scheme? (This case has seen some attention in the literature, as it corresponds to the so-called “interpolated digital waveguide mesh” [311].)

(c) Discuss the significance and ramifications of a choice of λ away from the stability condition, with reference to Rule of Thumb #1, given on page 140.

Problem 11.12 Show that the characteristic polynomial corresponding to the “nine-point” explicit scheme (11.16) is given by

$$z - 2 + 4\lambda^2 (p_x + p_y - 2(1 - \alpha)p_x p_y) + z^{-1}$$

where p_x and p_y are as defined in terms of wavenumber components as in (10.13), and take on values between 0 and 1. The stability condition is thus

$$0 \leq \lambda^2 (p_x + p_y - 2(1 - \alpha)p_x p_y) \leq 1$$

Show that these conditions lead immediately to the stability conditions given in (11.17).

Hint: Begin with the left inequality, and derive a condition on α alone, then use the right inequality to find the condition on λ . (Your result from Problem 10.2 will be of great use here).

Problem 11.13 Show that the characteristic polynomial corresponding to the compact implicit scheme (11.18) is given by

$$z - 2 + \frac{4\lambda^2 (p_x + p_y - 2(1 - \alpha)p_x p_y)}{1 + 2(1 - \theta)\lambda^2 (p_x + p_y - 2(1 - \alpha)p_x p_y)} + z^{-1} = 0$$

where p_x and p_y are again as defined in (10.13), and take on values between 0 and 1. The stability condition is thus

$$0 \leq \frac{\lambda^2 (p_x + p_y - 2(1 - \alpha)p_x p_y)}{1 + 2(1 - \theta)\lambda^2 (p_x + p_y - 2(1 - \alpha)p_x p_y)} \leq 1$$

Show that these conditions lead immediately to the stability conditions given in (11.19).

This is much trickier than the above problem, in that now the function to be bounded is rational rather than polynomial. There are essentially three steps: 1) Find conditions under which the numerator of the expression above is non-negative. 2) Given this condition, find conditions under which the denominator is non-negative. 3) Given the conditions derived in 1) and 2) above, find conditions under which the numerator is less than or equal to the denominator. Your bounds on λ may overlap, depending on the choice of θ and α .

Problem 11.14 Consider the following family of implicit finite difference schemes for the 2D wave equation, generalizing scheme (11.18):

$$(1 + \theta\gamma^2 k^2 \delta_{\Delta\alpha_1}) \delta_{tt} u = \gamma^2 \delta_{\Delta\alpha_2} u$$

This scheme now depends on the parameters θ , α_1 and α_2 —the two nine-point approximations to the Laplacian are distinct. Using von Neumann analysis, find a stability condition for this scheme of the form $\lambda \leq \lambda^*(\theta, \alpha_1, \alpha_2)$.

Problem 11.15 Beginning from the definition of the grid variable $u_{l,m}^{n+1}$ in terms of wave variables, from (11.21), use the scattering operation (11.22) and the shifting operation (11.23) in order to show that the waveguide mesh calculates solutions to the finite difference scheme (11.10), under the special choice of $\lambda = \gamma k/h = 1/\sqrt{2}$.

Problem 11.16 The stability condition for scheme (11.25) for the wave equation in radial coordinates, relating the radial and angular grid spacings h_r and h_θ to the time step k , is given in (11.26). In order to set the grid spacings for a given sample rate, it is useful to set, beforehand, a parameter $q = h_\theta/h_r$. Show that for a given q , a bound on h_r is then

$$h_r^2 \geq \frac{\gamma^2 k^2}{2} \left(1 + \sqrt{1 + \frac{4}{q^2 \gamma^2 k^2}} \right)$$

Given that, in an implementation, the grid spacings must be quantized as $h_r = \frac{1}{N_r}$ and $h_\theta = \frac{2\pi}{N_\theta}$, for integer N_r and N_θ , can you find a stability condition in terms of N_θ and N_r ?

11.10 Programming Exercises

Programming Exercise 11.1 Modify the code implementation of scheme (11.10) for the 2D wave equation given in §A.11, such that the grid spacings h_x and h_y are not the same. Again, the problem is assumed defined over the unit area rectangle \mathbb{U}_ϵ^2 , and with Dirichlet conditions on all four sides. The main question here is the following: given a sample rate $f_s = 1/k$, how are h_x and h_y to be

chosen such that the bound (11.32) is satisfied as close to equality as possible, given the further restriction that $h_x = \sqrt{\epsilon}/N_x$, $h_y = 1/\sqrt{\epsilon}N_y$, for a given ϵ , and for integer N_x and N_y ? Once you have found a solution to this problem, and made the necessary changes to the rest of the code, try comparing the output of your new scheme to that of the scheme with equal grid spacing, for a variety of different choices of the aspect ratio ϵ and the wave speed γ . Under what conditions are these perceptually distinct?

Programming Exercise 11.2 Modify the code implementation of scheme (11.10) for the 2D wave equation given in §A.11, such that the output interpolation location is time-varying (i.e., moving). One simple way of specifying a trajectory is as follows: for a rectangular domain of aspect ratio ϵ , and thus side lengths $\sqrt{\epsilon}$ and $1/\sqrt{\epsilon}$, let the continuous output coordinates x_o and y_o be defined as

$$x_o(t) = \frac{\sqrt{\epsilon}}{2} + A \cos(2\pi f_o t) \quad y_o(t) = \frac{1}{2\sqrt{\epsilon}} + A \sin(2\pi f_o t)$$

Here, f_o is a scan frequency, typically on the order of 1 Hz or less, and A specifies the radius of a circle along which the output location travels (how large can A be?). (This means of obtaining output is similar to so-called scanned synthesis [400]—see also Programming Exercise 6.6, which deals with the 1D case.)

Employ bilinear interpolation at each sampling instant (see §10.2.1 and Programming Exercise 10.1). For which range of values of γ and f_s do you hear truncation effects? Extend your code such that the output is stereo, with each channel drawn from a separate output location, each specified by a given scan frequency and circle radius.

Programming Exercise 11.3 Modify the code implementation in §A.11 such that Neumann conditions are enforced—try both the first-order accurate conditions given in (10.20), and the second-order accurate conditions given in Problem 10.5. Because the solution is now free to drift, you will need to apply some sort of DC-blocking filter to your output signal u_o^n , if it is drawn directly from values computed on the grid. A simple one-zero filter output v_o^n is given by $v_o^n = (u_o^n - u_o^{n-1})/k$, and is equivalent to reading a velocity. Can you hear the difference in the resulting sound between the two types of boundary condition?

Programming Exercise 11.4 (2D Artificial Reverberation.) Now that you have a code implementation of the 2D wave equation under Neumann boundary conditions, it is possible to use it as a crude physical model of a 2D “room,” in order to apply artificial reverberation to an input audio signal. The finite difference scheme will be of the form

$$\delta_{tt}u = \gamma^2 \delta_{\Delta \boxplus} u + J(x_i, y_i)f$$

where $J(x_i, y_i)$ is an input spreading operator acting at the desired source position (x_i, y_i) , as described in §10.2.1—be careful to take these coordinates relative to the side lengths of the domain. In order to do this, first remove the initial condition from the code. Then, read in a mono soundfile (read about Matlab functions for doing this, such as, e.g., `wavread`), which will become $f = f^n$ in the above recursion.

The parameter $\gamma = c/L$ may be used in order to scale the “size” of the virtual reverberant room—do not be surprised if, for particularly low values of γ , the calculation takes quite a while, or if you run into an “out of memory” error. This is a big calculation! In fact, it will be essential for you to use a relatively low audio sample rate (such as 8000 Hz) in order to get the effect of a reasonably sized room in a short calculation. Make sure that your input soundfile is thus properly downsampled before beginning! Also, make sure that the input signal has a zero DC offset before processing—otherwise, your “room” will drift away (think of it as a membrane under free conditions).

You might also wish to generalize the code such that it generates stereo output, by reading from separate locations over the grid.

Programming Exercise 11.5 Modify the code implementation of scheme (11.10) for the 2D wave equation given in §A.11, such that it simulates a membrane coupled to a cavity, as described in Problems 11.5 and 11.9. (This should be a very minor operation!) Make sure that for a given k , γ and d , h is chosen according to the more general stability condition (11.33). Verify, by taking the Fourier transform of the response of the membrane to an impulsive excitation, that the modal frequencies deviate from those of the uncoupled case according to (11.30).

Programming Exercise 11.6 For the scheme (11.10) with $h_x = h_y$, defined over the square $\mathbb{U}_{N,N}^2$, calculate numerical modal frequencies using the first-order accurate Neumann conditions given as the second of each pair in (11.15), applied at all four edges of the domain, and the second-order accurate conditions given in Problem 11.10. In either case, the scheme, in vector-matrix form, will look like

$$\mathbf{u}^{n+1} = 2\mathbf{u}^n - \mathbf{u}^{n-1} + \gamma^2 k^2 \mathbf{D}_{\Delta \boxplus} \mathbf{u}^n$$

where \mathbf{u}^n is the grid function $u_{l,m}^n$ rewritten as a vector (see §10.2.4), and where $\mathbf{D}_{\Delta \boxplus}$ is matrix form of the Laplacian operator, incorporating the particular boundary conditions. The modal frequencies, in Hertz, will be given by $f = (1/\pi k) \sin^{-1}(\gamma k \sqrt{-\text{eig}(\mathbf{D}_{\Delta \boxplus})}/2)$. Assume the sample rate to be $f_s = 44100$ Hz, and $\gamma = 1000$. Produce a sorted list of these frequencies for both types of boundary condition, and compare the first few (say, 20) with the exact frequencies, which are given by

$$f_{p,q} = \frac{\gamma}{2} \sqrt{p^2 + q^2} \quad \text{for } p, q = 0, \dots$$

Programming Exercise 11.7 Implement the two-parameter scheme (11.18) for the 2D wave equation, defined over a rectangular region \mathbb{U}_ϵ^2 , according to the vector-matrix update form (11.20). Assume Dirichlet boundary conditions. In order to do this, you will need a matrix form of the operator $\mathbf{D}_{\Delta \alpha}$ —see Problem 10.4 and Programming Exercise 10.4. In order to perform the update, make use of the standard linear system updating package in Matlab. Compare the computing time required to that of the explicit scheme, which is a special case of scheme (11.18) with $\alpha = \theta = 1$.

In addition, compute the numerical modal frequencies of scheme (11.18) directly as

$$f = \frac{1}{2\pi k} \cos^{-1}(-\text{eig}(\mathbf{A}^{-1} \mathbf{B}))$$

Programming Exercise 11.8 Create a Matlab implementation of modal synthesis for the 2D wave equation, defined over the unit square \mathbb{U}^2 , under fixed, or Dirichlet boundary conditions, and for a plucked initial condition of the form of a 2D raised cosine. Here, the update is as in (11.24), with frequencies ω as given in (11.8). In fact, the update is very straightforward; the determination of the initializing values for the state Φ_m is more difficult (read about the two-dimensional FFT function `fft2` in Matlab).

Programming Exercise 11.9 Create a Matlab script which calculates a finite difference solution to the 2D wave equation, defined over the unit circle, using the family of schemes (11.27). Make use of a fixed (Dirichlet) condition at the outer edge of the circle. As this is an implicit scheme, a vector-matrix form, requiring linear system solutions, is essential—you will need to arrange the grid function as a vector \mathbf{u} , and generate the matrix form of the operator δ_Δ (see Programming Exercise 10.6). You will also need to ensure that you have satisfied the stability condition (11.28) as close to equality as possible. In order to do this, rewrite this condition in terms of h_r and $q = h_\theta/h_r$, as in Problem 11.16.

For a given value of γ , such as $\gamma = 2000$, perform a study of output bandwidth, as a function of the free parameter scheme α , as well as the ratio $q = h_\theta/h_r$. Initialize the scheme with a sharply peaked pluck-like distribution, so that you will excite all the modes sufficiently, and plot an output spectrum, from which the bandwidth should be easily observable—ignore any isolated spurious modes which appear high in the audio spectrum.

Chapter 12

Linear Plate Vibration

The 2D wave equation has been treated in the previous chapter as a test case for sound synthesis methods. But, aside from the case of the vibrating membrane, it is often materials with an inherent stiffness which are of interest in musical acoustics. When these are flat, they are referred to as plates, and when curved, as shells. The physics of vibrating plates is far more complex than that of the membrane, described by the 2D wave equation, and this complexity shows itself in the resulting equations of motion, even in the simplest case of thin linear plate vibration.

Because the 2D wave equation is so simply expressed, it is often assumed that the increased model complexity for systems such as plates must translate to more computational work. But, as seen in Chapter 7, stiffness tends to *reduce* computational costs. The same is true of plates—whereas simulation of membrane vibration in real time is, even now, quite daunting, plate synthesis is not. This is good news, as the world of sounds produced by plates is a very rich one indeed. The lossless Kirchhoff thin plate model, as well as modal analysis and finite difference schemes, is introduced in §12.1, and frequency-dependent loss in §12.2. Coupling to various excitation mechanisms, such as the mallet and bow as well as the related case of plate reverberation are treated in §12.3, and coupling to strings in §12.4. Anisotropic plate vibration is briefly discussed in §12.5, and finally, schemes for the thin plate equation are developed in radial coordinates in §12.6.

12.1 The Kirchhoff Thin Plate Model

The Kirchhoff model of a uniform thin isotropic plate [243] is defined as

$$\rho H u_{tt} = -D \Delta \Delta u \quad (12.1)$$

Here, u is the plate deflection in a transverse direction, ρ is a material density, H is the plate thickness, and the constant D , defined by

$$D = \frac{EH^3}{12(1-\nu^2)}$$

is sometimes known as the plate flexural rigidity, and depends on Young's modulus E , and Poisson's ratio $\nu < 1/2$. When spatially scaled with respect to a length parameter L , the Kirchhoff model may be written as

$$u_{tt} = -\kappa^2 \Delta \Delta u \quad (12.2)$$

where

$$\kappa^2 = \frac{D}{\rho H L^4} \quad (12.3)$$

As usual for problems which are second order in time, two initial conditions must be supplied (normally displacement and velocity). Boundary termination is a much more complex matter than in the case of the 2D wave equation; conditions will be given shortly, in §12.1.2.

The model above is but the simplest representation of plate dynamics. It does not take into account effects that occur at high amplitudes, which will be covered in the next chapter, nor does it hold when the plate becomes thick (i.e., when H/L becomes large in some sense), in which case a thick plate model (some examples of which are very well covered in the text by Graff [155]) is perhaps more appropriate. Most plates which occur in a musical setting, however, are quite thin, and the above model is sufficient for a preliminary foray into physical modeling synthesis. For a quantitative look at the range of applicability of the thin plate hypothesis in musical acoustics, through a comparison with the Mindlin-Reissner thick plate theory, see the next section.

12.1.1 Phase and Group Velocity

The characteristic equation or dispersion relation for the thin plate equation (12.2) is

$$s^2 = -\kappa^2|\beta|^2 \quad \longrightarrow \quad \omega = \pm\kappa|\beta|^2$$

and expressions for the phase and group velocity follow as

$$v_\phi = \kappa|\beta| \quad v_g = 2\kappa|\beta|$$

Again, just as in the case of the ideal bar in 1D, wave propagation is dispersive, with short wavelength components traveling faster than those of long wavelength. See Figure 12.1, which shows the time evolution of an initial displacement—the dispersive behavior may again be seen in the high-frequency ripples preceding the main body of the disturbance.

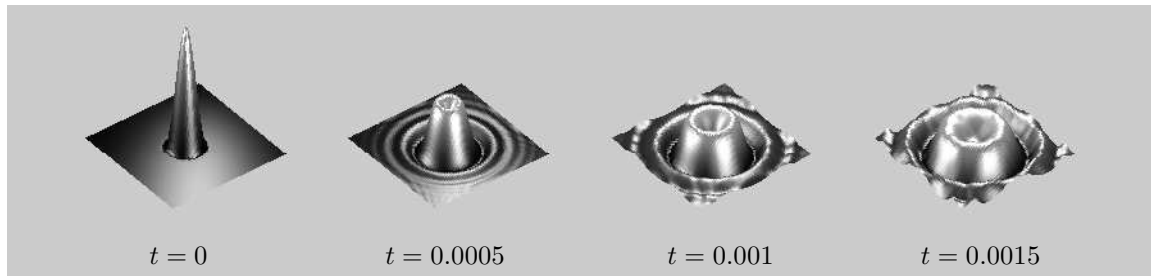


Figure 12.1: *Time evolution of the displacement of a plate. Here, the plate has stiffness parameter $\kappa = 5$, an aspect ratio of $\epsilon = 1$, and free boundary conditions are applied at the edges. The initial condition is of plucked type, in the form of a raised cosine at the domain center.*

This system, like the wave equation, is isotropic—again, though it would be possible to write the expressions for phase and group velocity in terms of frequency ω alone, the associated difference schemes lose this isotropic property, and the easiest comparison is through the expressions above, in terms of wavenumber β . An extension of the thin plate model to the anisotropic case is indeed of interest in musical acoustics as well, and will be described more fully in §12.5.

Thick vs. Thin Plate Models

Plates which occur as components of musical instruments are thin; one question which then arises is: are thin plate models sufficient to describe the behavior of such objects subject to the constraints

of human audition? One way of answering this question is through a comparison with certain thick plate models, via dispersion relations. For the sake of this comparison, consider the thin Kirchhoff plate model, and what is perhaps the simplest possible model of thick plate vibration (taking into account shear and rotatory inertia effects) due to Mindlin and Reissner [238, 155]; this model will not be presented here, but may be viewed as the direct extension of the Timoshenko beam theory to 2D. (The Timoshenko model is presented briefly in Problem 7.1.)

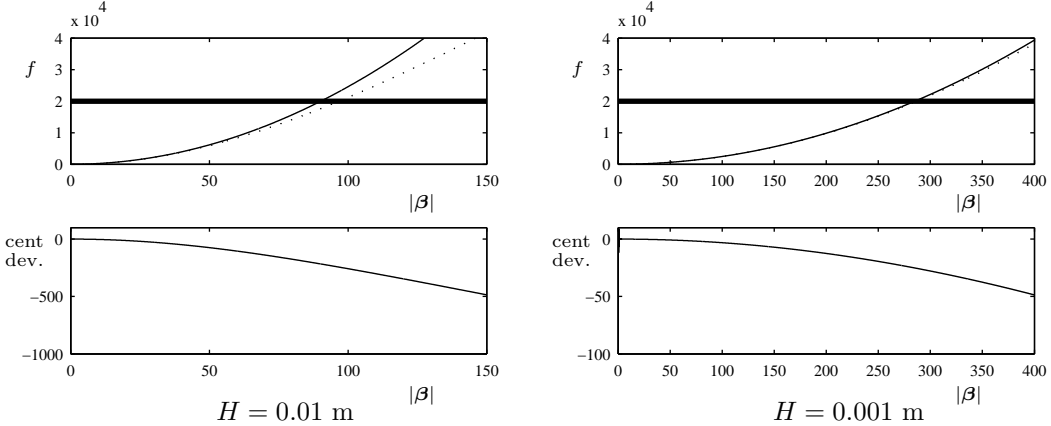


Figure 12.2: Comparison between thick and thin plate models, for a steel plate of thickness 1 cm (left) and 1 mm (right). Top: dispersion relation with frequency $f = f(\beta)$ (dimensional form) for the Kirchhoff thin plate model (solid line) and the Mindlin-Reissner thick plate model (dotted line). The upper limit of human hearing, at $f = 20$ kHz, is plotted as a thick black line. Bottom: the deviation, in cents, between the two profiles as a function of wavenumber.

From the plots in Figure 12.2, it should be clear that the deviation of the dispersion relation of the Kirchhoff model (and thus modal frequencies) from that of the thick plate model is pronounced at high frequencies—the thinner the plate, the less influence over frequencies in the audio range. For metal plates of roughly 1 mm thickness, the effect is minimal, though for other materials, such as glass, the effect may be more pronounced. Not shown in the dispersion plots are an additional family of frequencies, which lie well above the audio range for the two example thicknesses considered here.

Thick plate models are heavily used in finite element calculations, but may well be overkill when it comes to thin plates such as those which occur in musical acoustics; given that simulating the thick model involves a good deal more computational work, one should consider very carefully the use of standard finite element packages, designed for industrial applications, in physical modeling sound synthesis.

12.1.2 Energy and Boundary Conditions

For the Kirchhoff plate defined over a domain \mathcal{D} , the energy may be found, using the usual manipulations, as

$$\frac{d\mathfrak{H}_0}{dt} = \mathfrak{B}_0 \quad \text{with} \quad \mathfrak{H}_0 = \mathfrak{T} + \mathfrak{V}_0 \quad (12.4)$$

where \mathfrak{B}_0 is a term resolved on the boundary of \mathcal{D} , and

$$\mathfrak{T} = \frac{1}{2} \|u_t\|_{\mathcal{D}}^2 \quad \mathfrak{V}_0 = \frac{\kappa^2}{2} \|\Delta u\|_{\mathcal{D}}^2$$

which is similar to the expression for the ideal bar, from (7.5). The expression \mathfrak{V}_0 (and thus \mathfrak{H}_0), however, though valid in the case of the infinite plate, may need to be modified under certain boundary conditions—see below.

Edges and Fixed Boundary Conditions

At an edge of a Cartesian domain, say at $x = 0$ for $\mathcal{D} = \mathbb{R}^{2,x+}$, integration by parts leads, from (10.5), to the following expression for the boundary term \mathfrak{B}_0 in (12.4):

$$\mathfrak{B}_0 = \kappa^2 (\{u_t, (\Delta u)_x\}_{(0,\mathbb{R})} - \{u_{tx}, \Delta u\}_{(0,\mathbb{R})})$$

(Recall the use of the $\{\cdot, \cdot\}$ notation to indicate a 1D inner product over a boundary, from (10.7).) One may immediately extract the following two sets of boundary conditions:

$$u = u_x = 0 \quad \text{Clamped} \tag{12.5a}$$

$$u = u_{xx} = 0 \quad \text{Simply supported} \tag{12.5b}$$

(In fact, the simply supported condition is normally written in a slightly different form—see the following discussion of free boundary conditions.) These conditions are directly analogous to those for the ideal bar, from (7.7a) and (7.7b). One might also suppose, by analogy, that the conditions $u_{xx} = u_{xxx} = 0$ correspond to a free edge condition; in fact, they do not. The difficulty is that the \mathfrak{V}_0 may be interpreted as a potential energy only under a fixed termination. It may be modified in the following way.

The Operator $\mathcal{L}(\cdot, \cdot)$ and Free Boundary Conditions

In order to address the issue of free boundary conditions in a thin plate, it turns out to be useful to introduce an operator which appears with great frequency in problems in thin plate vibration [285]. The operator $\mathcal{L}(\cdot, \cdot)$ is defined, in Cartesian coordinates, with respect to two functions $\alpha(x, y)$ and $\beta(x, y)$, as

$$\mathcal{L}(\alpha, \beta) = \alpha_{xx}\beta_{yy} + \alpha_{yy}\beta_{xx} - 2\alpha_{xy}\beta_{xy} \tag{12.6}$$

Though this operator will crop up in a more central way in the study of nonlinear plate vibration in Chapter 13, it possesses several properties which are useful in arriving at free boundary conditions even in the linear case. First, it is bilinear, and also symmetric, so that $\mathcal{L}(\alpha, \beta) = \mathcal{L}(\beta, \alpha)$, implying further that, if α and β also depend on t ,

$$(\mathcal{L}(\alpha, \beta))_t = \mathcal{L}(\alpha_t, \beta) + \mathcal{L}(\alpha, \beta_t) \tag{12.7}$$

Next, assuming for the moment that $\mathcal{L}(\alpha, \beta)$ is defined over the half plane domain $\mathcal{D} = \mathbb{R}^{2,x+}$,

$$\begin{aligned} \langle \mathcal{L}(\alpha, \beta), 1 \rangle_{\mathbb{R}^{2,x+}} &= \int_{-\infty}^{\infty} \int_0^{\infty} \mathcal{L}(\alpha, \beta) dx dy = - \int_{-\infty}^{\infty} \alpha_x \beta_{yy} + \alpha \beta_{xxyy} dy \\ &= -\{\alpha_x, \beta_{yy}\}_{(0,\mathbb{R})} - \{\alpha, \beta_{xxyy}\}_{(0,\mathbb{R})} \end{aligned} \tag{12.8}$$

Thus $\mathcal{L}(\alpha, \beta)$, when integrated over the spatial domain, may be resolved into terms which act over the boundary alone—note in particular that if α and β are constrained to be zero over this boundary, then the integral vanishes.

With this in mind, one may now return to the problem of the free boundary condition over the half plane $\mathcal{D} = \mathbb{R}^{2,x+}$. Set $\alpha = \beta = u$, and define the quantity $\mathfrak{V}_{\text{free}}$ by

$$\mathfrak{V}_{\text{free}} = \frac{\kappa^2(\nu - 1)}{2} \langle \mathcal{L}(u, u), 1 \rangle_{\mathbb{R}^{2,x+}}$$

Then, using properties (12.7) and (12.8) above,

$$\frac{d\mathfrak{V}_{\text{free}}}{dt} = \mathfrak{B}_{\text{free}} = \kappa^2(1-\nu)(\{u_{xt}, u_{yy}\}_{(0,\mathbb{R})} + \{u_t, u_{xyy}\}_{(0,\mathbb{R})})$$

and, interpreting $\mathfrak{V}_{\text{free}}$ as a contribution to the potential energy of the plate, one has finally,

$$\frac{d\mathfrak{H}}{dt} = \mathfrak{B} \quad \text{where} \quad \mathfrak{H} = \mathfrak{H}_0 + \mathfrak{V}_{\text{free}} \quad (12.9)$$

and where the boundary term is

$$\mathfrak{B} = \mathfrak{B}_0 + \mathfrak{B}_{\text{free}} = \kappa^2 (\{u_t, u_{xxx} + (2-\nu)u_{xyy}\}_{(0,\mathbb{R})} - \{u_{tx}, u_{xx} + \nu u_{yy}\}_{(0,\mathbb{R})}) \quad (12.10)$$

Though \mathfrak{H}_0 is obviously non-negative, it is not immediately clear that $\mathfrak{H} = \mathfrak{H}_0 + \mathfrak{V}_{\text{free}}$ will be, given that $\mathcal{L}(u, u)$ is of indeterminate sign. With a little additional effort, one may show non-negativity of \mathfrak{H} —see Problem 12.1.

Upon inspection of the new boundary term \mathfrak{B} , the conventional lossless free boundary condition may be extracted:

$$u_{xx} + \nu u_{yy} = u_{xxx} + (2-\nu)u_{xyy} = 0 \quad \text{Free} \quad (12.11)$$

Notice that the boundary conditions now depend on ν and, as such, it is an extra parameter which must appear in any simulation, and which cannot be eliminated through scaling techniques¹. For steel, which is a common choice of material in musical instruments, ν is approximately 0.3. The more conventional form of the simply supported condition, equivalent to that given in (12.5b) also emerges—see Problem 12.2.

Though fixed and free conditions have been shown here for a domain with a single edge, it should be clear that, at least over a rectangular domain, they may be used at any edge, where x may be interpreted as a coordinate normal to the plate edge, and y to a tangential coordinate.

Corners

Corners pose slightly more difficulty in the case of the plate than for the 2D wave equation. Consider a thin Kirchhoff plate defined over the quarter plane $\mathcal{D} = \mathbb{R}^{2,x+y+}$. Through energy analysis (see Problem 12.3), one may show that under fixed conditions, no further condition at $x = 0, y = 0$ need be supplied other than $u = 0$. Under free conditions, however, a new condition intervenes:

$$u_{xy}|_{x=0,y=0} = 0 \quad \text{Free BC at corner} \quad (12.12)$$

which must be enforced in addition to the edge conditions.

12.1.3 Modes

Modal analysis for thin plates is similar to that applied to the 2D wave equation, in §11.1.3. As for the case of the ideal bar however (see §7.1.3), closed-form expressions for modal frequencies and shapes are rare—for a rectangular plate of aspect ratio ϵ , defined over the unit area rectangle $\mathcal{D} = \mathbb{U}_\epsilon^2$, only simply supported conditions such as (12.5b) applied on all edges lead to a simple expression:

$$U_{p,q}(x, y) = \sin(p\pi x/\sqrt{\epsilon}) \sin(q\pi\sqrt{\epsilon}y) \quad \omega_{p,q} = \pi^2 \kappa (p^2/\epsilon + \epsilon q^2) \quad (12.13)$$

¹In the simulation setting, this is a consideration which strongly affects modal algorithms—the modal shapes and frequencies will be dependent not just on geometry, but also on ν , and must be recalculated as the material is changed. Time domain methods, once the proper boundary conditions are inserted into the algorithm, are insensitive to this choice.

In all other cases of interest (and in particular, that of free termination, which plays a large role in models of percussion instruments), the shapes and frequencies must be computed numerically. See Figure 12.3 for an illustration of the modal shapes. Under free conditions at all edges of a rectangular plate, there will be three additional zero-frequency modes corresponding to “rigid body” motion—see Programming Exercise 12.1 for some exploration of this.

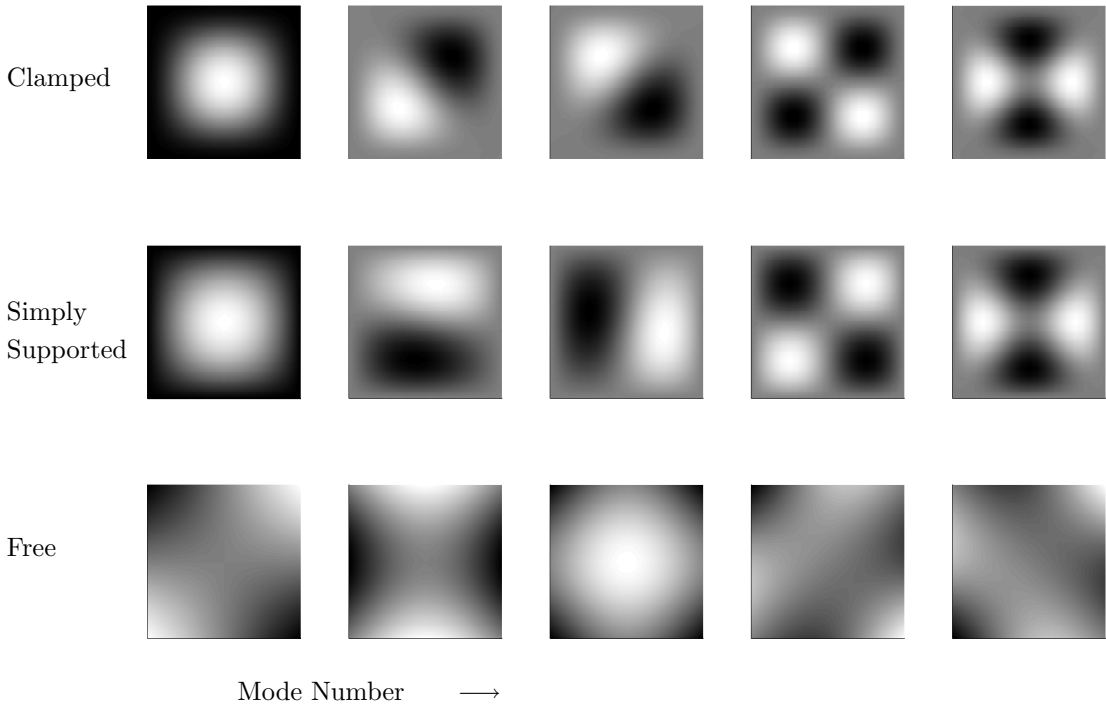


Figure 12.3: *The first five modes of vibration for a thin square plate, under clamped (top), simply supported (middle) and free (bottom) boundary conditions. In all cases, dark and light areas correspond to modal maxima and minima. In the case of the free condition, the first five modes of non-zero frequency are shown (i.e., three modes corresponding to rigid body motion are not shown here).*

Just as in the case of the ideal bar, it should be apparent that the frequencies increase more quickly with mode number for this stiff 2D system, with respect to those of the analogous non-stiff system, the 2D wave equation. From the above expression for the modal frequencies, one may arrive at the following count for the number of degrees of freedom $N_m(f_s/2)$ (twice the number of modal frequencies less than $f_s/2$):

$$N_m(f_s/2) = \frac{f_s}{2\kappa}$$

In comparison with the analogous expression for the 2D wave equation (or for a membrane) from (11.9), note that the number of modes depends linearly on f_s , implying a uniform density of modes. In fact, one has an average spacing between modes of 2κ Hz. See Figure 12.4. This implies, furthermore, a reduction in the number of degrees of freedom necessary to describe the plate up

to a given frequency. As a result, the simulation of plate vibration is far less computationally intensive than membrane vibration²—which is perhaps surprising! As usual, the same reduction in computational expense follows through to the case of finite difference schemes, which are covered next.

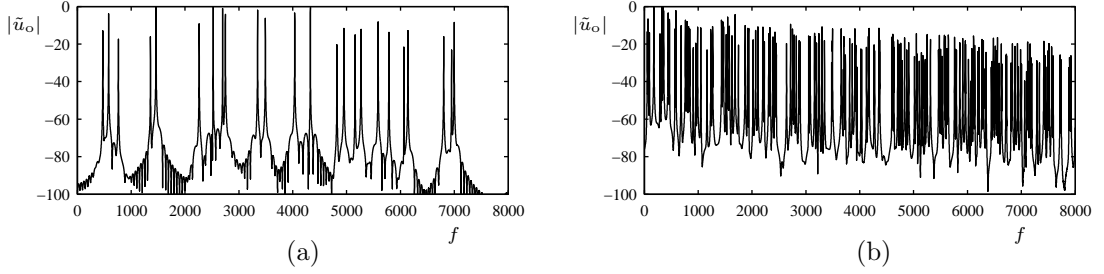


Figure 12.4: *Output spectra, showing an even distribution of modes, for a thin plate model. In this case, the plate is square, under free boundary conditions, and in (a), the stiffness parameter $\kappa = 200$, and in (b), $\kappa = 20$.*

12.1.4 A Simple Finite Difference Scheme

Probably the most straightforward finite difference method for the Kirchhoff plate employs the five-point approximation to the Laplacian, twice, as discussed in §10.2:

$$\delta_{tt} u = -\kappa^2 \delta_{\Delta \square, \Delta \square} u \quad (12.14)$$

When written out in full in terms of the grid function $u_{l,m}^n$, assuming that the grid spacing is equal to h in both the x and y directions, the scheme is of the form

$$\begin{aligned} u_{l,m}^{n+1} = & (2 - 20\mu^2) u_{l,m}^n + 8\mu^2 (u_{l,m+1}^n + u_{l,m-1}^n + u_{l+1,m}^n + u_{l-1,m}^n) \\ & - 2\mu^2 (u_{l+1,m+1}^n + u_{l+1,m-1}^n + u_{l-1,m+1}^n + u_{l-1,m-1}^n) \\ & - \mu^2 (u_{l,m+2}^n + u_{l,m-2}^n + u_{l+2,m}^n + u_{l-2,m}^n) - u_{l,m}^{n-1} \end{aligned}$$

and depends on the scheme parameter μ , defined as

$$\mu = \frac{\kappa k}{h^2}$$

As one might gather, there are many possibilities for the generalization of scheme (12.14), through parameterized approximations to $\Delta\Delta$ [48], and perhaps implicit constructions—one such parameterized family of schemes will be explored in §12.1.5, and other schemes used in investigations in musical acoustics appear in [315], for a system equivalent to (12.1). Finite difference schemes for rectangular plates are examined in much more detail in the book by Szilard [347].

von Neumann Analysis and Stability

The characteristic polynomial for scheme (12.14) is

$$z + (16\mu^2(p_x + p_y)^2 - 2) + z^{-1} = 0$$

²This is true for a thin plate model, but, when a full thick plate model is employed, one may expect an avalanche of modes in the high frequency range. Given the discussion of the applicability of the thick plate model in musical acoustics, on page 334, the increased modal density will not exhibit itself, at least for reasonably thin plates, until well beyond the upper reaches of the audio frequency range.

in terms of the variables $p_x = \sin^2(\beta_x h/2)$, and $p_y = \sin^2(\beta_y h/2)$. The roots are of unit magnitude under the conditions

$$0 \leq 4\mu^2(p_x + p_y)^2 \leq 1$$

which is satisfied when

$$\mu \leq \frac{1}{4} \quad \longrightarrow \quad h \geq 2\sqrt{\kappa k} \quad (12.15)$$

Energy and Numerical Boundary conditions

Finding numerical boundary conditions which correspond to typical lossless conditions of the type discussed in §12.1.2 is straightforward, but proving stability for a choice of such conditions can be a very delicate and involved matter. It is worth showing how this may be done, using energy methods, for one such set.

Consider the scheme (12.14), defined over the half-plane $\mathbb{Z}^{2,x+}$. Taking an inner product with $\delta_t u$ leads directly, using summation by parts from (10.19) to

$$\delta_{t+}\mathfrak{t} = -\kappa^2 \langle \delta_{\Delta \boxplus} \delta_t u, \delta_{\Delta \boxplus} u \rangle_{\mathbb{Z}^{2,x+}} + \mathfrak{b}_0 = -\delta_{t+}\mathfrak{v}_0 + \mathfrak{b}_0 \quad \longrightarrow \quad \delta_{t+}\mathfrak{h}_0 = \mathfrak{b}_0 \quad (12.16)$$

where $\mathfrak{h}_0 = \mathfrak{t} + \mathfrak{v}_0$, and

$$\mathfrak{t} = \frac{1}{2} \|\delta_{t-} u\|_{\mathbb{Z}^{2,x+}}^2 \quad \mathfrak{v}_0 = \frac{\kappa^2}{2} \langle \delta_{\Delta \boxplus} u, e_{t-} \delta_{\Delta \boxplus} u \rangle_{\mathbb{Z}^{2,x+}} \quad (12.17a)$$

$$\mathfrak{b}_0 = \kappa^2 \{ \delta_{t-} u, \delta_{x-} \delta_{\Delta \boxplus} u \}_{(0,\mathbb{Z})} - \kappa^2 \{ \delta_{x-} \delta_{t-} u, \delta_{\Delta \boxplus} u \}_{(0,\mathbb{Z})} \quad (12.17b)$$

One may immediately extract numerical clamped and simply supported conditions as

$$u = \delta_{x-} u = 0 \quad \text{Clamped} \quad (12.18a)$$

$$u = \delta_{xx} u = 0 \quad \text{Simply Supported} \quad (12.18b)$$

In either case the scheme conserves numerical energy. Stability follows, as usual, by finding conditions under which the energy remains non-negative.

The case of the free boundary condition is more complex. One may write, for the potential energy \mathfrak{v}_0 , and defining $v \triangleq \delta_t u$,

$$\begin{aligned} \delta_{t+}\mathfrak{v}_0 &= \kappa^2 \langle \delta_{\Delta \boxplus} v, \delta_{\Delta \boxplus} u \rangle_{\mathbb{Z}^{2,x+}} \\ &= \kappa^2 \nu \langle \delta_{\Delta \boxplus} v, \delta_{\Delta \boxplus} u \rangle_{\mathbb{Z}^{2,x+}} + \kappa^2 (1-\nu) \langle \delta_{\Delta \boxplus} v, \delta_{\Delta \boxplus} u \rangle_{\mathbb{Z}^{2,x+}} \\ &= \kappa^2 \nu \langle \delta_{\Delta \boxplus} v, \delta_{\Delta \boxplus} u \rangle_{\mathbb{Z}^{2,x+}} + \kappa^2 (1-\nu) (\langle \delta_{xx} v, \delta_{xx} u \rangle_{\mathbb{Z}^{2,x+}} + \langle \delta_{yy} v, \delta_{yy} u \rangle_{\mathbb{Z}^{2,x+}}) \\ &\quad + \kappa^2 (1-\nu) (\langle \delta_{xx} v, \delta_{yy} u \rangle_{\mathbb{Z}^{2,x+}} + \langle \delta_{yy} v, \delta_{xx} u \rangle_{\mathbb{Z}^{2,x+}}) \end{aligned}$$

Finally, using summation by parts on the final two terms in the above expression leads to

$$\begin{aligned} \delta_{t+}\mathfrak{v}_0 &= \kappa^2 \nu \langle \delta_{\Delta \boxplus} v, \delta_{\Delta \boxplus} u \rangle_{\mathbb{Z}^{2,x+}} + \kappa^2 (1-\nu) (\langle \delta_{xx} v, \delta_{xx} u \rangle_{\mathbb{Z}^{2,x+}} + \langle \delta_{yy} v, \delta_{yy} u \rangle_{\mathbb{Z}^{2,x+}}) \\ &\quad + 2\kappa^2 (1-\nu) \langle \delta_{x+y+} v, \delta_{x+y+} u \rangle_{\mathbb{Z}^{2,x+}} \\ &= \delta_{t+}\mathfrak{v} - \mathfrak{b}' \end{aligned}$$

where

$$\begin{aligned} \mathfrak{v} &= \frac{\kappa^2 \nu}{2} \langle \delta_{\Delta \boxplus} u, e_{t-} \delta_{\Delta \boxplus} u \rangle_{\mathbb{Z}^{2,x+}} + \frac{\kappa^2 (1-\nu)}{2} (\langle \delta_{xx} u, e_{t-} \delta_{xx} u \rangle_{\mathbb{Z}^{2,x+}} + \langle \delta_{yy} u, e_{t-} \delta_{yy} u \rangle_{\mathbb{Z}^{2,x+}}) \\ &\quad + \kappa^2 (1-\nu) \langle \delta_{x+y+} u, e_{t-} \delta_{x+y+} u \rangle_{\mathbb{Z}^{2,x+}} \end{aligned} \quad (12.19a)$$

$$\mathfrak{b}' = \kappa^2 (1-\nu) \{ \delta_{t-} u, \delta_{x-} \delta_{yy} u \}_{(0,\mathbb{Z})} + \kappa^2 (1-\nu) \{ \delta_{x-} \delta_{t-} u, \delta_{yy} u \}_{(0,\mathbb{Z})} \quad (12.19b)$$

and finally, from (12.16), to

$$\delta_{t+}\mathfrak{h} = \mathfrak{b} \quad (12.20)$$

where $\mathfrak{h} = \mathfrak{t} + \mathfrak{v}$, and where $\mathfrak{b} = \mathfrak{b}_0 + \mathfrak{b}'$ is of the form

$$\mathfrak{b} = \kappa^2 \{ \delta_t u, \delta_{x-} (\delta_{xx} + (2 - \nu) \delta_{yy}) u \}_{(0, \mathbb{Z})} - \kappa^2 \{ \delta_{x-} \delta_t u, (\delta_{xx} + \nu \delta_{yy}) u \}_{(0, \mathbb{Z})}$$

Clearly, the boundary term vanishes when

$$(\delta_{xx} + \nu \delta_{yy}) u = \delta_{x-} (\delta_{xx} + (2 - \nu) \delta_{yy}) u = 0 \quad \text{Free} \quad (12.21)$$

which corresponds directly to the boundary condition (12.11). Still, however, the above analysis is not sufficient to show stable behavior of the scheme. As usual, one must show that the conserved energy is a non-negative function of the state defined over the grid. Even in this simple case of the scheme defined over the half plane, this is complicated by the fact the expressions for the energy now include values outside the domain, at virtual grid locations. This analysis is performed in [46], and in a step-by-step fashion, in Problem 12.4.

Scheme (12.14), under the above conditions (12.18a), (12.18b) or (12.21) is conservative, over the half plane. It is direct to extend this analysis to the quarter plane; if the scheme (12.14) is defined over the region $\mathcal{D} = \mathbb{Z}^{2,x+y+}$, the numerical boundary conditions above continue to hold at the boundary at $x = 0$, and the same conditions hold, with x and y reversed, at the boundary at $y = 0$. For free boundary conditions on both edges, the corner condition corresponding to (12.12) will be

$$\delta_{x-y-} u_{0,0} = 0 \quad (12.22)$$

See Problem 12.5. These conditions may be extended, by symmetry, to a rectangular region. For more on the construction of the related operator $\delta_{\Delta\Box, \Delta\Box}$, see Problem 12.6 and Programming Exercise 12.2.

12.1.5 An Implicit Family of Schemes

Just as in the case of the ideal bar, the dispersive behavior of scheme (12.14) leads to an audible mistuning of modes—see Figure 12.5(b), showing the numerical phase velocity for this scheme relative to the phase velocity of the model system, as a function of wavenumber, and Table 12.1, which compares numerical modal frequencies to exact values for a particular instance of a plate under simply supported boundary conditions.

As before, for very fine modeling, particularly for high-pitched plates (i.e., for high values of κ), an implicit generalization of scheme (12.14) may be of use. Consider, thus, the two-parameter family of schemes, given by

$$(1 + \alpha k \kappa \delta_{\Delta\Box} + \phi k^2 \kappa^2 \delta_{\Delta\Box, \Delta\Box}) \delta_{tt} u = -\kappa^2 \delta_{\Delta\Box, \Delta\Box} u \quad (12.23)$$

where α and ϕ are the free parameters. When $\alpha = \phi = 0$, the scheme reduces to (12.14).

Stability analysis, though now more complex, yields the bounds $\mu \leq \mu_{\max}(\alpha, \phi)$, as given over regions of the α, ϕ plane in Figure 12.5(a); notice that, as in the case of schemes mentioned earlier for the wave equation and the ideal bar, there are choices of the parameters such that the scheme is unconditionally stable. See Problem 12.7.

As expected, it is possible to choose the parameters such that dispersion is minimized, particularly in the low-frequency limit, and the accuracy of the numerical modal frequencies is much greater. See Figure 12.5(c) and Table 12.1. The poor performance of the explicit scheme is clearly in evidence in the table; deviations of a semitone or more are possible even for relatively low frequencies. The parameters α and ϕ have been chosen here in an ad hoc manner—computer optimization techniques are advisable, perhaps with a goal of minimizing the variation in relative phase velocity over the entire range of wavenumbers, though one must bear in mind that the choice of μ , which is dependent

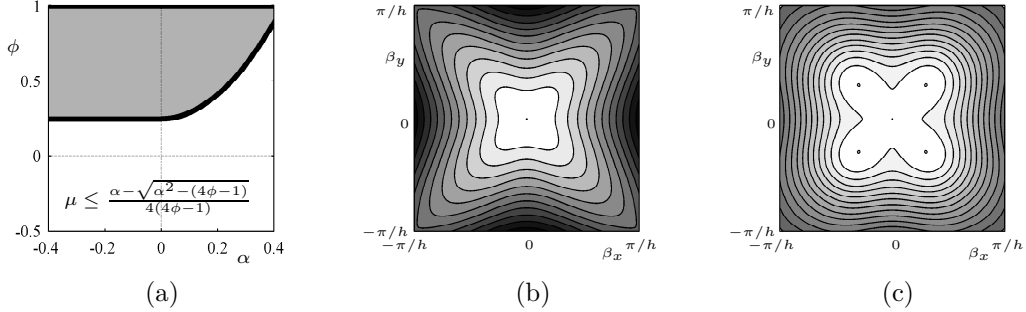


Figure 12.5: (a) Regions of unconditional (shaded), and conditional (unshaded) stability for scheme (12.23), in the α, ϕ parameter space. Over the region of conditional stability, the bound $\mu \leq \mu_{\max}(\alpha, \phi)$ is as indicated. In (b), a contour plot of numerical phase velocity relative to the exact phase velocity for the plate equation, as a function of the wavenumber components β_x and β_y , for the explicit scheme (12.14), and in (c), a similar plot for the implicit scheme (12.23) with $\alpha = 0.47$ and $\phi = 0.3$. Contours indicate deviations of 5% from the exact value of 1.

on α and ϕ , will have great bearing on computational cost, and such an attribute must be accounted for in any optimization procedure.

12.2 Loss and Tension

As in the case of the ideal bar, loss modeling in plates is a very involved matter—there are various sources of such loss, including thermoelasticity, viscoelasticity and radiation; see [79] for a complete picture of such effects. Tension may also be added, as in the case of the stiff string, in order to yield a general model for a stiff membrane [135]. A simple, perceptually correct plate model is a direct extension of the case of the bar:

$$u_{tt} = -\kappa^2 \Delta \Delta u + \gamma^2 \Delta u - 2\sigma_0 u_t + 2\sigma_1 \Delta u_t$$

As before, σ_0 , in the absence of the other term with coefficient σ_1 gives rise to frequency-independent damping, and when this other term is added, increasing damping at higher frequencies is modeled. As before, it is possible to rewrite σ_0 and σ_1 in terms of two chosen values of decay constant T_{60} at specified frequencies—the expressions are identical to those given in (7.29). The obvious explicit extension of scheme (12.14) is

$$\delta_{tt}u = -\kappa^2 \delta_{\Delta \Delta, \Delta \Delta} u + \gamma^2 \delta_{\Delta \Delta} u - 2\sigma_0 \delta_{t, t} u + 2\sigma_1 \delta_{t-t} \delta_{\Delta \Delta} u \quad (12.24)$$

Implicit versions are of course available, useful both in reducing numerical dispersion, and in improved (centered) modeling of the frequency-dependent damping term. See Programming Exercise 12.3.

12.3 Plate Excitation

Excitation, using physical models of a hammer-like object, and a bow has been covered in the lumped context in §4.2.3 and §4.3.1, and in the case of 1D systems such as strings and bars in §7.5 and §7.4. From a functional point of view, the situation is not extremely different in the case of 2D systems such as plates, though, of course, the sound output is of an entirely different character.

Table 12.1: Comparison among modal frequencies for the plate equation, defined over a square, under simply supported conditions, with $\kappa = 100$, and modal frequencies (as well as their cent deviations from the exact frequencies) of the simple explicit scheme (12.14), and the implicit scheme (12.23), with $\alpha = 0.47$ and $\phi = 0.3$, with a sample rate $f_s = 44100$ Hz. μ is chosen so as to satisfy the stability condition given in Figure 12.5(a) in each case as close to equality as possible.

Mode number	Exact Freq.	Explicit		Implicit	
		Freq.	Cent Dev.	Freq.	Cent Dev.
(1,1)	314.2	311.6	-14.1	315.9	9.5
(1,2)	785.4	764.1	-47.6	792.2	14.9
(2,2)	1256.6	1217.4	-54.9	1281.9	34.5
(1,3)	1570.8	1470.6	-114.1	1583.0	13.4
(2,3)	2042.0	1926.1	-101.2	2092.9	42.6
(1,4)	2670.4	2366.5	-209.2	2672.7	1.5
(2,5)	4555.3	3838.7	-296.3	4573.0	6.7

In both cases, one may connect the plate to the excitation by using a distribution $e_{\text{exc}}(x, y)$ representing the spatial extent of the excitation. In the case of an ideal thin plate with loss, but without tension, for example, the combined system is of the following form:

$$u_{tt} = -\kappa^2 \Delta \Delta u - 2\sigma_0 u_t + 2\sigma_1 \Delta u_t + e_{\text{exc}}(x, y)F \quad (12.25)$$

where $F(t)$ is a force divided by the total plate mass. Usually it is simplest to use a localized distribution of the form of a 2D Dirac delta function $e_{\text{exc}}(x, y) = \delta(x - x_i, y - y_i)$; this is certainly sufficient for bowing, though for large mallets (or small plates) a more general distribution (such as, e.g., a 2D raised cosine, as per (11.3)) may be advisable. The excitation point, $x = x_i$, $y = y_i$ has been left fully general here. In the case of the bow, however, it is only physically reasonable to bow at an edge, though in simulation, of course, one can bow wherever one likes!

F may derive from a physical model of an excitation mechanism, generally driven by gestural data at a control rate. On the other hand, in one very interesting application of physical modeling, namely plate reverberation, F is an audio signal, and is “processed” by a plate—see §7.9 for more on the use of physical modeling principles in the emulation of analog audio effects.

A simple scheme, assuming that the excitation acts at a point with coordinates x_i , y_i , then, is the following:

$$\delta_{tt}u = -\kappa^2 \delta_{\Delta, \Delta} u - 2\sigma_0 \delta_{t-} u + 2\sigma_1 \delta_{t-} \delta_{\Delta} u + J_p(x_i, y_i)F \quad (12.26)$$

where $J_p(x_i, y_i)$ is a p th-order spreading function, as described in §10.2.1. Notice that as in the case of the bar, a backward difference has been employed to approximate the frequency-dependent loss term—this could be adjusted to a centered difference, at the expense of requiring an implicit update.

12.3.1 Coupling to a Mallet Model

The interaction with a mallet-like object may be generalized directly from the case of the hammer-string interaction in 1D, as described in §7.5. In this case, if the vertical position of the mallet is $u_H(t)$, the force term F is given by

$$F = -\mathcal{M} \frac{d^2 u_H}{dt^2} = \omega_H^{1+\alpha} ([u_H - \langle e_{\text{exc}}, u \rangle_D]^+)^{\alpha}$$

As before, the interaction is modeled using a one-sided power law nonlinearity. \mathcal{M} is the ratio of the mass of the mallet to that of the plate, ω_H is a stiffness parameter, and α the stiffness exponent. Again, the operation $[.]^+$ indicates the “positive part of,” and thus the interaction is active only when the mallet and plate are in contact. Such a model, when coupled to a membrane rather than a plate, has been employed in time domain simulations of drums [282, 215] as well as anisotropic plates [216].

Given the previous encounters with this type of nonlinearity in §4.2.2 and §7.5, a well-behaved difference approximation to the force equations above is of semi-implicit type:

$$F = -\mathcal{M}\delta_{tt}u_H = \omega_H^{1+\alpha}\mu_t(u_H - I_p(x_i, y_i)u)([u_H - I_p(x_i, y_i)u]^+)^{\alpha-1} \quad (12.27)$$

where $I_p(x_i, y_i)$ is a p th order interpolation operator, as described in §10.2.1. As expected, such an approximation allows for a unique update, when coupled with (12.26). The major effect of the nonlinearity can be seen to be a reduction in the total contact duration and increase in brightness with increasing strike velocity—see Figure 12.6. Notice also the characteristic deformation of the force curves, resulting from reflections from the plate boundaries—recontact phenomena are also possible.

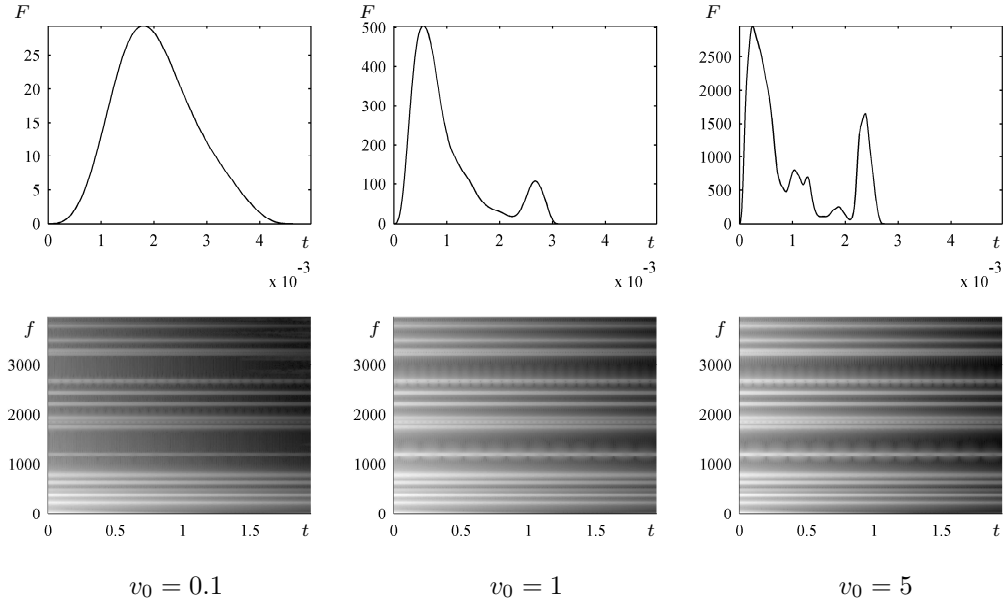


Figure 12.6: Force profiles (top), and output spectra (bottom), for a mallet striking a plate. Here, the plate has $\kappa = 100$, aspect ratio 1.3, a uniform decay time of $T_{60} = 2$ s, and is under free boundary conditions. The mallet/plate mass ratio is $\mathcal{M} = 0.4$, and the stiffness parameters are $\omega_H = 1000$ and $\alpha = 3$. The plate is struck at the plate center, and readout is taken at coordinates $x_o = 0.8$, $y_o = 0.6$. Striking velocities v_0 are as indicated. Scheme (12.26) is employed, accompanied by (12.27), running at a sample rate of 44.1 kHz.

A Synthesis Shortcut

Given that the total contact time between a mallet or hammer and a plate (or a string for that matter) is often quite short (usually on the order of 1–5 ms), one might remark that, to a first approximation, the precise details of the force interaction may not be of great psychoacoustic importance. On the other hand, as mentioned above, the nonlinearity of the mallet interaction does lead to a change in the contact duration, which will indeed affect the brightness of the resulting sound.

One convenient way of avoiding explicitly integrating the nonlinear coupled system, then, is to simply specify an excitation function $F(t)$ in system (12.25), and subsequently in scheme (12.26). Because the system is linear, stability concerns are eased considerably. Here is simple pulse-like choice of excitation function:

$$F = F_{\text{exc}}(t) = \begin{cases} \frac{F_{\text{max}}}{2} \left(1 - \cos\left(\frac{2\pi(t-t_0)}{T_{\text{exc}}}\right)\right) & t_0 \leq t \leq t_0 + T_{\text{exc}} \\ 0 & \text{otherwise} \end{cases} \quad (12.28)$$

which is parameterized by F_{max} , the maximum force, T_{exc} , the pulse duration, and t_0 , the time at which the pulse occurs. For curves of relatively simple form, the difference in sound output compared to that generated using a full mallet model is minimal. See Figure 12.7.

The main difficulty here is that due to the departure from a strict physical model, one must have a convenient means of parameterizing the curve $F(t)$ in terms of initial strike velocity, which will involve additional experimentation. Still, it is a relatively safe way of generating sound in a first attempt. See §13.2.6 for an application to synthesis using a nonlinear plate vibration model.

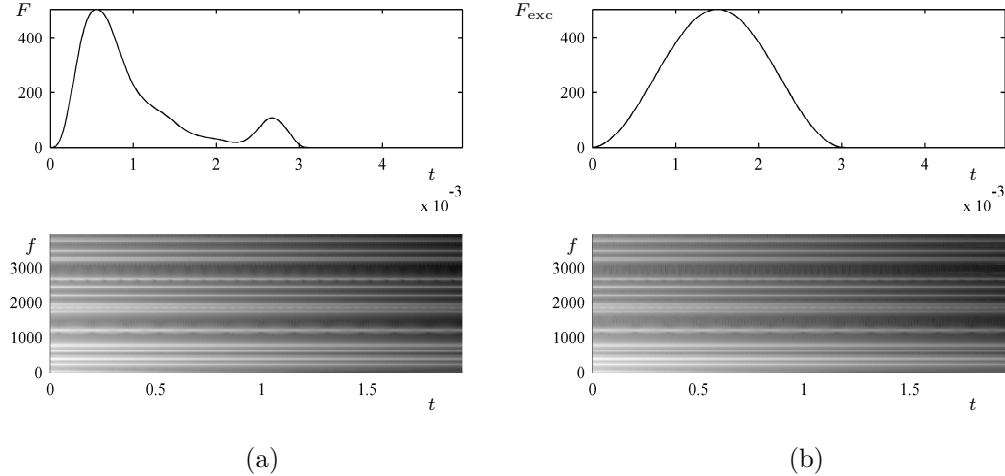


Figure 12.7: Comparison between outputs for (a) the mallet-plate interaction, using the parameters and scheme as described in the caption to Figure 12.6, with $v_0 = 1$, and (b) output using a synthetic excitation function $F_{\text{exc}}(t)$.

12.3.2 Coupling to a Bow Model

The bow model, presented earlier in §4.3.1 and §7.4, may also be used an excitation to a vibrating plate; now, assuming an excitation distribution of the form of a Dirac delta function, F in (12.25)

is of the form:

$$F = -F_B \phi(v_{\text{rel}}) \quad \text{where} \quad v_{\text{rel}} = u_t(x_i, y_i) - v_B \quad (12.29)$$

Here, $F_B = F_B(t)$ is interpreted as a bowing force/total plate mass, and $v_B = v_B(t)$ is the bow velocity. The function ϕ is a friction characteristic of the form discussed in §4.3.1. Using scheme (12.26), with

$$v_{\text{rel}} = I_p(x_i, y_i) \delta_t u - v_B \quad (12.30)$$

leads to a scheme which may be updated explicitly, using Newton's method; as in the case of the string interaction, an additional condition on μ arises which must be satisfied for uniqueness—see Problem 12.8. The variety of sounds which may be produced using such a bow model is enormous; some configurations produce quasi-harmonic tones, others produce more noise-like outputs. A good choice of boundary condition for the plate under bowing conditions, is to leave one edge free, where the bow is applied, and to use simply supported or clamped conditions at all other edges—see Figure 12.8.

12.3.3 Plate Reverberation

Plate reverberation, the granddaddy of all analog audio effects, developed in the 1950s [211], and subsequently became the high-end artificial reverberation device of choice for decades, until the advent of digital reverberation decades later. Operation is relatively straightforward—a large metal plate, of varying dimensions, but sometimes as long as two meters, is fed with a dry input signal, and a pickup reads an output signal at a given position on the plate. The typical plate reverberation characteristic is very different from that of a room, mainly due to the absence of strong early reflections, and to the modal distribution, which is nearly uniform—both result from the inherently dispersive nature of wave propagation in a plate, as discussed in §12.1.1. In spite of this, the plate reverb sound has become one of the most sought after effects in digital audio. Simulation, as in the case of the helical spring (see §7.9), is another interesting application of physical modeling principles not to a musical instrument, but a processing unit.

Finite difference schemes are an excellent match to this problem, as the geometry of typical units is rectangular; some recent studies have been carried out by various this author [44, 47] and others, primarily Arcas [12]. The basic system is of the form of (12.25), and the associated difference scheme is (12.26), where for a typical plate reverb unit, κ is on the order of approximately 2, or less. The function F , in this case, is an input waveform, perhaps after having undergone equalization—the precise form of such equalization is not important for the present purposes, but is described in detail in [12]. A single output $m(t)$ is normally drawn from the plate through an accelerometer placed at given coordinates x_o, y_o relative to the plate corner; in terms of the finite difference scheme (12.26), a sequence m^n may be obtained as

$$m^n = \delta_{tt} I(x_o, y_o) u^n$$

where $I(x_o, y_o)$ is an interpolation operator. This operation eliminates the need to consider rigid body motion of the plate, essentially filtering out any DC drift. (A more physical approach would be to model the means by which the plate is supported). On the other hand, it does impose a high-pass character to the output, which must be rectified through filtering operations (or, again, through a model of equalization at the input stage). See Figure 12.9 for a typical example of an impulse response generated using such a scheme. The character of the response, as shown in (a) is nearly noise-like—notice in particular the uniform spacing of modal frequencies, as shown over different frequency ranges in (b) and (c).

A finite difference implementation has many desirable features, not least of which are: the ability

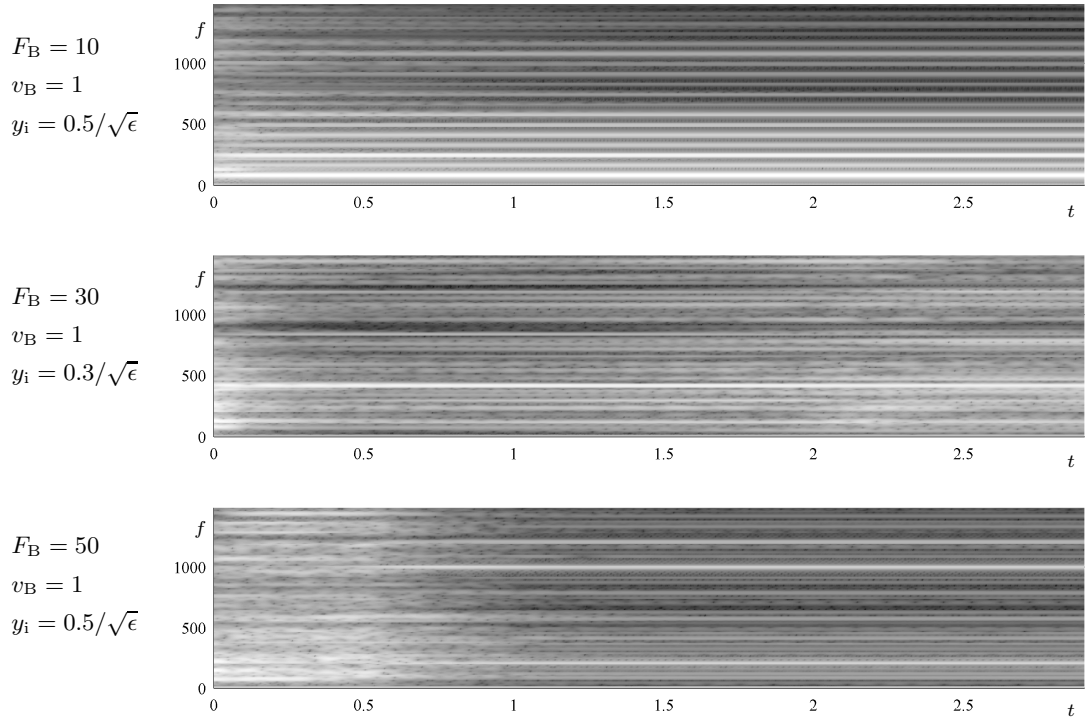


Figure 12.8: Spectrograms of output from a bowed plate model. In this case, the plate has stiffness parameter $\kappa = 20$, aspect ratio $\epsilon = 1$, and $T_{60} = 4$ s, and is under free conditions at $x = 0$, and clamped conditions on all other sides. The bow force/total plate mass F_B , bow velocity v_B and bowing position $(0, y_i)$ are as given above, in three cases. Scheme (12.26) is used, accompanied by (12.29) and (12.30), at a sample rate of 44.1 kHz, and output is read at $x_o = 0.7$, $y_o = 0.7$. At top, a quasi-harmonic tone is produced, at a low pitch. As the bowing point is varied, various harmonics of the plate may be singled out, as shown in the middle panel. Finally, at high bow forces, a dramatic scraping, or noise-like sound may be generated initially, before settling down to a pitched tone.

to obtain multiple outputs cheaply, at distinct and possibly time-varying locations (thus generalizing the functionality of the physical plate reverberation unit), and the possibility of introducing other features such as point-wise clamping (for the sake of tuning) along the boundary, and possibly the clamping of regions of the boundary along the corners. Such features are discussed in [44]. Note that, even in the simple case of a rectangular plate with free edges, there is not, in general, a closed form expression for the modal shapes and frequencies, and thus a modal implementation, while possible, may require an enormous amount of precomputation for each new input/output/boundary condition configuration—there can be upward of 10 000 modes in the audio range for a typical plate reverberation unit.

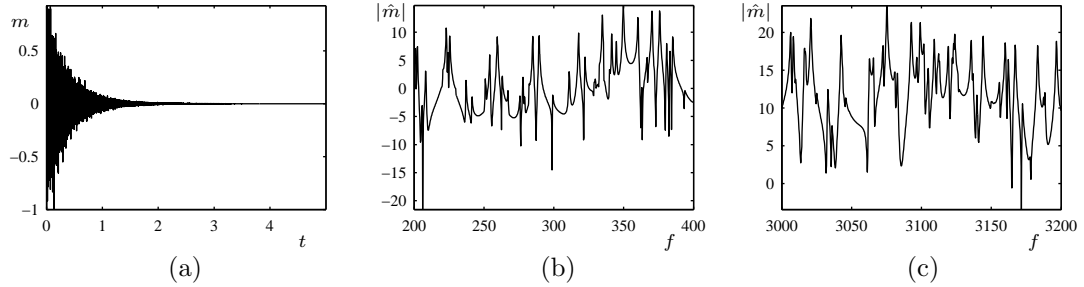


Figure 12.9: *Acceleration response of a plate model to a force impulse. Here, the plate model is of the form of (12.25), with $\kappa = 2$, aspect ratio $\epsilon = 2$, under free boundary conditions, and with T_{60} decay times of 10 s at 500 Hz and 8 s at 2000 Hz. The impulse is inserted at the location $x_i = 0.807$, $y = 0.353$, and output acceleration m is read from $x_o = 0.607$, $y_o = 0.303$. The difference scheme (12.26) is used, at a sample rate 44.1 kHz.* (a) Time response, (b) frequency response over a low-frequency range, and (c) frequency response over a mid-frequency range.

12.4 Plate-string Connections

Another use of the plate-like structure in musical acoustics is as a soundboard, particularly in the piano and other keyboard instruments. Here, it functions as an auxiliary element connected to the main resonator (usually a string), and is employed so as to increase the radiation efficiency of the resonator. For an overview, see [135] and the references therein. Simulation routines, typically for use in comparing measurement with theory, have been developed by various authors—given the geometrical complexity of real-world soundboards, this may involve finite element methods (a wise choice) [346]. For applications closer to synthesis, finite difference schemes have been employed [153], and are a good choice, especially if one is interested in programming simplicity, efficiency, as well as exploring situations which are more than a little removed from strict acoustical modeling of real world instruments! When digital waveguides are employed for the strings, a common technique for the emulation of the soundboard effect on the resulting sound is known as “commuted synthesis” [337, 374]—the waveguides are terminated with filters derived from measured soundboard responses. While allowing for very realistic sound output, the interest here is in design flexibility, rather than high-fidelity sound synthesis based on a fixed instrument configuration.

Real soundboards, as mentioned above, are enormously complicated objects [152]. Not only is there the geometrical complexity of the board, which is often of an irregular shape, of variable thickness, strongly anisotropic, and perhaps accompanied by struts, but there is also the nature of the coupling to the strings, through the bridge. Such an object responds to longitudinal string vibrations as well as transverse—indeed, phenomena such as phantom partials in piano and guitar strings are audible precisely because of the transfer of longitudinal motion through the bridge [86]. As a first stab, however, it is worth spending some time, examining the most rudimentary possible connection between a string and a plate, and how it may be implemented using time domain methods. The situation is not enormously different from the case of coupled bars, as discussed in §7.8, with the exception that one must now pay special attention to the string boundary conditions.

Consider the following system, in dimensional form:

$$\rho_P H u_{tt} = -D \Delta \Delta u + \delta(x - x_{S1}, y - y_{S1}) f_1 + \delta(x - x_{S2}, y - y_{S2}) f_2 \quad \rho_S A w_{tt} = T_0 w_{\eta\eta} \quad (12.31)$$

Here, $u(x, y, t)$ is the transverse displacement of a thin linear lossless and isotropic plate, of material

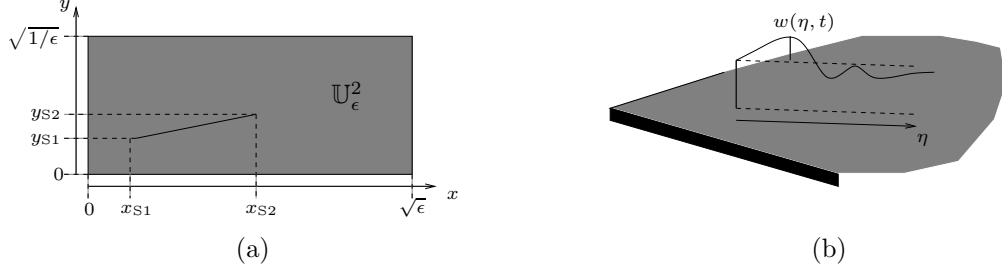


Figure 12.10: Geometry of the plate-string connection described by (12.32). (a): Top view, and (b), side view.

density ρ_P , thickness H , and stiffness parameter D , defined over a rectangle of side lengths L_x and L_y , and $w(\eta, t)$ is the transverse displacement of an ideal string, of material density ρ_S , cross-sectional area A , under tension T_0 , and of length L . Notice that the spatial coordinate η is used in the case of the string so as not to confuse it with the coordinates describing the plate. The string is connected to the plate at coordinates (x_{S1}, y_{S1}) at one end, and (x_{S2}, y_{S2}) at the other end, exerting pointwise transverse forces F_1 and F_2 . Note the use of two-dimensional Dirac delta functions here (these could be generalized to forces operating over a region of the plate without much difficulty).

When the coordinates x , y and η are spatially scaled, with respect to a characteristic length $\sqrt{L_x L_y}$ in the case of the plate, and L in the case of the string, the following system results:

$$u_{tt} = -\kappa^2 \Delta \Delta u + \delta(x - x_{S1}, y - y_{S1})F_1 + \delta(x - x_{S2}, y - y_{S2})F_2 \quad \mathcal{M}w_{tt} = \mathcal{M}\gamma^2 w_{\eta\eta} \quad (12.32)$$

where $F_1 = f_1/\rho_P H L_x L_y$, $F_2 = f_2/\rho_P H L_x L_y$, and where the string/plate mass ratio \mathcal{M} is $\rho_S A L / \rho_P H L_x L_y$. See Figure 12.10.

The one missing piece, here, is the relationship between the pointwise forces F_1 and F_2 , and the string displacement. Energy analysis deals with this nicely.

Energy Analysis

First, for simplicity, assume that the plate boundary is fixed (in the case of the soundboard, it is often assumed clamped [346]). Taking inner products with u_t over \mathbb{U}_ϵ^2 , in the case of the plate equation, and with w_t over \mathbb{U} in the case of the ideal string equation leads to the following energy balance:

$$\frac{d}{dt} (\mathfrak{H}_P + \mathfrak{H}_S) = \mathfrak{B} + F_1 u_t(x_{S1}, y_{S1}, t) + F_2 u_t(x_{S2}, y_{S2}, t)$$

where

$$\begin{aligned} \mathfrak{H}_P &= \frac{1}{2} \|u_t\|_{\mathbb{U}_\epsilon^2}^2 + \frac{\kappa^2}{2} \|\Delta u\|_{\mathbb{U}_\epsilon^2}^2 & \mathfrak{H}_S &= \frac{\mathcal{M}}{2} \|w_t\|_{\mathbb{U}}^2 + \frac{\gamma^2 \mathcal{M}}{2} \|w_\eta\|_{\mathbb{U}}^2 \\ \mathfrak{B} &= -\gamma^2 \mathcal{M} (w_\eta(0, t) w_t(0, t) - w_\eta(1, t) w_t(1, t)) \end{aligned}$$

The system is lossless when

$$F_1 u_t(x_{S1}, y_{S1}) + F_2 u_t(x_{S2}, y_{S2}) - \gamma^2 \mathcal{M} (w_\eta(0, t) w_t(0, t) - w_\eta(1, t) w_t(1, t)) = 0$$

from which the following conditions for a rigid connection may be extracted:

$$w(0, t) = u(x_{S1}, y_{S1}, t) \quad w(1, t) = u(x_{S2}, y_{S2}, t) \quad F_1 = \mathcal{M}\gamma^2 w_\eta(0, t) \quad F_2 = -\mathcal{M}\gamma^2 w_\eta(1, t) \quad (12.33)$$

The first two conditions specify that the displacements of the string and plate should be the same at the connection points, and the second two that the forces acting on the plate are proportional to the string slopes at its endpoints. Such conclusions are, of course, obvious from simple dynamic considerations, but, as usual, the explicit relation to energy principles allows one to deduce similar conditions in the discrete case. One could, of course, go much further in specifying more complex connection conditions, involving lumped masses, springs, dampers etc., exactly along the lines of the coupled bar system in §7.8. Such conditions could be of use in describing, say, the effects of ribs often attached to real soundboards, which serve to alter the frequency response considerably.

A Finite Difference Scheme

The obvious discretization for system (12.32) is as follows:

$$\delta_{tt}u = -\kappa^2 \delta_{\Delta\eta, \Delta\eta} u + J(x_{S1}, y_{S1})F_1 + J(x_{S2}, y_{S2})F_2 \quad (12.34a)$$

$$\mathcal{M}\delta_{tt}w = \mathcal{M}\gamma^2 \delta_{\eta\eta} w \quad (12.34b)$$

Note the use, now, of the two-dimensional spreading function J , as described in §10.2.1; any interpolant may be used, but in practice, for a static connection, simple truncation (i.e., using J_0) is probably sufficient. In the simulations which follow, the grid spacing is chosen as $h_x = h_y = h_P$ for the plate, and h_S for the string. For stability, in addition to the stability condition (12.15) for the plate relating h_P and k , a CFL-type condition $h_S \geq \gamma k$ must also hold. The numerical boundary conditions corresponding to (12.33) are

$$w_0 = I(x_{S1}, y_{S1})u \quad w_N = I(x_{S2}, y_{S2})u \quad F_1 = \mathcal{M}\gamma^2 \delta_{\eta-} w_0 \quad F_2 = -\mathcal{M}\gamma^2 \delta_{\eta+} w_N \quad (12.35)$$

which are provably numerically stable, and which lead to a unique update—see Problem 12.9.

Variation of the String/Plate Mass Ratio

Though the string/plate mass ratio in most instrument configurations is rather small, it is interesting to examine the effects of varying this ratio. See Figure 12.11, which shows temporal vibration envelopes for such a string, as well as spectra, under different choices of this ratio. When the string and plate are of widely differing material properties, (e.g., when \mathcal{M} is very small), then the modal frequencies of the plate appear as a form of coloration—as the ratio is increased, one begins to see such components featuring strongly in the string’s vibration spectrum, as well as interesting modulation of the temporal envelope, reflecting the gradual trade of energy between plate and string.

It is important to point out, though, that even though for small mass ratios, the modal frequencies of the plate and string remain generally uninfluenced by one another, in general, the concept of a “modal frequency” for a part of a coupled system is not well-defined. In fact, there is no simple way of determining the frequencies of the combined system without some sort of eigenvalue analysis for the combined global system. In the case of the piano, a very useful simplification, proposed by Smith and van Duyne [337] involves prefiltering an impulse (such as a hammer strike excitation function) by a measured response for the soundboard—such a technique is known as commuted synthesis, as mentioned earlier. One must beware, however, the temptation to conclude that such an operation is generally valid, even in the linear case, although it is beyond question a good idea in the case of fixed instrument configurations such as the piano.

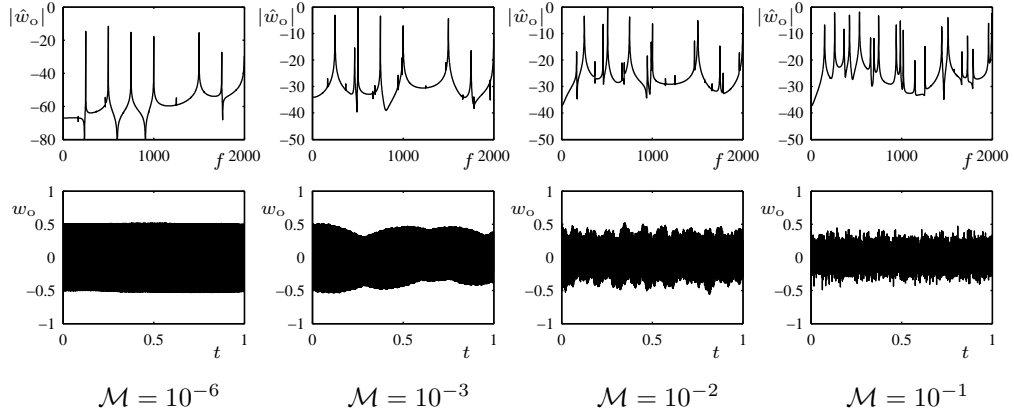


Figure 12.11: *Plate-string connection.* Referring to system (12.32), a string, with $\gamma = 500$, is connected to plate, of aspect ratio 1.3, under simply supported boundary conditions, and of stiffness $\kappa = 50$, at coordinates $(0.3, 0.5)$ and $(0.7, 0.8)$. The string is initialized with a narrow raised cosine distribution. The output spectrum $|\hat{w}_o|$ in dB, and temporal envelope w_o of the string vibration, taken at position $\eta = 0.2$ on the string are plotted for a variety of choices of the string/plate mass ratio, as indicated.

Sympathetic Vibration

It is not a huge step to move from the case of one string connected to a plate to several. The model described by system (12.32) may be generalized directly to the case of M strings as follows:

$$u_{tt} = -\kappa^2 \Delta u + \sum_{q=1}^M \delta(x - x_{S1}^{(q)}, y - y_{S1}^{(q)}) F_1^{(q)} + \delta(x - x_{S2}^{(q)}, y - y_{S2}^{(q)}) F_2^{(q)} \quad (12.36a)$$

$$\mathcal{M}^{(q)} w_{tt}^{(q)} = \mathcal{M}^{(q)} (\gamma^{(q)})^2 w_{\eta^{(q)} \eta^{(q)}}^{(q)} \quad q = 1, \dots, M \quad (12.36b)$$

where now, the displacement of the q th string, of wave speed $\gamma^{(q)}$ and string/plate mass ratio $\mathcal{M}^{(q)}$, and defined over spatial coordinate $\eta^{(q)}$, is $w^{(q)}$. The q th string is connected to the plate at coordinates $(x_{S1}^{(q)}, y_{S1}^{(q)})$ at one end, and $(x_{S2}^{(q)}, y_{S2}^{(q)})$ at the other. Needless to say, there is almost no additional “intellectual overhead” associated with generalizing finite difference scheme (12.34); each term in the sum in (12.36a) may be treated exactly as in (12.34a), and each of (12.36b) as (12.34b).

This, now, is a rather complex object, musically speaking, and a full exploration of this system could occupy an entire volume, but the main feature is the ability of energy to be passed back and forth between the strings and the soundboard, a phenomenon known as sympathetic vibration. As a simple example, consider the case of two strings attached to a plate, as illustrated in Figure 12.12, which shows the time evolution of the displacements of the plate and strings, when one of the strings is subjected to a plucked excitation.

All properties of numerical conservation and stability carry over directly to the discrete case—see Figure 12.13.

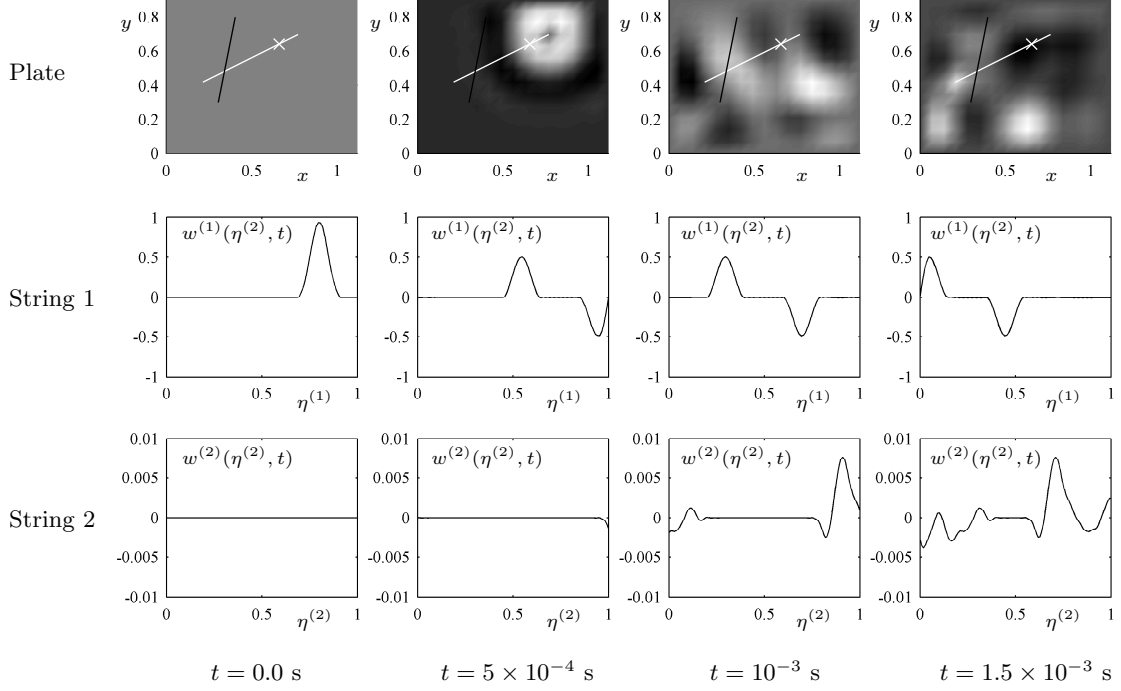


Figure 12.12: *Simulation of a plate connected with two strings; the white and black lines in the upper row of plots indicate the first and second strings, and the first string is initialized with a narrow raised cosine distribution (pluck) at time $t = 0$, at the location marked with a white cross. From left to right, snapshots of the time evolution of the plate displacement (top row), the first string (middle row) and second string (bottom row) are plotted. Referring to system (12.36), the plate is of aspect ratio 0.8, and stiffness $\kappa = 50$, and the strings have $\gamma^{(1)} = 500$ and $\gamma^{(2)} = 400$, respectively, and have mass ratios $\mathcal{M}^{(1)} = \mathcal{M}^{(2)} = 0.01$ with respect to the plate. A scheme generalizing (12.34) is used, at sample rate 44100 Hz.*

12.5 Anisotropic Plates

The model presented above for a connection between a string and a plate is extremely crude, but the basic idea can be significantly extended, by introducing effects of stiffness and frequency-dependent loss in the string, as described in §7.3, as well as loss in the plate itself, as per §12.2. There is one feature of plate vibration, however, which is peculiar to 2D systems, and which is rather important with regard to typical soundboards, namely anisotropy, or variation in the properties of a plate with the direction of propagation of a wave³. Anisotropic plate vibration has been studied with regard to loss models by Chaigne and Lambour [79], and finite difference schemes for use in simulation by the same authors, [216] as well as Giordano and his group [151, 153], in the context of piano

³Note that the concept of anisotropy is distinct from that of point-to-point spatial variation in a system. A spatially-uniform anisotropic system behaves in the same way at every point, and is thus LSI, and amenable to spatial Fourier analysis, whereas a spatially varying, but isotropic system will not be.

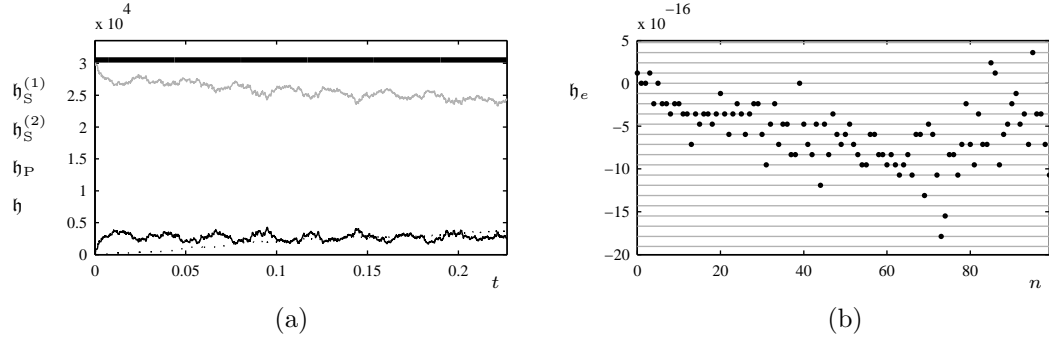


Figure 12.13: *Variation in numerical energy for the two string-plate system described in the caption to Figure 12.12. (a) The energy of the first (struck) string $\hbar_S^{(1)}$, in grey, the second string $\hbar_S^{(2)}$, in dashed black, the plate \hbar_P , in black, and the total energy \hbar , as a thick black line. (b) Relative variation in error, $\hbar_e^n = (\hbar^n - \hbar^0)/\hbar^0$, as a function of time step. Multiples of machine epsilon are indicated by solid grey lines.*

soundboard modeling.

The simplest type of anisotropic thin plate model is referred to as orthotropic, and may be described by the following equation [55]:

$$\rho H u_{tt} = -D_x u_{xxxx} - D_y u_{yyyy} - D_{xy} u_{xxyy} \quad (12.37)$$

where the density ρ and thickness H are as for the isotropic model given in (12.1), but where the stiffness constants D_x , D_y and D_{xy} are defined as

$$D_x = \frac{E_x H^3}{12(1 - \nu_{xy}\nu_{yx})} \quad D_y = \frac{E_y H^3}{12(1 - \nu_{xy}\nu_{yx})} \quad D_{xy} = \nu_{yx} D_x + \nu_{xy} D_y + \frac{G_{xy} H^3}{3}$$

for material constants E_x and E_y (Young's modulus in the coordinate directions), ν_{xy} and ν_{yx} (Poisson's ratios) and G_{xy} (a shear coefficient). When $E_x = E_y = E$, $\nu_{xy} = \nu_{yx} = \nu$, and $G_{xy} = E/2(1 + \nu)$, (12.37) reduces to the isotropic plate equation (12.1). Certain materials, in particular wooden soundboards with an anisotropic character due to grain and ribbing, the ratio of Young's moduli may be as high as 10:1 or 20:1 [151, 216]. The equation above is often written as a system of second-order equations in displacement and moments [216].

When spatially scaled with respect to a length L , equation (12.37) may be written as

$$u_{tt} = -\kappa_x^2 u_{xxxx} - \kappa_y^2 u_{yyyy} - \kappa_{xy}^2 u_{xxyy} \quad (12.38)$$

where $\kappa_x^2 = D_x/\rho H L^4$, $\kappa_y^2 = D_y/\rho H L^4$ and $\kappa_{xy}^2 = D_{xy}/\rho H L^4$.

Dispersion Relation

The dispersion relation for (12.38) is given by

$$\omega^2 = \kappa_x^2 \beta_x^4 + \kappa_y^2 \beta_y^4 + \kappa_{xy}^2 \beta_x^2 \beta_y^2$$

in terms of components of the wavenumber $\boldsymbol{\beta} = [\beta_x, \beta_y]$. Without resorting to the definition of a directional phase or group velocity, it should be clear that propagation speed, for a given wavenumber magnitude, will be different by a factor of κ_x/κ_y in direction x with respect to direction y .

Table 12.2: Simulation results for anisotropic wooden plate, corresponding to that investigated in [216], under simply supported conditions. The plate is of aspect ratio 1.248, and the stiffness parameters (referring to (12.38)) are $\kappa_x = 36.5$, $\kappa_y = 8.41$, and $\kappa_{xy} = 18.1$. Scheme (12.39) is used, with a sample rate of 44100 Hz. Exact modal frequencies are given, as well as numerical frequencies employing an equal grid spacing $h_x = h_y$, and an unequal spacing given by (12.41), as well as deviations in cents.

Mode number	Exact Freq.	$r = 1$		$r = \sqrt{\kappa_y/\kappa_x}$	
		Freq.	Cent Dev.	Freq.	Cent Dev.
(1,1)	56.5	56.4	-2.5	56.4	-3.1
(1,2)	98.4	97.9	-9.6	98.2	-4.4
(2,2)	225.9	224.5	-10.1	224.3	-12.2
(1,3)	177.1	174.4	-26.5	176.1	-9.7
(2,3)	291.2	288.1	-18.9	289.1	-12.8
(1,4)	290.7	282.2	-51.3	287.8	-18.0
(2,5)	533.1	512.64	-67.7	525.1	-26.1

Finite Difference Schemes

Time domain finite difference schemes of various types have been proposed—see the references at the beginning of this section. A simple explicit scheme, equivalent to one of those presented in [216], is of the following form:

$$\delta_{tt}u = -\kappa_x^2\delta_{xxxx}u - \kappa_y^2\delta_{yyyy}u - \kappa_{xy}^2\delta_{xx}\delta_{yy}u \quad (12.39)$$

Due to the anisotropy of the system, one can perhaps foresee problems in the choice of the grid spacing; here, the grid spacings h_x and h_y will remain, generally, independent of one another. The reasoning against the use of a uniform grid is straightforward, and may be related to Rule of Thumb #1, on page 140—a uniform grid means that, in at least one of the coordinate directions, the grid spacing will not be optimal, and thus one will observe mistuning of modal frequencies, which can potentially be very severe for great differences in the directional stiffnesses.

Given this choice, and writing $r = h_y/h_x$ for what might be called the grid aspect ratio, the stability condition for scheme (12.39) may be arrived at using the usual von Neumann techniques (see Problem 12.10):

$$h_x \geq (4k^2(\kappa_x^2 + \kappa_y^2/r^4 + \kappa_{xy}^2/r^2))^{1/4} \quad (12.40)$$

A good guess at a useful setting for r is the following:

$$r = \sqrt{\frac{\kappa_y}{\kappa_x}} \quad (12.41)$$

which symmetrizes the effects of stiffness in the two coordinate directions. As an example, consider the case of a wood plate of parameters as given in Table 12.2, which exhibits a strong anisotropy. Under simply supported conditions, one may compare numerically computed frequencies with exact values—clearly the choice (12.41) allows for a greater degree of accuracy than a choice of equal grid spacings (or $r = 1$), at virtually no added computational expense.

12.6 The Thin Plate in Radial Coordinates

As some percussion instruments (such as the cymbal) may be modeled, to a first approximation, as circular plates, it is worth examining finite difference schemes in radial coordinates. The discussion in this section is a continuation of that of §10.3 and §11.7, and will be extended to the case of nonlinear shell vibration in §13.3.

In radial coordinates, the thin plate equation is as in (12.2), but the Laplacian operator is as defined in the second of (10.2). The problem, when spatially scaled, is defined over the unit circle $\mathcal{D} = \mathbb{U}_o$, and thus the constant κ is defined by $\kappa = \sqrt{\frac{D}{\rho H R^4}}$, where R is the physical radius of the plate.

In radial coordinates, the clamped and simply supported conditions at $r = 1$ take on a relatively simple form:

$$u = u_r = 0 \quad \text{Clamped} \quad (12.42a)$$

$$u = u_{rr} + \nu u_r + \nu u_{\theta\theta} = 0 \quad \text{Simply supported} \quad (12.42b)$$

In general, however, it is the free edge condition which is of most interest in musical acoustics:

$$u_{rr} + \nu u_r + \nu u_{\theta\theta} = u_{rrr} + u_{rr} - u_r + (\nu - 3)u_{\theta\theta} + (2 - \nu)u_{r\theta\theta} = 0 \quad \text{Free} \quad (12.43)$$

If the plate is free to vibrate at its center, then no further condition is required. In the case of some instruments, such as cymbals, however, this is clearly not the case. Here, as a first stab, is a crude clamped condition, when the plate is assumed defined over the annular region $\epsilon \leq r \leq 1$:

$$u = u_r = 0 \quad \text{at} \quad r = \epsilon \quad (12.44)$$

For small ϵ , this is a good starting point for, say, a high-hat model. See Figure 12.14 for a comparison of the behavior of a free-edge plate under this condition and with no condition applied—from the figure, the behavior is not noticeably different, but there will be a slight shifting of the lower modal frequencies. Needless to say, rigid body motion is ruled out under condition (12.44).

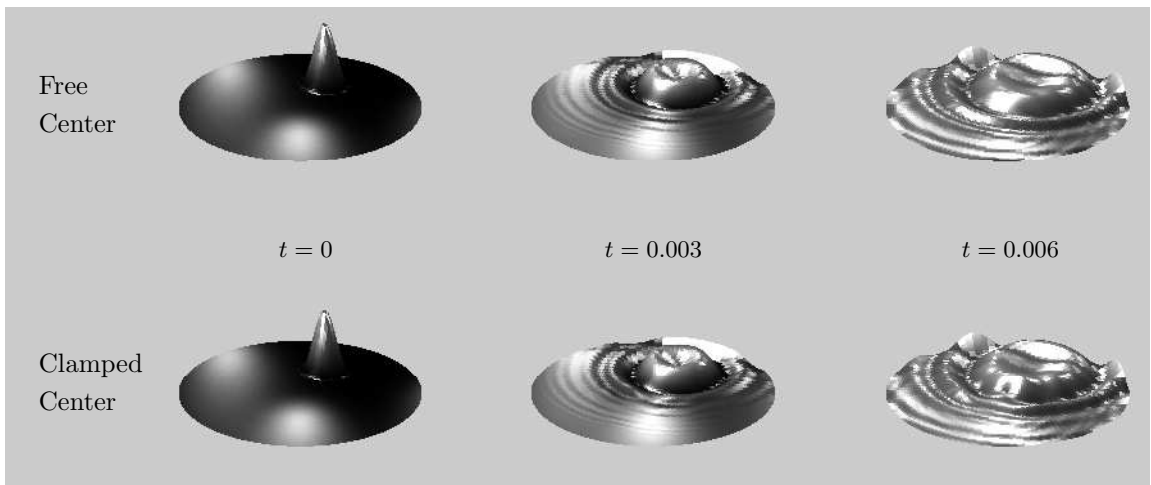


Figure 12.14: *Snapshots of the time evolution of the displacement of a thin circular plate, with $\kappa = 3$, at times as indicated, under free edge conditions, and with no condition at the plate center (at top) and with a clamped center condition (at bottom). The plate is initialized using a raised cosine distribution.*

12.6.1 Finite Difference Schemes

Given that explicit schemes for the 2D wave equation in radial coordinates behave poorly, with regard to numerical dispersion and output bandwidth, it is perhaps useful to begin from a parameterized implicit scheme:

$$(1 + \alpha\kappa^2 k^2 \delta_{\Delta\circ, \Delta\circ}) \delta_{tt} u = -\kappa^2 \delta_{\Delta\circ, \Delta\circ} u \quad (12.45)$$

Here, $\delta_{\Delta\circ, \Delta\circ}$ is an approximation to the biharmonic operator as discussed on page 304.

Numerical boundary conditions corresponding to the clamped edge have been addressed in Programming Exercise 10.7. For the free edge, conservative boundary conditions analogous to (12.43) may be arrived at through analysis similar to the case of Cartesian coordinates. There are many possibilities; here is a set of first-order accurate conditions:

$$((\mu_r + r)\delta_{\Delta\circ} - (1 - \nu)\delta_{r+} - (1 - \nu)\delta_{\theta\theta}) u_{N_r, m} = 0 \quad (12.46a)$$

$$((\mu_r + r)\delta_{r+}\delta_{\Delta\circ} + (1 - \nu)\delta_{r+}\delta_{\theta\theta} - (1 - \nu)\delta_{\theta\theta}) u_{N_r, m} = 0 \quad (12.46b)$$

These are relatively easy to implement, and suitable when the grid is dense (i.e., when κ is low, as in the case of large gongs). Second-order accurate conditions may be employed as well:

$$(\delta_{\Delta\circ} - (1 - \nu)\delta_{r+} - (1 - \nu)\delta_{\theta\theta}) u_{N_r, m} = 0 \quad (12.47a)$$

$$(\mu_r - ((\mu_r + r)\delta_{r+}\delta_{\Delta\circ}) + (1 - \nu)\delta_{r+}\delta_{\theta\theta} - (1 - \nu)\delta_{\theta\theta}) u_{N_r, m} = 0 \quad (12.47b)$$

The free center condition has been discussed on page 304. For the clamped center condition (12.44), assuming that the clamping radius is small, one may set

$$u_{0,0} = u_{1,m} = 0 \quad \text{for all } m \quad (12.48)$$

See also Programming Exercise 12.5.

Stability conditions for this scheme may be arrived at, through extensive analysis—when $\alpha > 1/4$, the scheme is unconditionally stable, but for $\alpha \leq 1/4$, the scheme update at the center point has an influence on the form of the condition. Here are two conditions of interest:

$$\frac{2\sqrt{1 - 4\alpha\kappa} k}{h_r^2} \left(1 + \frac{1}{h_\theta^2} \right) \leq 1 \quad \text{Free center} \quad (12.49a)$$

$$\frac{2\sqrt{1 - 4\alpha\kappa} k}{h_r^2} \left(1 + \frac{1}{4h_\theta^2} \right) \leq 1 \quad \text{Clamped center} \quad (12.48)$$

The stability condition under clamped conditions allows for a smaller choice of h_r , for a given sample rate, than the free center stability condition. As it turns out, good results are obtained when α is chosen slightly below $1/4$.

In Figure 12.15 appears a comparison of output spectra for this scheme under the choice $\alpha = 0$, corresponding to an explicit scheme, and for a value of $\alpha = 0.2495$. As expected, the bandwidth of the explicit scheme, except for various spurious modes, is limited to approximately 2 kHz, which is useless for synthesis purposes. The implicit scheme does somewhat better in that the over-all distribution of modal frequencies is correct for a large part of the spectrum, but even still, only the lowest frequencies are reasonably accurate. See also Programming Exercise 12.6.

Given the previous discussion in §11.7.1, one may infer the following:

Rule of Thumb #5

Finite difference schemes in radial coordinates exhibit heavy numerical dispersion, and explicit schemes in particular produce a severely bandlimited result.

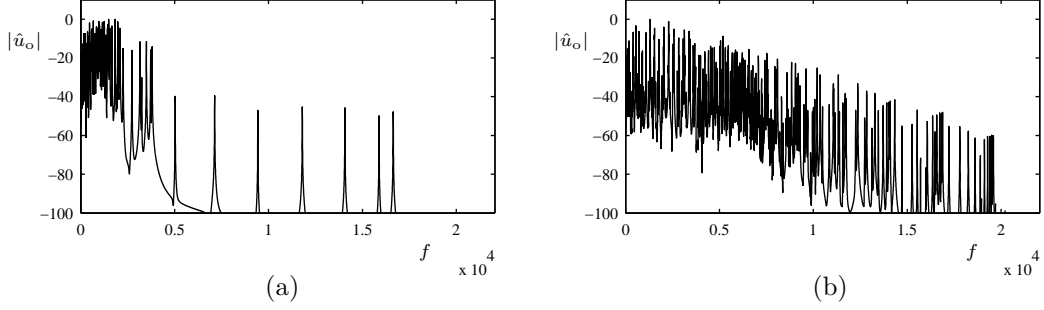


Figure 12.15: *Typical difference scheme output spectra for a circular plate, with $\kappa = 30$, under free edge and clamped center conditions. The family of schemes (12.45) is used, at 44.1 kHz, with (a) $\alpha = 0$ and (b), $\alpha = 0.2495$.*

12.7 Problems

Problem 12.1 For the plate defined over the half plane $\mathcal{D} = \mathbb{R}^{2,x+}$, show that the total energy \mathfrak{H} , as given in (12.9), may be rewritten, using the definition of $\mathcal{L}[\cdot, \cdot]$, as

$$\mathfrak{H} = \frac{1}{2} \|u_t\|_{\mathbb{R}^{2,x+}}^2 + \frac{\nu\kappa^2}{2} \|\Delta u\|_{\mathbb{R}^{2,x+}}^2 + \frac{(1-\nu)\kappa^2}{2} (\|u_{xx}\|_{\mathbb{R}^{2,x+}}^2 + \|u_{yy}\|_{\mathbb{R}^{2,x+}}^2 + 2\|u_{xy}\|_{\mathbb{R}^{2,x+}}^2)$$

and conclude that $\mathfrak{H} \geq 0$, because every term is non-negative.

Problem 12.2 Show that the simply supported condition at the edge of a free plate at $x = 0$,

$$u = 0 \quad u_{xx} + \nu u_{yy} = 0$$

which may be arrived at through inspection of the boundary term \mathfrak{B} in the energy balance (12.10), is equivalent to the condition (12.5b).

Problem 12.3 Consider a plate defined over the quarter plane $\mathcal{D} = \mathbb{R}^{2,x+y+}$. Show that an energy balance of the form $d\mathfrak{H}/dt = \mathfrak{B}$ holds as before, where \mathfrak{H} is as defined as in (12.9), but over $\mathbb{R}^{2,x+y+}$, but where the boundary term is now

$$\begin{aligned} \mathfrak{B} = & \kappa^2 (\{u_t, u_{xxx} + (2-\nu)u_{xyy}\}_{(0,\mathbb{R}^+)} - \{u_{tx}, u_{xx} + \nu u_{yy}\}_{(0,\mathbb{R}^+)}) \\ & + \kappa^2 (\{u_t, u_{yyy} + (2-\nu)u_{yxx}\}_{(\mathbb{R}^+, 0)} - \{u_{ty}, u_{yy} + \nu u_{xx}\}_{(\mathbb{R}^+, 0)}) \\ & + 2\kappa^2 (1-\nu) u_t u_{xy}|_{x=0, y=0} \end{aligned}$$

Thus, if a free boundary condition such as (12.11) is satisfied along both edges, and if the corner condition (12.12) holds, the plate is lossless.

Problem 12.4 Consider the scheme (12.14) for the Kirchhoff thin plate equation, defined over the half plane $\mathcal{D} = \mathbb{Z}^{2,x+}$. It has been shown, in the analysis beginning on page 340, that the boundary conditions (12.18a), (12.18b) and (12.21) lead to exact numerical energy conservation, for a function $\mathfrak{h} = \mathfrak{t} + \mathfrak{v}$, where \mathfrak{t} and \mathfrak{v} are as defined in (12.17a) and (12.19a), respectively. It remains to show that this energy function is a non-negative function of the state u defined over $\mathbb{Z}^{2,x+}$.

(a) Show, using identity (2.22f), that \mathfrak{v} may be bounded from below as

$$\mathfrak{v} \geq -\frac{\kappa^2 k^2 \nu}{8} \|\delta_{\Delta \boxplus} \delta_{t-u}\|_{\mathbb{Z}^{2,x+}}^2 - \frac{\kappa^2 k^2 (1-\nu)}{8} (\|\delta_{xx} \delta_{t-u}\|_{\mathbb{Z}^{2,x+}}^2 + \|\delta_{yy} \delta_{t-u}\|_{\mathbb{Z}^{2,x+}}^2 + 2\|\delta_{x+y} \delta_{t-u}\|_{\mathbb{Z}^{2,x+}}^2)$$

and, using the definition of $\delta_{\Delta \boxplus}$, from (10.9), as

$$\mathfrak{v} \geq -\frac{\kappa^2 k^2}{8} (\|\delta_{xx} \delta_{t-u}\|_{\mathbb{Z}^{2,x+}}^2 + \|\delta_{yy} \delta_{t-u}\|_{\mathbb{Z}^{2,x+}}^2 + 2\nu \langle \delta_{xx} u, \delta_{yy} u \rangle_{\mathbb{Z}^{2,x+}} + 2(1-\nu) \|\delta_{x+y} \delta_{t-u}\|_{\mathbb{Z}^{2,x+}}^2)$$

(b) Using summation by parts of the term involving the inner product above, show that

$$\mathfrak{v} \geq -\frac{\kappa^2 k^2}{8} (\|\delta_{xx}\delta_{t-}u\|_{\mathbb{Z}^{2,x+}}^2 + \|\delta_{yy}\delta_{t-}u\|_{\mathbb{Z}^{2,x+}}^2 + 2\|\delta_{x+y+}\delta_{t-}u\|_{\mathbb{Z}^{2,x+}}^2) + \frac{\kappa^2 k^2 \nu}{4} \{\delta_{yy}u, \delta_{x-}u\}_{(0,\mathbb{Z})}$$

Besides the boundary term, the only term in the above expression that depends on values of the grid function u outside $\mathbb{Z}^{2,x+}$ is the first in brackets above.

(c) Show that, for any grid function f defined over $\mathbb{Z}^{2,x+}$,

$$\begin{aligned} \|\delta_{yy}f\|_{\mathbb{Z}^{2,x+}}^2 &\leq \frac{16}{h^4} \|f\|_{\mathbb{Z}^{2,x+}} \\ \|\delta_{x+y+}f\|_{\mathbb{Z}^{2,x+}}^2 &\leq \frac{16}{h^4} \|f\|_{\mathbb{Z}^{2,x+}} \\ \|\delta_{xx}f\|_{\mathbb{Z}^{2,x+}}^2 &\leq \frac{16}{h^4} \|f\|_{\mathbb{Z}^{2,x+}} - 2\{\delta_{x-}f, \delta_{xx}f\}_{(0,\mathbb{Z})} \end{aligned}$$

and thus that

$$\mathfrak{v} \geq -\frac{8\kappa^2 k^2}{h^4} \|\delta_{t-}u\|_{\mathbb{Z}^{2,x+}}^2 + \frac{\kappa^2 k^2}{4} \{(\delta_{xx} + \nu\delta_{yy})u, \delta_{x-}u\}_{(0,\mathbb{Z})}$$

(d) Finally, show that when any of the boundary conditions (12.18a), (12.18b), or (12.21) holds, the boundary term in the above inequality vanishes, and it is true that

$$\mathfrak{h} = \mathfrak{t} + \mathfrak{v} \geq \left(\frac{1}{2} - \frac{8\kappa^2 k^2}{h^4} \right) \|\delta_{t-}u\|_{\mathbb{Z}^{2,x+}}^2$$

The above expression is non-negative under condition (12.15), obtained using von Neumann analysis.

Problem 12.5 Consider the scheme (12.14), defined now over the quarter plane $\mathcal{D} = \mathbb{Z}^{2,x+y+}$. Using an analysis similar to that carried out beginning on page 340, show that an energy balance of the form $\delta_{t+}\mathfrak{h} = \mathfrak{b}$, where $\mathfrak{h} = \mathfrak{t} + \mathfrak{v}$, for \mathfrak{t} and \mathfrak{v} as defined in (12.17a) and (12.19a), respectively, but over the quarter plane, but where \mathfrak{b} is now given by

$$\begin{aligned} \mathfrak{b} = & \kappa^2 \{\delta_{t-}u, \delta_{x-}(\delta_{xx} + (2 - \nu)\delta_{yy})u\}_{(0,\mathbb{Z})} - \kappa^2 \{\delta_{x-}\delta_{t-}u, (\delta_{xx} + \nu\delta_{yy})u\}_{(0,\mathbb{Z})} \\ & + \kappa^2 \{\delta_{t-}u, \delta_{y-}(\delta_{yy} + (2 - \nu)\delta_{xx})u\}_{(\mathbb{Z},0)} - \kappa^2 \{\delta_{y-}\delta_{t-}u, (\delta_{yy} + \nu\delta_{xx})u\}_{(\mathbb{Z},0)} \\ & + 2\kappa^2(1 - \nu)\delta_{t-}u_{0,0}\delta_{x-y-}u_{0,0} \end{aligned}$$

and deduce clamped, simply supported and free numerical boundary conditions.

Problem 12.6 Consider the operator $\delta_{\Delta\boxplus, \Delta\boxplus}$, defined over the quarter plane $\mathbb{Z}^{2,x+y+}$, assuming equal grid spacings $h_x = h_y = h$, and free boundary conditions (12.21), and the corner condition (12.22). Use these conditions, and the definition of $\delta_{\Delta\boxplus, \Delta\boxplus}$ in order to find an explicit expression for $\delta_{\Delta\boxplus, \Delta\boxplus} u_{l,m}$ at any point $l \geq 0, m \geq 0$ in the interior of the domain. You need only construct the operator at six representative locations (l, m) : $(0, 0), (1, 0), (1, 1), (2, 0), (2, 1), (2, 2)$; the operator will take one of these forms at all other points in the domain.

Hint: as an example, consider the explicit form of the operation at $l = 2, m = 0$:

$$\begin{aligned} h^4 \delta_{\Delta\boxplus, \Delta\boxplus} u_{2,0} = & (11 - 4\nu - 6\nu^2)u_{2,0} + (-6 + 2\nu + 4\nu^2)(u_{3,0} + u_{1,0}) + (-6 + 2\nu)u_{2,1} \\ & + (2 - \nu)(u_{3,1} + u_{1,1}) + (1 - \nu^2)(u_{4,0} + u_{0,0}) + u_{2,2} \end{aligned}$$

Continue, and consider the case of the operator $\delta_{\Delta\boxplus, \Delta\boxplus}$ defined over the rectangular domain \mathbb{U}_{N_x, N_y}^2 , with free boundary conditions on all four sides, and corner conditions analogous to (12.22) at the four corners. Construct the matrix form $\mathbf{D}_{\Delta\boxplus, \Delta\boxplus}$, which will be a $(N_x + 1)(N_y + 1) \times (N_x + 1)(N_y + 1)$ sparse matrix. See also Programming Exercise 12.2.

Problem 12.7 For the family of schemes given in (12.23), which depends on the free parameters α and ϕ , use von Neumann analysis to prove the stability bound given in Figure 12.5(a), namely that

$$\begin{cases} \mu \leq \frac{\alpha - \sqrt{\alpha^2 - (4\phi - 1)}}{4(4\phi - 1)}, & \phi \leq \frac{1}{4} \quad \text{or} \quad \alpha \geq 0 \quad \text{and} \quad \phi \leq \frac{1+\alpha^2}{4} \\ \mu \text{ unconstrained,} & \text{otherwise} \end{cases} \quad (12.50)$$

Problem 12.8 Consider the case of the scheme (12.26) simulating plate vibration, with equal grid spacings $h_x = h_y = h$, coupled with a bow model of bow force $F_B(t)$ and velocity $v_B(t)$, through (12.29) and (12.30), and suppose that the plate is lossless (i.e., $\sigma_0 = \sigma_1 = 0$). The scheme is stable when $\mu \leq 1/4$, where $\mu = k\kappa/h^2$. Show that the condition for uniqueness of numerical solutions is that

$$\mu \leq -\frac{2\kappa}{\max(F_B) \min(\phi')}$$

when $\min(\phi') \leq 0$, and when the interpolant J_p satisfies $\|J_p\|_{\mathcal{D}} \leq 1/h^2$.

Hint: Proceed as in the case of the bow string interaction, as outlined in §7.4, by taking the inner product of (12.26) with $J_p(x_i, y_i)$.

Problem 12.9 Consider scheme (12.34) for the plate-string connection.

(a) Show that, if the numerical boundary conditions (12.35) for the string are employed, and the plate has lossless boundary conditions, the scheme conserves a numerical energy $\mathfrak{h} = \mathfrak{h}_P + \mathfrak{h}_S$, where \mathfrak{h}_P is a numerical energy corresponding to the plate (see page 340) and \mathfrak{h}_S an energy corresponding to a scheme for the 1D wave equation (see §6.2.6). Show that each term is individually non-negative if the conditions $h_P \geq 2\sqrt{\kappa k}$ and $h_S \geq \gamma k$ are respected, and that the combination is thus stable.

(b) By applying the interpolation operators $I(x_{S1}, y_{S1})$ and $I(x_{S2}, y_{S2})$ to the finite difference scheme (12.34a), and assuming that the two endpoints of the string are sufficiently separated, show, by combination with (12.34a) and the numerical boundary conditions (12.35), that the forces F_1 and F_2 may be determined, at each time step, in terms of previously computed values of the string and plate states, and thus the scheme may be updated explicitly.

Problem 12.10 Using von Neumann analysis, prove the stability condition (12.40) for scheme (12.39) for the linear lossless orthotropic plate.

12.8 Programming Exercises

Programming Exercise 12.1 Consider the thin plate equation (12.2), defined over the rectangular region \mathbb{U}_ϵ^2 . A modal function $U(x, y)$, at frequency ω , satisfies:

$$\omega^2 U = \kappa^2 \Delta \Delta U$$

In order to approximate these modal functions, one might employ a finite difference operator $\delta_{\Delta \boxplus, \Delta \boxplus}$ applied to a grid function $\phi = \phi_{l,m}$, defined over \mathbb{U}_{N_x, N_y}^2 , and approximate the modal equation above as

$$\omega^2 \phi = \kappa^2 \delta_{\Delta \boxplus, \Delta \boxplus} \phi$$

In matrix form, when ϕ is reconstituted as a vector ϕ consisting of concatenated vertical strips of ϕ , and $\delta_{\Delta \boxplus, \Delta \boxplus}$ is written as a sparse matrix $D_{\Delta \boxplus, \Delta \boxplus}$, incorporating boundary conditions, the m th modal frequency and shape may be found as

$$\omega_m = \kappa \sqrt{\text{eig}_m(D_{\Delta \boxplus, \Delta \boxplus})} \quad \phi_m = \text{eigenvector}_m(D_{\Delta \boxplus, \Delta \boxplus})$$

where eig_m and eigenvector_m signify the “ m th eigenvalue, and associated eigenvector of.”

Write a Matlab script which generates, for such a rectangular plate, plots of the first 25 modal functions, under simply supported or clamped conditions at all four sides of the domain. In order to do this, you will need to have generated the matrix $D_{\Delta \boxplus, \Delta \boxplus}$ —see Programming Exercise 10.5. Also, in the case of simply-supported conditions, perform a study of the accuracy of these numerical modal frequencies through comparison with exact values, from (12.13), and under different choices of the grid spacing. (You may find, however, that, even for relatively small choices of the grid dimensions N_x and N_y , the calculation of eigenvalues can take a very long time, so be sure to keep these numbers small.)

Programming Exercise 12.2 Extend the code you have written in Programming Exercise 10.5, which generates a sparse matrix form $\mathbf{D}_{\Delta \boxplus, \Delta \boxplus}$ corresponding to the discrete biharmonic operator $\delta_{\Delta \boxplus, \Delta \boxplus}$, operating over the rectangular domain \mathbb{U}_{N_x, N_y}^2 , to the case of the free boundary conditions

(12.21) at the edge with $x = 0$, and conditions (12.22) at the corner at $x = 0, y = 0$, and equivalent conditions, obtained by interchanging x and y , at the other three edges and corners. The results of Problem 12.6 will be of use here.

Programming Exercise 12.3 Create a Matlab script which calculates the response of a rectangular plate to a given initial condition, using the finite difference scheme (12.24) for a plate with frequency-dependent loss. Assume that the applied tension is zero, and that the excitation is an initial velocity with a 2D raised-cosine distribution, according to (11.3). Your code will depend on a number of parameters:

- sample rate f_s
- simulation duration T_f
- plate stiffness parameter κ
- plate aspect ratio ϵ
- loss parameters σ_0 and σ_1 , or, equivalently, two values of T_{60} specified at distinct frequencies f_1 and f_2
- excitation center coordinates x_i, y_i , excitation radius r_{hw} and amplitude c_0
- readout coordinates x_o, y_o
- boundary condition type (clamped, simply supported or free)

It is probably easiest to program this algorithm by making use of the sparse matrix form $\mathbf{D}_{\Delta\Box, \Delta\Box}$ of the discrete biharmonic operator—see Programming Exercise 12.2.

Programming Exercise 12.4 Extend the plate synthesis algorithm from Programming Exercise 12.3 to allow, simultaneously:

- Mallet strikes, as described in §12.3.1. Control data, in this case, should consist of times, velocities, and locations of strikes, and extra necessary parameters will be the mallet/plate mass ratio \mathcal{M} , a stiffness parameter ω_H and a nonlinearity exponent α .
- Bowing gestures, as described in §12.3.2. Control data should consist of bow force and velocity curves, and a bowing location, and you will need to specify a friction characteristic ϕ as well.
- Input from an external audio source, as described in §12.3.3, where control data will consist of a readin location (or perhaps trajectory).
- The connection to multiple strings, as described in §12.4. You will need to specify, for each string, the string/plate mass ratio \mathcal{M} , wave speed γ , and connection coordinates (x_{S1}, y_{S1}) and (x_{S2}, y_{S2}) for the two string ends. You may wish to allow for readout from the strings themselves.

The main programming work here will be managing a) the control data, and b) the connection points. Use bilinear interpolation for these connections, and make sure that your code does not allow more than a single connection at a given location (though there is no reason why this cannot be done, at least in a virtual environment).

Programming Exercise 12.5 Extend the code you have written in Programming Exercise 10.7, which generates a sparse matrix form $\mathbf{D}_{\Delta\circ, \Delta\circ}$ of the biharmonic operator in radial coordinates, in the following way:

- implement the free edge conditions given in (12.46) and (12.47).
- implement the clamped center condition, according to conditions (12.48).

The user should be able to decide between clamped/free conditions at the center or edge through the specification of an input flag. Note that the size of the output matrix will depend on these conditions. For example, under clamped edge and center conditions, the matrix will be of size $(N_\theta(N_r - 2)) \times (N_\theta(N_r - 2))$, but under clamped edge/free center conditions, it will be of size $(N_\theta(N_r - 1) + 1) \times (N_\theta(N_r - 1) + 1)$.

Programming Exercise 12.6 Implement the implicit scheme (12.45) for the plate defined over a circular geometry; here, you will need to rewrite the scheme in a vector-matrix update form, and determine the update matrices, which will depend on $\mathbf{D}_{\Delta\phi,\Delta\phi}$, which you have generated, under a variety of edge and center conditions, in the previous exercise. Make sure that you choose the grid spacings such that the appropriate stability condition from (12.49) is satisfied. Use, as an initial condition, a plucked raised cosine distribution of the form given in (11.3).

Perform a study of output bandwidth, as a function of α , and the parameter $q = h_\theta/h_r$, and for a given value of κ , such as $\kappa = 20$. How does computational complexity depend on α ?

Chapter 13

Nonlinear Plate Vibration

Perhaps the most dramatic example of nonlinear behavior in all of musical acoustics is afforded by the vibration of a metal plate at high amplitudes. Various percussion instruments, and especially gongs and cymbals, owe their characteristic sound almost entirely to this behavior [299]. To the listener, the perceptual results of the nonlinearity are dominant, and include effects such as the rapid buildup of high-frequency energy as heard in cymbal crashes, subharmonic generation, as well as pitch glides, which have been discussed in some detail in the case of the string in Chapter 8. For sound synthesis purposes, a linear model does not even begin to approximate the sound of these instruments.

There are a variety of models of nonlinear plate vibration; when the plate is thin, and vibration amplitudes are low, all of these reduce to the Kirchhoff model discussed in §12.1. (Plates which appear in a musical setting are generally thin, and so there is little reason to delve into the much more involved topic of thick plate vibration, which, even in the linear case, is orders of magnitude more involved than dealing with simple thin plate models—see the comments on page 334.) Perhaps the simplest nonlinear thin plate model is that of Berger [37], which is discussed in §13.1; this system is a 2D analogue of the Kirchhoff-Carrier, or “tension-modulated” string discussed in §8.1, and the predominant perceptual result of employing such a model is the pitch glide. Though this model leads to computationally attractive finite difference schemes, it is not capable of rendering the more interesting effects mentioned above, which are defining characteristics of some percussion instruments. To this end, the more complex model of von Kármán [251, 347] is introduced in §13.2, as are various finite difference schemes. Extensions to the nonlinear vibration of spherical shells appear in §13.3. For the sake of brevity, only simple rectangular and circular structures are covered in this chapter.

13.1 The Berger Plate Model

The simplest model of nonlinear plate vibration is due to Berger [37, 280]; as mentioned above, it is a direct generalization of the Kirchhoff-Carrier system (12.1) to 2D (or rather, the nonlinear bar vibration model presented in §8.1.4, which includes effects of stiffness). Because of the earlier extended discussion of the string model, the treatment here will be brief. 2D models similar to that of Berger have recently seen some exploration in the context of sound synthesis [270].

When defined over a domain \mathcal{D} , Berger’s equation takes the following form:

$$\rho H u_{tt} = -D \Delta \Delta u + \left(\frac{6D}{|\mathcal{D}|H^2} \int_{\mathcal{D}} |\nabla u|^2 dA \right) \Delta u - 2\rho H \sigma_0 u_t$$

Here, the parameters D , H and ρ are as for the case of linear plate vibration, $|\mathcal{D}|$ is the surface area of the plate, and ∇u is the gradient of u . A linear loss term has been included. Clearly, the equation above reduces to the linear model (12.1) at low vibration amplitudes, and under lossless conditions.

When scaled, using (in Cartesian coordinates, for example) $x' = x/\sqrt{|\mathcal{D}|}$, and $y' = y/\sqrt{|\mathcal{D}|}$, and $u' = u/u_0$, with $u_0 = H/\sqrt{6}$, after removing primes the equation is of the form

$$u_{tt} = -\kappa^2 (\Delta \Delta u - \mathfrak{M} \Delta u) - 2\sigma_0 u_t \quad \mathfrak{M} = \int_{\mathcal{D}} |\nabla u|^2 dA \quad (13.1)$$

where the integral \mathfrak{M} above is defined over a unit area region \mathcal{D} . As in the case of the string, the most obvious effect of the nonlinear term is to allow for a change in pitch with vibration amplitude—the loss term leads to pitch glide effects. In Cartesian coordinates, fixed boundary conditions such as (12.5) may be shown to be lossless, but the free conditions must be altered slightly—see Problem 13.1.

It is rather simple to arrive at a difference scheme simulating the Berger model. Consider the equation (13.1) defined over the unit area rectangle \mathbb{U}_ϵ^2 , of aspect ratio ϵ in Cartesian coordinates. A general choice of scheme for (13.1) is

$$\delta_{tt} u = -\kappa^2 (\delta_{\Delta \square, \Delta \square} u - [\mathfrak{m}] \delta_{\Delta \square} u) - 2\sigma_0 \delta_t u \quad (13.2)$$

where $[\mathfrak{m}]$ is some discrete approximation to \mathfrak{M} as given in (13.1). The scheme above is defined over the rectangular region \mathbb{U}_{N_x, N_y}^2 . There are, as before, many approximations available for the nonlinear term—given the extended discussion in §8.1.2, here is a good choice:

$$[\mathfrak{m}] = \mu_{t+} \left(\sum_{l=1}^{N_x} \sum_{m=0}^{N_y} h^2 \delta_{x-} u e_t - \delta_{x-} u + \sum_{l=0}^{N_x} \sum_{m=1}^{N_y} h^2 \delta_{y-} u e_t - \delta_{y-} u \right)$$

which leads to stable behaviour under the condition (12.15), under conservative or lossy boundary conditions. Like scheme (8.7) for the Kirchhoff-Carrier equation, with the nonlinearity discretized as in (8.9), though this scheme is apparently implicit, it may be rewritten in a fully explicit form.

Some typical pitch glides are shown in Figure 13.1; as before, the precise details of the loss model will be of great importance in determining the pitch trajectory. As one might expect, though stable, this scheme exhibits many of the same deficiencies as the related scheme for the Kirchhoff-Carrier string, as discussed on page 231. In particular, numerical oscillations can appear when the stability condition is satisfied near equality, accompanied by a suppression of the pitch glide effect. Improved θ schemes are a good remedy. A modal approach, such as that outlined in §8.1.3 is again a possibility, but with the added complication that now, in general, the modal shapes and frequencies for the plate are not available in closed form, except under simply supported conditions at all edges, and thus must be precomputed.

Instead of dwelling on the details of algorithms for the Berger model, however, it is probably best to turn to a more detailed approximation, which better captures the important perceptual effects of nonlinear plate vibration.

13.2 The von Kármán Plate Model

A widely used model of nonlinear vibration of plates at moderate amplitudes is the so-called dynamic analogue of the system of von Kármán [347, 251]. Its form is quite compact:

$$\rho H u_{tt} = -D \Delta \Delta u + \mathcal{L}(\Phi, u) \quad (13.3a)$$

$$\Delta \Delta \Phi = -\frac{EH}{2} \mathcal{L}(u, u) \quad (13.3b)$$

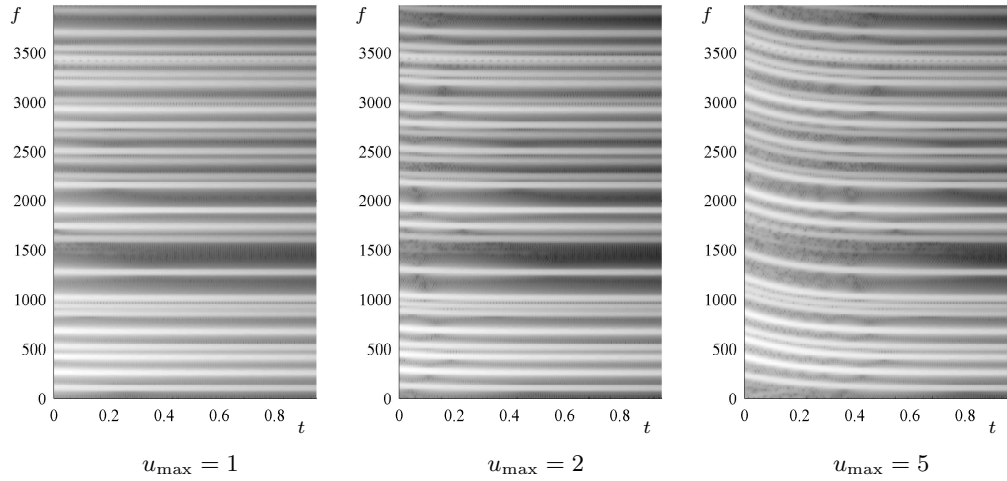


Figure 13.1: Spectrograms of output from scheme (13.2) for the Berger system, for a square plate with $\kappa = 34$, under simply supported boundary conditions, and with $\sigma_0 = 3.18$. The excitation is of the form of a narrow raised cosine distribution, of amplitude u_{\max} centered at the plate center. Pitch glides become apparent as u_{\max} is raised. The sample rate is 44.1 kHz.

Here, as in the linear case, $u(x, y, t)$ is the transverse plate deflection and the new variable $\Phi(x, y, t)$ is often referred to as the Airy stress function. Both are defined over a region $(x, y) \in \mathcal{D} \subset \mathbb{R}^2$. E , H , ρ as well as D are as defined for the linear thin plate system in §12.1, and the nonlinear operator $\mathcal{L}(\cdot, \cdot)$ is defined (in Cartesian coordinates) in (12.6). The system is initialized using the functions $u(x, y, 0)$ and $u_t(x, y, 0)$ —note that no initial condition is required for Φ , which may be set from the initial condition for u from (13.3b). Clearly, system (13.3) reduces to the linear thin plate equation (12.1) in the limit of small amplitudes (note that the terms involving the operator \mathcal{L} are second order in u and Φ).

It is worth noting that there are several variants of the von Kármán system; that given above is simplified from the so-called “full” or “complete” system, in which in-plane displacements appear explicitly [204, 251, 203]; all such systems may themselves be derived from even more general forms [416]. The Berger model, described in §13.1, may be derived from this form, under somewhat subtle assumptions. Interestingly, it is possible to arrive at a nonlinear modal description of the von Kármán system, especially useful in the study of mode couplings and bifurcations in the case of plates defined over a circular geometry—see, e.g., [359, 355].

13.2.1 More on the Operator $\mathcal{L}(\cdot, \cdot)$

The operator $\mathcal{L}(\cdot, \cdot)$ is defined in (12.6), in Cartesian coordinates, as a means of analyzing boundary conditions in the case of thin linear plate vibration. It plays, obviously, a much greater role in the nonlinear case, and possesses a useful symmetry property beyond those described in the earlier section. This symmetry property, first noted in [46], and also described recently in [354], will be called, for lack of a better term, “triple self-adjointness”: For any three smooth functions α , β and

γ defined over \mathcal{D} ,

$$\iint_{\mathcal{D}} \alpha \mathcal{L}(\beta, \gamma) d\sigma = \iint_{\mathcal{D}} \mathcal{L}(\alpha, \beta) \gamma d\sigma + \mathcal{J} \quad (13.4)$$

In other words, variables may be interchanged in the above integral, leading only to terms \mathcal{J} which are resolved on the boundary of the region \mathcal{D} . In the case of, for instance, the half plane $\mathcal{D} = \mathbb{R}^{2,x+}$, \mathcal{J} is of the form

$$\mathcal{J} = \int_{-\infty}^{\infty} \alpha_x \beta_{yy} \gamma - \alpha (\beta_{yy} \gamma)_x - \alpha_y \beta_{xy} \gamma + \alpha (\beta_{xy} \gamma)_y dy$$

In designing a stable numerical scheme for (13.3), it is crucial that a discrete analogue of the property (13.4) be maintained—see §13.2.7.

13.2.2 Scaled Form

As in the case of nonlinear string vibration, it is of interest to scale not only the spatial coordinates (in Cartesian coordinates, one may choose $x' = x/L$, $y' = y/L$, for some constant L of dimensions of length, such as $L = \sqrt{|\mathcal{D}|}$ in problems defined over a rectangular region), but also the dependent variables u and Φ , by introducing dimensionless variables $u' = u/u_0$, $\Phi' = \Phi/\Phi_0$. The particular choice of the scaling constants u_0 and Φ_0 is important in an analysis setting, but numerically the problem is insensitive to the choice, and it is thus best to choose them such that the problem is expressible in terms of the fewest number of parameters. Under the choices

$$\Phi_0 = D \quad u_0 = H/\sqrt{6(1 - \nu^2)} \quad (13.5)$$

and after substitution in system (13.3), the following system results:

$$u_{tt} = -\kappa^2 \Delta \Delta u + \kappa^2 \mathcal{L}(\Phi, u) \quad (13.6a)$$

$$\Delta \Delta \Phi = -\mathcal{L}(u, u) \quad (13.6b)$$

where the sole parameter is κ is as defined in (12.3).

13.2.3 Energy Analysis

The energy analysis of system (13.6) is a simple extension of that carried out in §12.1.2 in the case of linear plate vibration. In this case, an inner product of (13.6a) with u_t over the domain \mathcal{D} leads directly to

$$\frac{d\mathfrak{H}_{\text{lin}}}{dt} = \kappa^2 \langle u_t, \mathcal{L}(\Phi, u) \rangle_{\mathcal{D}} + \mathfrak{B}_{\text{lin}}$$

where $\mathfrak{H}_{\text{lin}}$ is the total energy of the plate due to linear effects, and $\mathfrak{B}_{\text{lin}}$ is the accompanying boundary term (particular forms of these expressions are given in the case of the quarter plane in §12.1.2). Now, employing various properties the operator \mathcal{L} , and integration by parts, beginning

with the triple self-adjointness property (13.4) leads to

$$\frac{d\mathfrak{H}_{\text{lin}}}{dt} \stackrel{(13.4)}{=} \kappa^2 \langle \Phi, \mathcal{L}(u_t, u) \rangle_{\mathcal{D}} + \mathfrak{B}_{\text{lin}} + \mathfrak{B}_{\text{nonlin}} \quad (13.7a)$$

$$\stackrel{(12.7)}{=} \frac{\kappa^2}{2} \langle \Phi, (\mathcal{L}(u, u))_t \rangle_{\mathcal{D}} + \mathfrak{B}_{\text{lin}} + \mathfrak{B}_{\text{nonlin}} \quad (13.7b)$$

$$\stackrel{(13.6b)}{=} -\frac{\kappa^2}{2} \langle \Phi, \Delta \Delta \Phi_t \rangle_{\mathcal{D}} + \mathfrak{B}_{\text{lin}} + \mathfrak{B}_{\text{nonlin}} \quad (13.7c)$$

$$\stackrel{(10.6)}{=} -\frac{\kappa^2}{2} \langle \Delta \Phi, \Delta \Phi_t \rangle_{\mathcal{D}} + \mathfrak{B}_{\text{lin}} + \mathfrak{B}_{\text{nonlin}} + \mathfrak{B}'_{\text{nonlin}} \quad (13.7d)$$

$$= -\frac{\kappa^2}{4} \frac{d}{dt} \|\Delta \Phi\|_{\mathcal{D}}^2 + \mathfrak{B}_{\text{lin}} + \mathfrak{B}_{\text{nonlin}} + \mathfrak{B}'_{\text{nonlin}} \quad (13.7e)$$

and thus

$$\frac{d\mathfrak{H}}{dt} = \mathfrak{B} \quad \text{with} \quad \mathfrak{H} = \mathfrak{H}_{\text{lin}} + \frac{\kappa^2}{4} \|\Delta \Phi\|_{\mathcal{D}}^2$$

and where $\mathfrak{B} = \mathfrak{B}_{\text{lin}} + \mathfrak{B}_{\text{nonlin}} + \mathfrak{B}'_{\text{nonlin}}$ are boundary terms. \mathfrak{H} is again non-negative, and conserved when the boundary terms vanish.

Boundary Conditions

In order to examine boundary conditions, consider the system defined over the half-plane $\mathcal{D} = \mathbb{R}^{2,x+}$. For losslessness, the boundary terms $\mathfrak{B}_{\text{lin}}$, $\mathfrak{B}_{\text{nonlin}}$ and $\mathfrak{B}'_{\text{nonlin}}$ should vanish. $\mathfrak{B}_{\text{lin}}$ is the term which appears in the case of linear plate vibration, in (12.10). As such, the boundary conditions (12.5a), (12.5b) and (12.11), corresponding to clamped, simply supported and free termination, should continue to hold in the nonlinear case.

There is not a consensus in the literature as to how to set boundary conditions for Φ (two required at an edge) in the three cases mentioned above—for a simply supported condition, for example, a variety of settings are considered by different authors [247, 176, 81]. See [148] for some general comments on this topic. An examination of the boundary terms $\mathfrak{B}_{\text{nonlin}}$ and $\mathfrak{B}'_{\text{nonlin}}$, which involve the function Φ over the boundary, is revealing:

$$\begin{aligned} \mathfrak{B}_{\text{nonlin}} &= -\kappa^2 \{u_t u_{yy}, \Phi_x\}_{(0,\mathbb{R})} - 2\kappa^2 \{u_{ty} u_{xy}, \Phi\}_{(0,\mathbb{R})} - \kappa^2 \{u_t u_{xyy}, \Phi\}_{(0,\mathbb{R})} + \kappa^2 \{u_{tx} u_{yy}, \Phi\}_{(0,\mathbb{R})} \\ \mathfrak{B}'_{\text{nonlin}} &= \frac{\kappa^2}{2} \{\Phi, (\Delta \Phi)_x\}_{(0,\mathbb{R})} - \frac{\kappa^2}{2} \{\Phi_x, \Delta \Phi\}_{(0,\mathbb{R})} \end{aligned}$$

(Note that $\mathfrak{B}_{\text{nonlin}}$ results from the triple self-adjointness property (13.4).) Consider the following pair of conditions on Φ , for which the boundary terms above vanish:

$$\Phi = \Phi_x = 0 \quad (13.8)$$

The conditions (13.8), when combined with conditions (12.5a), correspond to a clamped condition [174] and are also sometimes argued to correspond to a simply supported condition [314, 81], in conjunction with (12.5b). For the free boundary, a condition is often given in terms of higher derivatives of Φ , but conditions (13.8) can be shown to be equivalent (see Problem 13.2). For this reason, in the remainder of this chapter, it will be assumed that conditions (13.8) are satisfied at any edge of the domain (where x is interpreted as an outward normal coordinate). Note, however, that other conditions, such as $\Phi = \Delta \Phi = 0$ in conjunction with any fixed condition with $u = 0$ also lead to lossless behavior.

13.2.4 Nonlinear Behaviour in the Frequency Domain

Just as for the system describing large amplitude vibration of strings, described in §8.2, one of the main perceptual effects of the nonlinearity in the von Kármán model is in the complexity of the resulting response, especially when viewed in the frequency domain. The big distinction between the case of the plate and that of the string, though, under musical playing conditions, is in the relative importance of these effects—for the string, it is possible to generate phantom partials, which lend an extra coloration to the resulting sound, but for plates at high amplitudes, the effects are perceptually dominant.

As the system is nonlinear, one should expect that the modes which describe linear vibration of a plate will interact in the nonlinear case—see Figure 13.2, which illustrates the time evolution of the state of a rectangular plate initialized in a configuration corresponding to the lowest mode, under both low amplitude and high amplitude conditions. At high amplitudes, higher modal components are spontaneously generated—this is also visible in a plot of the spectrum of plate displacement, where new harmonics (as well as subharmonics) show an increasing presence at higher amplitudes—see Figure 13.3. Coupling between modes in the von Kármán system is an extremely complex matter, but has been studied extensively, especially for circular plates, in which case closed form expressions for the modal shapes are sometimes available—see, e.g., [359, 354, 355].

Other important perceptual effects, such as pitch glides and crashes, are intimately related to loss modeling; more examples will be shown in §13.2.6.

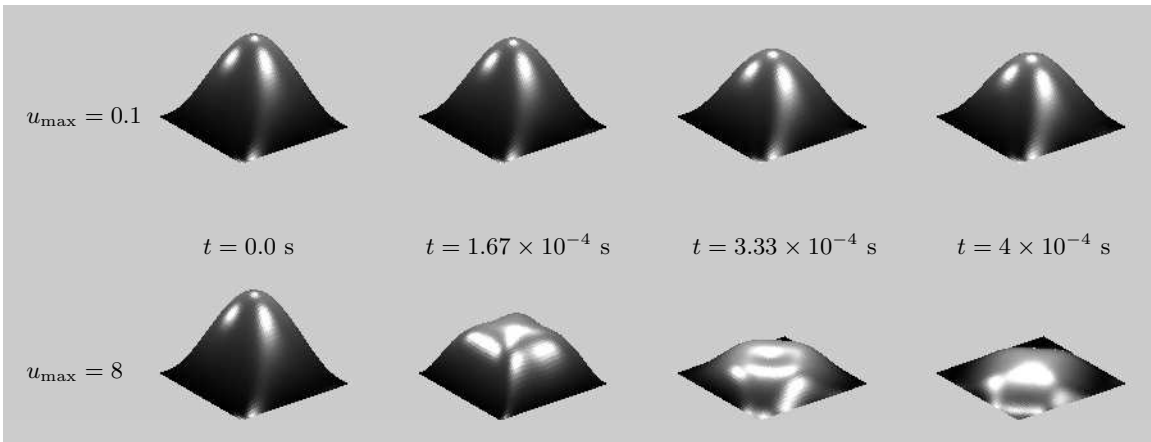


Figure 13.2: *Snapshots of the solution to the von Kármán system, at times as indicated. The plate is square, with $\kappa = 114.4$, and is under simply supported conditions. The plate is initialized with a distribution corresponding to the lowest-frequency mode of the plate under linear conditions, with maximum amplitude u_{\max} . At top, under low amplitude conditions, for $u_{\max} = 0.1$, the plate remains in the modal configuration, but at a higher amplitude of $u_{\max} = 8$, the evolution is more complex, with a generation of higher frequency modes.*

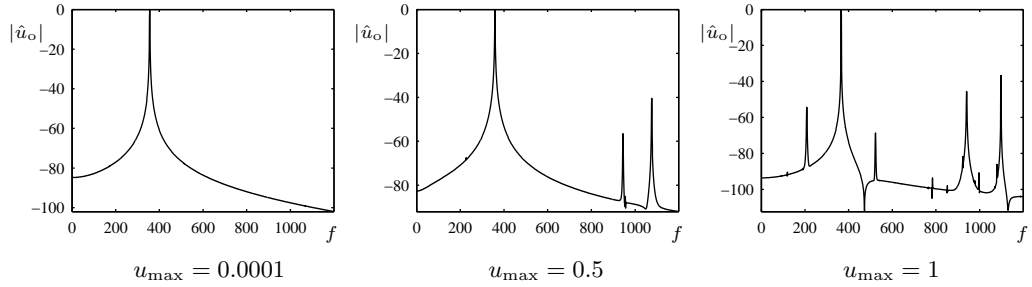


Figure 13.3: Frequency spectrum of output displacement, at plate center, for a square von Kármán plate, with $\kappa = 114.4$, under simply supported conditions. In all cases, the plate is initialized with a distribution corresponding to the lowest-frequency mode of the plate under linear conditions, with maximum amplitude u_{\max} as given.

13.2.5 Loss and Excitation

It is convenient to make use of a simple model of frequency-dependent loss, which is a simple extension of that applied to the case of the linear plate, in §12.2:

$$u_{tt} = -\kappa^2 \Delta \Delta u + \kappa^2 \mathcal{L}(\Phi, u) - 2\sigma_0 u_t + 2\sigma_1 \Delta u_t + e_{\text{exc}} F(t) \quad (13.9a)$$

$$\Delta \Delta \Phi = -\mathcal{L}(u, u) \quad (13.9b)$$

As before, the term with coefficient $2\sigma_0$ gives rise to frequency independent loss, and, when the term with coefficient $2\sigma_1$ is included, frequency-dependent loss is modeled. This is, of course, an enormously over-simplified loss model—see [79] for a more complete treatment of the various sources of loss in the case of linear plate vibration.

The term $e_{\text{exc}} F(t)$ represents a possible excitation, where e_{exc} is a spatial distribution (perhaps localized, so as to correspond to a strike), and where $F(t)$ results from coupling to a model of an excitation element, or is perhaps given as a function of time—see §12.3.

13.2.6 Finite Difference Schemes

Simulation of different varieties of the von Kármán system has seen a rather large amount of activity. The dynamic case has been much less investigated than the static, and many different techniques have been employed—see, e.g., [204, 222] as representative recent examples in the literature. So as not to stray too far from basic principles, it is worth taking a look at some very simple (and perhaps not extremely accurate!) difference schemes—there is a wide variety of possibilities, due to the number of possible discretization choices for the nonlinearities, represented by the terms involving the operator \mathcal{L} . Here is one family, simulating the lossy system (13.9):

$$\delta_{tt} u = -\kappa^2 \delta_{\Delta, \Delta} u + \kappa^2 [\mathcal{L}(\Phi, u)] - 2\sigma_0 \delta_{t, u} + 2\sigma_1 \delta_{\Delta} \delta_{t-u} + e_{\text{exc}} F \quad (13.10a)$$

$$\delta_{\Delta, \Delta} \Phi = -[\mathcal{L}(u, u)] \quad (13.10b)$$

Here, the two instances of $[\mathcal{L}]$ indicates some unspecified (possibly distinct) second-order accurate approximations to the nonlinear terms. As in the case of nonlinear string vibration, one may observe that, because the scheme reduces to scheme (12.14) for the Kirchhoff plate at low amplitudes, a necessary condition for stability will be (12.15) (which should be slightly modified when σ_1 is non-zero). A complication results from the second difference equation (13.10b), which is not time

dependent—it will be necessary to solve a linear system involving the operator $\delta_{\Delta} \boxplus \delta_{\Delta}$ at each time step in order to obtain values of the grid function Φ . Thus, all such schemes have an implicit character. This feature is peculiar to the assumptions underlying this particular model of plate vibration, in which the effects of in-plane displacements are condensed into a single potential function Φ . If the in-plane displacements are explicitly modeled, as is the case for the full von Kármán system [204], then the resulting system becomes similar to the model of nonlinear string vibration covered in §8.2, which can be integrated explicitly—but new in-plane wave speeds will appear, and simulating the resulting system will again require specialized numerical techniques, such as interpolation or θ schemes. In this light, the system (13.9), despite the required implicit update in scheme (13.10), is a simple and elegant choice of model.

The discretization of the nonlinear bracket operator \mathcal{L} is an important first step—here is one choice, defined for any two grid functions α and β :

$$\mathfrak{l}(\alpha, \beta) = \delta_{xx}\alpha\delta_{yy}\beta + \delta_{yy}\alpha\delta_{xx}\beta - \frac{1}{2}\mu_x - \mu_y - (\delta_{x+y} + \alpha\delta_{x+y} + \beta) \quad (13.11)$$

This is perhaps not the simplest possible choice, but it is one which possesses properties which are of great use in proving stability in conservative schemes—see [46], and the analysis in §13.2.7. See also Programming Exercise 13.1.

Once one has made a choice of the particular discrete form \mathfrak{l} , a simple scheme then follows from (13.10) under the choice

$$[\mathcal{L}] = \mathfrak{l} \quad (13.12)$$

In this case, it is only (13.10b) which requires a linear system solution; (13.10a) may be updated explicitly. The same is not true of other types of schemes, and in particular those with superior stability properties—see §13.2.7, as well as Problem 13.5.

Simulation Results: Pitch Glides and Crashes

Scheme (13.10) is a good ad hoc means of generating synthetic sound, and the results are surprisingly rich. Consider the case of a struck excitation, in which case the excitation function F would result from coupling to a mallet model, as described in §12.3.1. As a simple alternative, consider using a pulse-like function $F = F_{\text{exc}}(t)$ of the form given in (12.28); the spatial distribution e_{exc} is taken to be a two-dimensional Dirac delta function. As the strength of the excitation increases, beyond the pitch glide effect exhibited by the Berger model, there is the generation of new partials, and a noise-like component to the output—see Figure 13.4, and for comparison, Figure 13.1. For low values of κ , crash-like sounds can be produced—at high striking amplitudes, there is a slow build-up of high-frequency energy—see Figure 13.5. These sounds need to be heard to be appreciated—and are excellent examples of synthetic sounds with a dense character which could almost certainly not be generated using anything other than a physical model. See Programming Exercise 13.2.

Numerical Instability

Scheme (13.10), with the nonlinearity discretized as in (13.12) is, unfortunately, unstable at high excitation amplitudes—see Figure 13.6. As is common in nonlinear simulation (see the rudimentary case of the cubic nonlinear oscillator in Figure 4.3), this instability can occur without warning after many time steps of apparently stable behavior. Though it is very difficult to analyze the properties of this scheme in a rigorous way, as a general rule, instability occurs when vibration amplitudes approach the limit of validity of the von Kármán model itself (i.e., when the amplitude u takes on values approaching 5 or higher, corresponding, in the case of dimensional variables, to plate

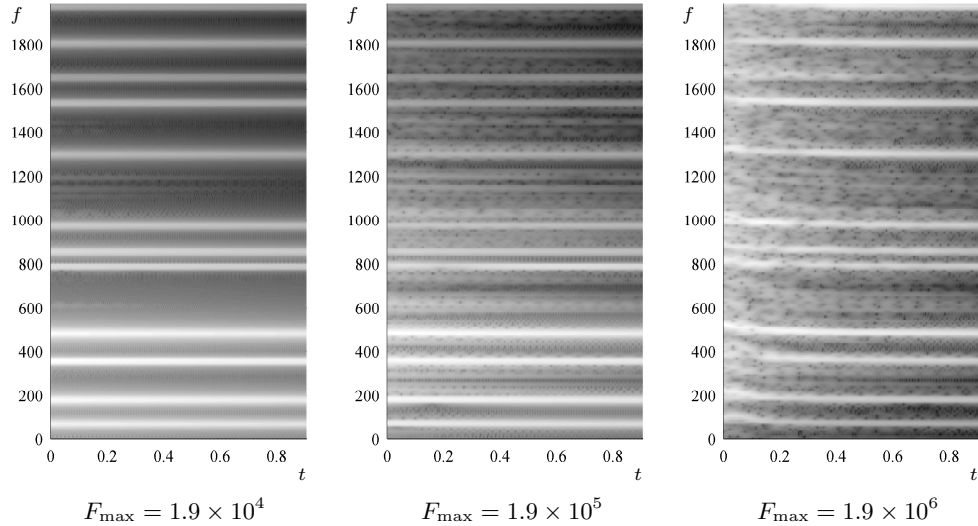


Figure 13.4: Spectrograms of output from scheme (13.10) for the von Kármán system, using discretization (13.12) for the nonlinearity, for a square plate with $\kappa = 20$, under free boundary conditions, and with $\sigma_0 = 1.38$ and $\sigma_1 = 0.001$. Excitation is applied at the plate center, using a spatial distribution e_{exc} of the form of a Dirac delta function, and with a forcing pulse of the form $F = F_{\text{exc}}(t)$ as given in (12.28), with a duration of 3 ms, and with varying amplitudes F_{max} as given in the panels above. The sample rate is 44.1 kHz.

displacements on the order of several times the thickness). This is not unexpected, but there is an additional dependence on the exact form of the initial conditions and/or the excitation function $F(t)$ and distribution e_{exc} , making such a scheme somewhat unwieldy in practice—often the most interesting sounds are generated quite near the stability limit, when nonlinear effects are strongest. Obviously, a more robust scheme is preferable.

13.2.7 Conservation and Numerical Stability

Scheme (13.10), with the nonlinearity discretized as in (13.12) has somewhat obscure stability properties. As one might guess, it is indeed possible to go further and find schemes with more robust behavior. As might be expected from the sequence of steps in (13.7), energy techniques provide a means of showing stable behavior. In this section, for the sake of clarity, only the lossless unforced problem (13.6) is considered.

A preliminary consideration is that the operator \mathbf{l} satisfy a self-adjointness property analogous to (13.4). For the particular choice of \mathbf{l} from (13.11), this is indeed true—for any three grid functions α , β , and γ defined over a domain \mathcal{D} which is a subset of \mathbb{Z}^2 ,

$$\langle \alpha, \mathbf{l}(\beta, \gamma) \rangle_{\mathcal{D}} = \langle \mathbf{l}(\alpha, \beta), \gamma \rangle_{\mathcal{D}} + j \quad (13.13)$$

where j is a boundary term. This property does not hold for all possible discretizations of \mathbf{l} . See Problem 13.3.

Because the operator \mathbf{l} is, like its continuous counterpart, bilinear, an identity corresponding to

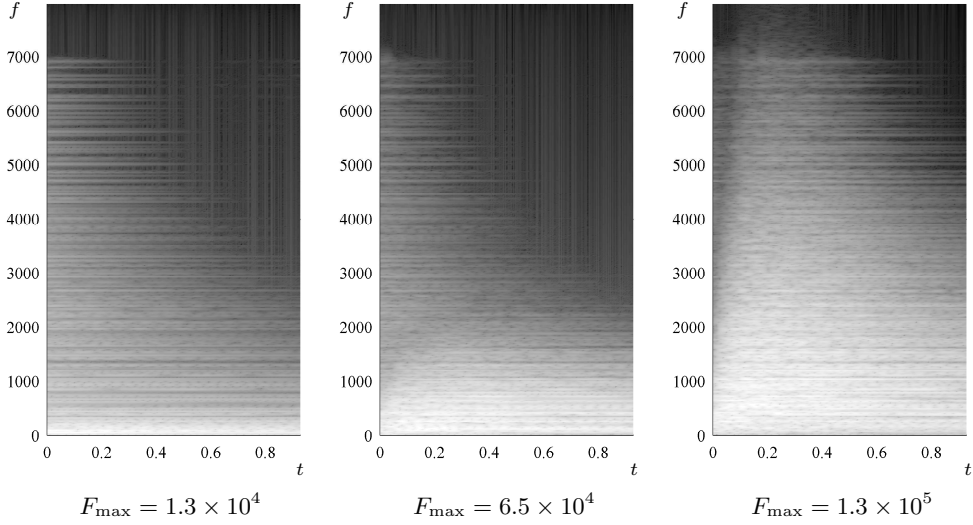


Figure 13.5: Spectrograms of crash-like output from scheme (13.10) for the von Kármán system, using discretization (13.12) for the nonlinearity, for a square plate with $\kappa = 5$, under free boundary conditions, and with $\sigma_0 = 1.38$ and $\sigma_1 = 0.005$. Excitation is applied at coordinates $x_i = 0.2$, $y_i = 0.3$ relative to the plate corner, using a spatial distribution e_{exc} of the form of a Dirac delta function, and with a forcing pulse of the form $F = F_{\text{exc}}(t)$ as given in (12.28), with a duration of 16 ms, and with varying amplitudes F_{max} as given in the panels above. The sample rate is 16 kHz.

(12.7) follows:

$$\delta_{t+} \mathbf{l}(\alpha, e_{t-} \alpha) = 2 \mathbf{l}(\delta_t \alpha, \alpha) \quad (13.14)$$

A Stable Scheme

Consider now the following scheme:

$$\delta_{tt} u = -\kappa^2 \delta_{\Delta \boxplus, \Delta \boxplus} u + \kappa^2 \mathbf{l}(\mu_t \Phi, u) \quad (13.15a)$$

$$\mu_{t-} \delta_{\Delta \boxplus, \Delta \boxplus} \Phi = -\mathbf{l}(u, e_{t-} u) \quad (13.15b)$$

Notice that this scheme has an implicit character beyond that of scheme (13.10), in that time averaging is applied inside the first instance of the bracket operator—see Problem 13.5 for more on implementation details for this scheme. To analyze this scheme, assume, for simplicity, that it is defined over the plane $\mathcal{D} = \mathbb{Z}^2$. Following a similar series of steps to the continuous case, as outlined in §13.2.3, one has

$$\delta_{t+} \mathfrak{h}_{\text{lin}} = \kappa^2 \langle \delta_t u, \mathbf{l}(\mu_t \Phi, u) \rangle_{\mathbb{Z}^2}$$

where $\mathfrak{h}_{\text{lin}}$ is the discrete energy corresponding to the linear scheme (12.14), as given in (12.20) (with boundary terms ignored here).

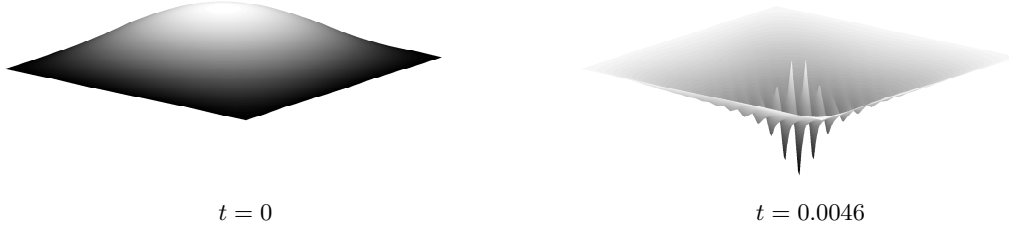


Figure 13.6: *Unstable behaviour in scheme (13.10) for the von Kármán system. In this case, the plate is square, with $\kappa = 11.44$, lossless, and under simply supported boundary conditions. The scheme, running at 44.1 kHz, is initialized with the first modal shape for the linear problem, with a peak amplitude of 14. Generally, in the unstable regime, the larger the amplitude of the initial condition, the shorter the time to the explosion of the solution.*

The following series of manipulations exactly mirrors that of the continuous case, from (13.7):

$$\begin{aligned} \delta_{t+}\mathfrak{h}_{\text{lin}} &\stackrel{(13.13)}{=} \kappa^2 \langle \mu_t \cdot \Phi, \mathfrak{l}(\delta_t u, u) \rangle_{\mathbb{Z}^2} \\ &\stackrel{(13.14)}{=} \frac{\kappa^2}{2} \langle \mu_t \cdot \Phi, \delta_{t+} \mathfrak{l}(u, e_t - u) \rangle_{\mathbb{Z}^2} \\ &\stackrel{(13.15b)}{=} -\frac{\kappa^2}{2} \langle \mu_t \cdot \Phi, \delta_t \cdot \delta_{\Delta \boxplus, \Delta \boxplus} \Phi \rangle_{\mathbb{Z}^2} \\ &\stackrel{(10.17)}{=} -\frac{\kappa^2}{2} \langle \mu_t \cdot \delta_{\Delta \boxplus} \Phi, \delta_t \cdot \delta_{\Delta \boxplus} \Phi_t \rangle_{\mathbb{Z}^2} \\ &= -\frac{\kappa^2}{4} \delta_{t+} \mu_t - \|\delta_{\Delta \boxplus} \Phi\|_{\mathbb{Z}^2}^2 = -\delta_{t+} \mathfrak{v}_{\text{nonlin}} \end{aligned}$$

where

$$\mathfrak{v}_{\text{nonlin}} = \frac{\kappa^2}{4} \mu_t - \|\delta_{\Delta \boxplus} \Phi\|_{\mathbb{Z}^2}^2$$

is the contribution to potential energy due to nonlinear effects. As a result, the scheme is conservative, i.e., $\delta_{t+}\mathfrak{h} = 0$, with $\mathfrak{h} = \mathfrak{h}_{\text{lin}} + \mathfrak{v}_{\text{nonlin}}$. In this case, the added energy is non-negative, so numerical stability is ensured under condition (12.15) which applies to the linear case.

Though boundary conditions are not treated here, conditions analogous to (13.8) may be extracted. At a plate edge at $x = 0$, for example, the conditions

$$\Phi = \delta_{x-} \Phi = 0$$

may easily be shown to be conservative. See [46] for full details. Boundary conditions for u are exactly as in the linear case—see page 340. As for all conservative methods, numerical energy is conserved to machine accuracy—see Figure 13.7.

Scheme (13.15) is but one member of a larger family of conservative methods for the von Kármán system [46]; the members of this family vary considerably in terms of properties such as stability, as well as computability—see Problem 13.4.

13.3 Spherical Shell Vibration

Real plates, when used as percussion instruments, are often curved—the models described in the previous sections must be extended considerably to account for the effects of this curvature (which are not necessarily small, even for very mildly curved structures!). Shell models, for general curved

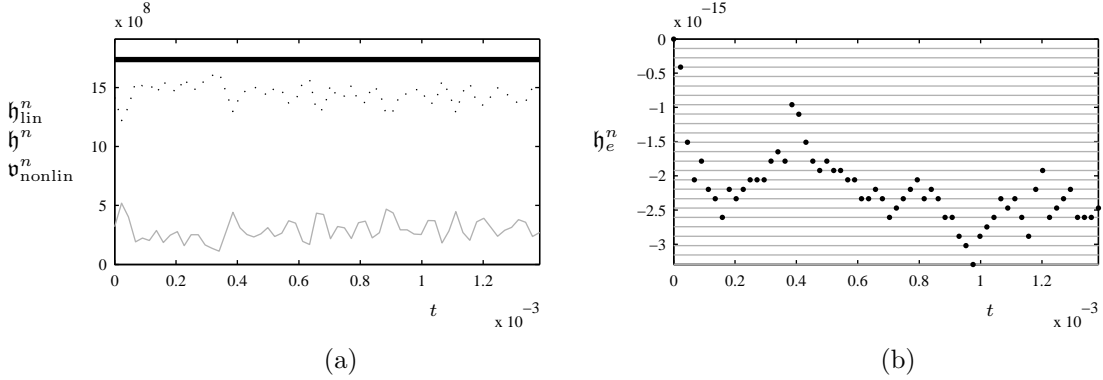


Figure 13.7: (a) Variation of the discrete potential energy due to nonlinear effects $\mathfrak{v}_{\text{nonlin}}^n$ (solid grey line), that due to linear effects $\mathfrak{h}_{\text{lin}}^n$ (dotted black line) and total discrete energy \mathfrak{h}^n (solid black line), plotted against time t , for the output of scheme (13.15) for the von Kármán system. In this case, $\kappa = 127$, the plate aspect ratio is 1.5, and boundary conditions are of free type. The scheme is run at 44.1 kHz, and is initialized with a raised cosine distribution centered at the plate center, of amplitude 10. (b) Variation of the error in energy \mathfrak{h}_e^n , defined, at time step n , as $\mathfrak{h}_e^n = (\mathfrak{h}^n - \mathfrak{h}^0) / \mathfrak{h}^0$, plotted as black points. Multiples of single bit variation are plotted as grey lines.

geometries, are highly complex objects, and there is no possibility of doing justice to this topic in the twilight sections of this book. See [220] for an overview of this vast topic. Indeed, in simulating such a general shell structure, a finite difference scheme is probably not the best choice of method, given that the curvature may make the use of a regular set of coordinates impossible; finite element methods are really the only option under such conditions.

On the other hand, shells as they occur in musical acoustics (such as the cymbal or gong) often have a particularly simple form. If, as a first approximation, the shell is modeled as a spherical cap, a particularly compact extension of the von Kármán system is available [356]:

$$\rho H u_{tt} = -D \Delta \Delta u + \mathcal{L}(\Phi, u) - \frac{1}{R_s} \Delta \Phi \quad (13.16a)$$

$$\Delta \Delta \Phi = -\frac{EH}{2} \mathcal{L}(u, u) + \frac{EH}{R_s} \Delta u \quad (13.16b)$$

Here, the constants D , ρ , H are as for the von Kármán system, and E is Young's modulus. The new parameter R_s is the radius of curvature of the spherical cap—notice that the system reduces to the von Kármán system (13.3) as the radius of curvature becomes large. The system is defined over a circle of radius R , and is obviously best dealt with in radial coordinates. See Figure 13.8.

A necessary component in the above description is a form of the bracket operator \mathcal{L} in radial coordinates:

$$\mathcal{L}(\alpha, \beta) = \frac{\alpha_{rr}}{r} \left(\beta_r + \frac{\beta_{\theta\theta}}{r} \right) + \frac{\beta_{rr}}{r} \left(\alpha_r + \frac{\alpha_{\theta\theta}}{r} \right) - \frac{2}{r^2} \left(\alpha_{r\theta} - \frac{\alpha_\theta}{r} \right) \left(\beta_{r\theta} - \frac{\beta_\theta}{r} \right) \quad (13.17)$$

Scaled Form, Loss and Excitation

In scaled form, for coordinates $r' = r/R$, and using the scaling of variables $u' = u/u_0$ and $\Phi' = \Phi/\Phi_0$, where u_0 and Φ_0 are as given for the von Kármán system in (13.5), the form of the system is, after

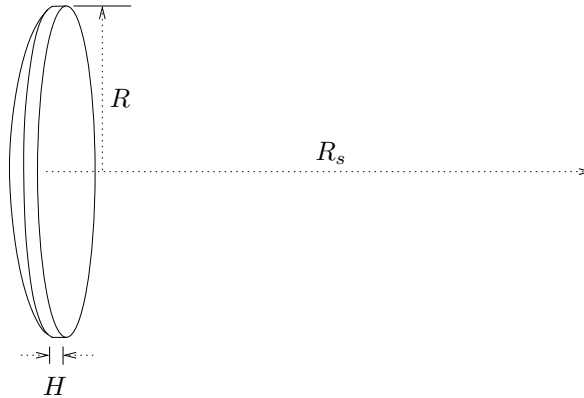


Figure 13.8: *Geometry of a spherical cap, with radius R , thickness H and radius of curvature R_s .*

removing primed variables and introducing frequency-dependent loss terms and an excitation,

$$u_{tt} = -\kappa^2 (\Delta \Delta u - \mathcal{L}(\Phi, u) + q \Delta \Phi) - 2\sigma_0 u_t + 2\sigma_1 \Delta u_t + F_{\text{exc}}(t) e_{\text{exc}} \quad (13.18a)$$

$$\Delta \Delta \Phi = -\mathcal{L}(u, u) + q \Delta u \quad (13.18b)$$

so that the problem is now defined over the unit circle $\mathcal{D} = \mathbb{U}_o^2$, and where the parameters κ and q are given by

$$\kappa = \sqrt{\frac{D}{\rho H R^4}} \quad q = \frac{R^2 \sqrt{6(1-\nu^2)}}{H R_s}$$

The terms involving σ_0 and σ_1 are the usual loss terms, and the excitation is modeled here in terms of a force-like excitation function F_{exc} and spatial distribution $e_{\text{exc}}(r, \theta)$. As discussed earlier, F_{exc} can result from coupling to a mallet model, or, in the simplest case, is supplied externally.

Boundary and Center Conditions

Boundary conditions, at the shell rim at $r = 1$ will be assumed here to be of free type—for the variable u , the conditions (12.43) should be used, and for Φ , the conditions

$$\Phi = \Phi_r = 0$$

though free conditions are often given in terms of higher derivatives of Φ —see [356].

Special care is necessary at the center of the domain. In some cases, there may be no support at the center (as in the case of the gong, but one should also be alert to the need for modeling the raised central dome which is often seen in such instruments), in which case, no further condition is necessary. In other cases, such as some types of cymbals, the shell is fixed to a support. There are obviously many modeling issues—clearly the center should be fixed, but the support may allow the shell to tilt, and may also involve a distributed connection to an annular support structure, which will have its own physical properties. As a simple first approximation to such a support, and one which is not necessarily realistic, but rather easy to work with, it is supposed here that the shell is clamped over an inner circumference of radius $\epsilon \ll 1$:

$$u = u_r = 0 \quad \text{and} \quad \Phi = \Phi_r = 0 \quad \text{at} \quad r = \epsilon \quad (13.19)$$

which generalizes condition (12.44) applied to the case of the flat circular plate.

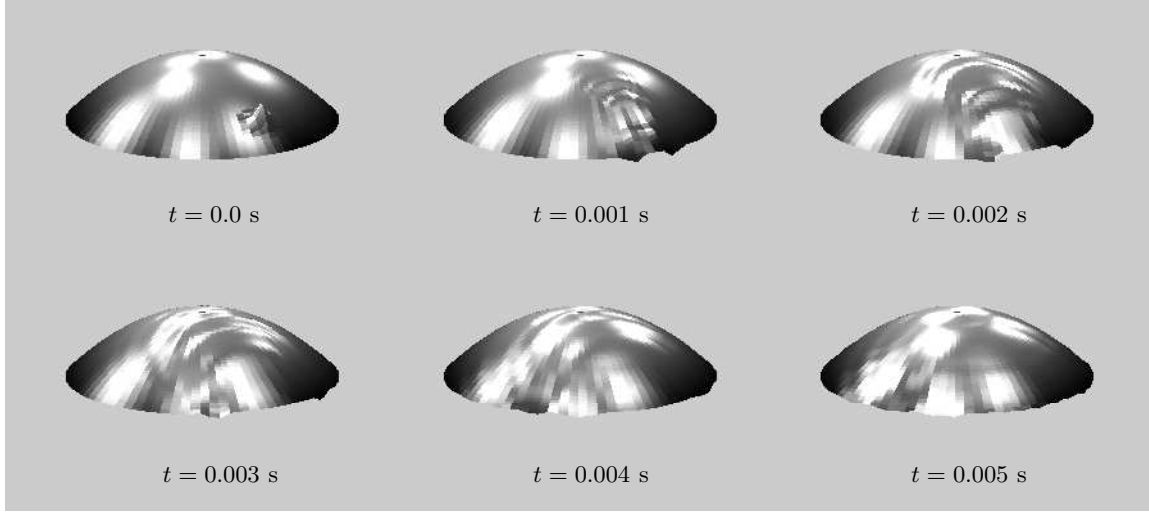


Figure 13.9: Snapshots of the time evolution of a spherical shell, according to (13.18), at times as indicated. Here, the shell is lossless, with $\kappa = 5$ and $q = 60$, and is under free edge conditions, with a clamped center condition. Scheme (13.20) is used under unforced conditions $F_{\text{exc}} = 0$, and the initial condition is a displacement of the form of a raised cosine distribution.

13.3.1 Difference Schemes

Without further delay, one may move directly to a difference scheme for system (13.18), which is an extension of scheme (13.10) for the von Kármán system, now in radial coordinates:

$$(1 + \alpha\kappa^2 k^2 \delta_{\Delta_0, \Delta_0}) \delta_{tt} u = -\kappa^2 (\delta_{\Delta_0, \Delta_0} u - [\mathcal{L}(\Phi, u)] + q\delta_{\Delta_0} \Phi) - 2\sigma_0 \delta_{t.} u_t + 2\sigma_1 \delta_{\Delta_0} \delta_{t-} u + F_{\text{exc}} e_{\text{exc}} \quad (13.20a)$$

$$\delta_{\Delta_0, \Delta_0} \Phi = -[\mathcal{L}(u, u)] + q\delta_{\Delta_0} u \quad (13.20b)$$

The scheme is defined over the circular region $\mathbb{U}_{\circ, N_r, N_\theta}^2$, with grid spacings h_r and h_θ , and the discrete Laplacian and biharmonic operators δ_{Δ_0} and $\delta_{\Delta_0, \Delta_0}$ are as described beginning on page 304. Taking a cue from the discussion of schemes for the circular plate, in §12.6.1, the scheme has a free parameter α , useful in maximizing output bandwidth.

One form of the discrete operator $[\mathcal{L}]$ approximating (13.17), is

$$[\mathcal{L}] = \mathfrak{l} = \frac{\delta_{rr}\alpha}{r} \left(\delta_{r.}\beta + \frac{\delta_{\theta\theta}\beta}{r} \right) + \frac{\delta_{rr}\beta}{r} \left(\delta_{r.}\alpha + \frac{\delta_{\theta\theta}\alpha}{r} \right) - \frac{2}{r^2} \left(\delta_{r.}\delta_{\theta.}\alpha - \frac{\delta_{\theta.}\alpha}{r} \right) \left(\delta_{r.}\delta_{\theta.}\beta - \frac{\delta_{\theta.}\beta}{r} \right) \quad (13.21)$$

As in the case of the discrete Laplacian (see (10.24)), a special form of \mathfrak{l} is necessary if the center of the shell is unconstrained. Here is the simplest possible second-order accurate form, for radial grid functions $\alpha_{l,m}$ and $\beta_{l,m}$:

$$\mathfrak{l}_{0,0}(\alpha, \beta) = \frac{4}{N_\theta^2 h_r^4} \sum_{p=0}^{N_\theta-1} \sum_{q=0}^{N_\theta-1} (1 - 4c_p c_q - 4s_p s_q) \alpha_{1,p} \beta_{1,q} - 2\alpha_{1,p} \beta_{0,0} - 2\alpha_{0,0} \beta_{1,q} + 2\alpha_{0,0} \beta_{0,0} \quad (13.22)$$

where $c_l = \cos(4\pi l/N_\theta)$ and $s_l = \sin(4\pi l/N_\theta)$. See Programming Exercise 13.1.

Necessary stability conditions for this scheme, distinct for clamped and free center conditions,

are

$$\begin{aligned} \frac{2\kappa k \sqrt{1-4\alpha}}{h_r^2 \sqrt{1-k^2\kappa^2 q^2/4}} \left(1 + \frac{1}{h_\theta^2}\right) &\leq 1 && \text{Free center} \\ \frac{2\kappa k \sqrt{1-4\alpha}}{h_r^2 \sqrt{1-k^2\kappa^2 q^2/4}} \left(1 + \frac{1}{4h_\theta^2}\right) &\leq 1 && \text{Clamped center (13.19)} \end{aligned}$$

for $\alpha < 1/4$ —especially good (i.e., wideband) behavior is observed when α is slightly less than $1/4$. See programming Exercise 13.3.

See Figure 13.9 for plots of output generated using this scheme.

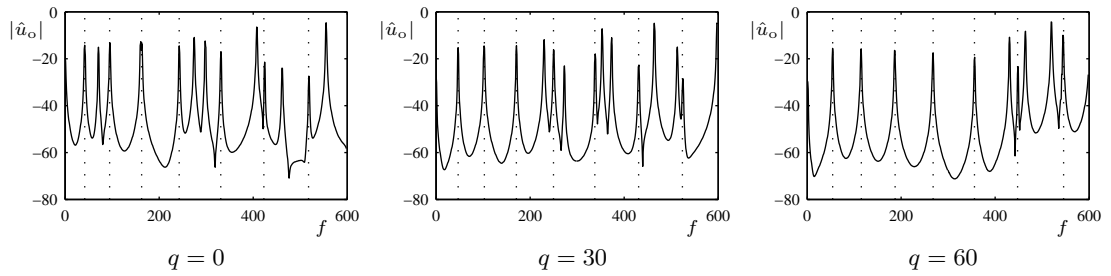


Figure 13.10: *Typical output spectra for a spherical shell, according to (13.18), under low-amplitude conditions. Here, $\kappa = 50$, and the curvature parameter q is as indicated in the panels above; boundary and center conditions are of free type. The vertical dotted lines indicate frequencies corresponding to the series of asymmetric modes without a nodal circle.*

13.3.2 Shifting of Mode Locations

For even a very light degree of curvature in a shell, the spectral characteristics can be dramatically changed with respect to the case of the flat plate. In the absence of nonlinear effects (i.e., when the bracket terms in system (13.18) are neglected), it is useful to examine some plots of typical output spectra for a shell under free boundary and center conditions, under different choices of the curvature parameter q , as shown in Figure 13.10. As pointed out in [356], there are essentially two families of modes: the series of asymmetric modes without nodal circles, the frequencies of which are affected only very slightly by an increase in curvature, and the remaining modes, the frequencies of which exhibit a strong upward shift with increased curvature. As such, for strongly curved shells, the majority of the spectrum is shifted upwards, leaving a very sparse distribution of modes in the lower end of the spectrum. Perceptually, the resulting sound is brighter, with an extra degree of dissonance due to the increased density of modes in the mid range of the spectrum. This over-all trend is roughly similar for free-edge shells under a clamped center condition.

13.3.3 Crashes

The variety of crash-like sounds which can be produced using a shell model is quite large—there is a dependence on amplitude of excitation as well as the curvature parameter q . See Figure 13.11 for some exploration of this. (There is also, of course, a strong additional dependence on the striking location.)

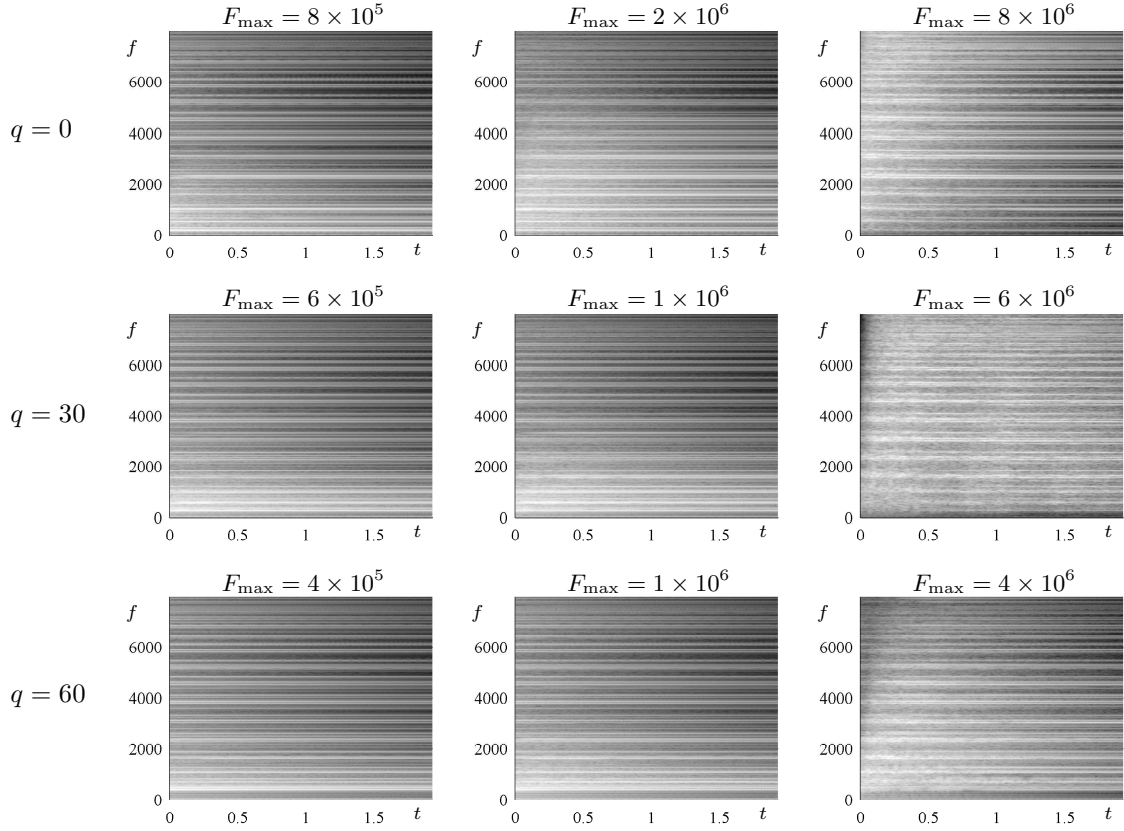


Figure 13.11: Spectrograms of sound output from scheme (13.20) for a spherical shell, with $\kappa = 50$, $\sigma_0 = 1.34$ and $\sigma_1 = 0.003$, and under conditions of zero curvature ($q = 0$), at top, moderate curvature ($q = 30$) in the middle row, and high curvature ($q = 60$), at bottom. In all cases, the shell is excited using a forcing function $F_{\text{exc}}(t)$, of the form given in (12.28), applied at time $t = 0$, duration 3 ms, at a point half-way from the center to the rim, and of maximum value F_{max} as indicated in the panels above. The center point of the shell is clamped, and the sample rate is 32 kHz.

As the closing example in this book, and one which is an excellent example of the power of physical modeling at its best, consider the shell model, subject to a periodic striking gesture, as illustrated in Figure 13.12. The resulting sound possesses a metallic pitched quality, superimposed on a bed of noise, which grows in amplitude as more energy is injected into the system; very uneven fluctuations in the output amplitude result, and it is clear that a linear model would be unable to react in such a manner. Furthermore, it is difficult to imagine how to construct an abstract synthesis method that would give such interesting unpredictability, given such a basic input gesture—see the comments on page 25.

13.4 Problems

Problem 13.1 For Berger's equation, in Cartesian coordinates, and defined over a rectangular region \mathbb{U}_ϵ^2 , show an energy balance of the form $d\mathfrak{H}/dt = -\mathfrak{Q} + \mathfrak{B}$, and determine \mathfrak{H} , \mathfrak{Q} and \mathfrak{B} . Show

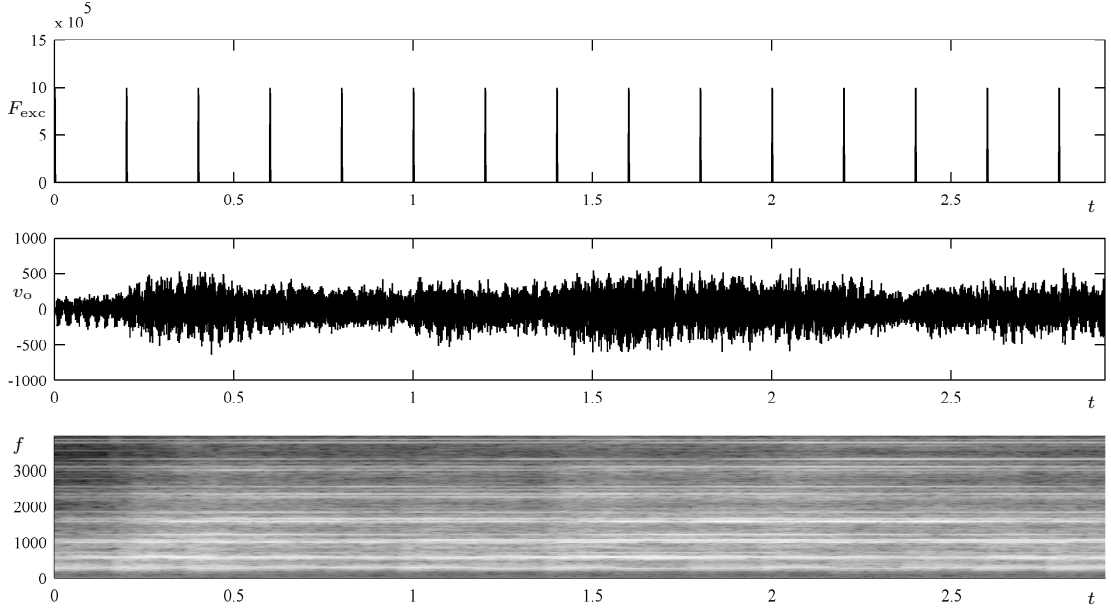


Figure 13.12: Response of a spherical shell model to an excitation function F_{exc} (shown at top) consisting of a series of sharp pulses, approximating a percussionist's gesture. here, the shell has $q = 30$, with all other parameters as in the caption to Figure 13.11, and is clamped at the center; the excitation is applied at a point mid way between the center and edge. The output velocity at a point on the shell's surface is shown in the middle panel, and its spectrogram at bottom. Scheme (13.20) is used, at 32 kHz.

that under clamped or simply supported conditions (12.5) at any edge, the system remains lossless, but free boundary conditions (12.11) should be altered to

$$u_{nn} + \nu u_{ss} = 0 \quad u_{nnn} + (2 - \nu)u_{nss} - \mathfrak{M}u_n = 0$$

at an edge with outward normal coordinate n , and tangential coordinate s . Do you anticipate any difficulties in implementing these conditions in a finite difference scheme? Discuss.

Problem 13.2 Consider the von Kármán system, defined over the half plane $\mathcal{D} = \mathbb{R}^{2,x+}$. The free boundary condition for Φ at $x = 0$ is often given not as (13.8), but as

$$\Phi_{yy} = \Phi_{xy} = 0 \quad (13.23)$$

Argue that these conditions are equivalent to those given in (13.8) using the following reasoning.

(a) Assume that conditions (13.8) hold at $x = 0$, and that these imply the conditions (13.23).

(b) Now, assume that conditions (13.23) hold at $x = 0$. At any point $x = 0, y = y_0$ along the boundary, $\Phi(x, y, t)$ may be expanded in Taylor series as follows, assuming that it is smooth:

$$\Phi(x, y, t) = \sum_{l=0}^{\infty} \sum_{m=0}^{\infty} q_{l,m}(y_0, t) x^l (y - y_0)^m$$

Show that if conditions (13.23) hold, then the coefficients $q_{l,m}(y_0, t)$ must vanish for $l = 0, m \geq 2$, and for $l = 1, m \geq 1$.

(c) Following from the above reasoning, the expansion for Φ is now of the form

$$\Phi(x, y, t) = q_{0,0}(y_0, t) + q_{1,0}(y_0, t)x + q_{0,1}(y_0, t)(y - y_0) + Q(x, y, t)$$

where $Q(x, y, t)$ is an expansion possessing only terms in the second power of x or higher. Evaluate this expression, as well as Φ_x at $x = 0$, and from the uniqueness of Φ at the boundary, argue that the

expression for $\Phi(x, y, t)$ must be independent of the expansion point, i.e., $\Phi = a(t) + b(t)x + c(t)y + Q(x, y, t)$.

(d) From the definition of the von Kármán system in (13.6), argue that if $\Phi(x, y, t)$ is a solution, so is any function $\Phi'(x, y, t) = \Phi(x, y, t) - a(t) - b(t)x - c(t)y$. (In other words, it is only second and higher spatial derivatives of Φ which appear in the system.)

(e) Show that if Φ satisfies boundary conditions (13.23), then there is a function Φ' which satisfies conditions (13.8) and which is also a solution to the von Kármán system.

Problem 13.3 Show condition (13.11) for the discrete operator \mathbf{l} .

Problem 13.4 Scheme (13.15) for the von Kármán system is one member of a larger family of second-order accurate conservative numerical methods:

$$\begin{aligned}\delta_{tt}u &= -\kappa^2 \delta_{\Delta\boxplus, \Delta\boxplus} u + \kappa^2 \mathbf{l}(\bar{\Phi}, \bar{u}) \\ \mu_{t-} \delta_{\Delta\boxplus, \Delta\boxplus} \Phi &= -(\alpha \mathbf{l}(u, e_{t-} u) + (1-\alpha) \mu_{t-} \mathbf{l}(u, u))\end{aligned}$$

where

$$\bar{u} = \alpha u + (1-\alpha) \mu_{t-} u \quad \bar{\Phi} = \beta \Phi + (1-\beta) \mu_{t-} \Phi$$

This family depends on two free parameters, α and β .

(a) Generalize the analysis of §13.2.7, and find the form $\mathbf{v}_{\text{nonlin}}$ of the additional energy due to nonlinear effects. Under what conditions on α and β is it guaranteed to be non-negative?

(b) For which values of α and β does this set of schemes admit a unique update?

Problem 13.5 Consider the conservative scheme (13.15) for the von Kármán system. Because of the time averaging operators applied within the first instance of the nonlinear bracket operator \mathbf{l} , u cannot be updated explicitly. On the other hand, recall that the operator \mathbf{l} is bilinear—thus unknowns u^{n+1} in the resulting recursion appear linearly. Find a vector-matrix update form of the scheme suitable for implementation.

As a starting point, it is useful to rewrite the scheme as

$$\begin{aligned}\mathbf{u}^{n+1} - 2\mathbf{u}^n + \mathbf{u}^{n-1} &= -\kappa^2 k^2 \mathbf{D}_{\Delta\boxplus, \Delta\boxplus}^{(1)} \mathbf{u}^n + \frac{\kappa^2 k^2}{2} (\mathbf{l}(\Phi^{n+1}, \mathbf{u}^n) + \mathbf{l}(\Phi^{n-1}, \mathbf{u}^n)) \\ \frac{1}{2} \mathbf{D}_{\Delta\boxplus, \Delta\boxplus}^{(2)} (\Phi^{n+1} + \Phi^n) &= -\mathbf{l}(\mathbf{u}^{n+1}, \mathbf{u}^n)\end{aligned}$$

where here, \mathbf{u}^n and Φ^n are the grid functions u and Φ arranged as vectors, and where $\mathbf{D}_{\Delta\boxplus, \Delta\boxplus}^{(1)}$ and $\mathbf{D}_{\Delta\boxplus, \Delta\boxplus}^{(2)}$ are two distinct matrix forms of the discrete biharmonic operator $\delta_{\Delta\boxplus, \Delta\boxplus}$, with boundary conditions appropriate to u and Φ , respectively. You must now find a linear system which, when solved, yields the unknowns \mathbf{u}^{n+1} and Φ^{n+1} . For more details, see [46].

13.5 Programming Exercises

Programming Exercise 13.1 Create a Matlab script which calculates, for two given grid functions α and β , the value of the discrete bracket operator \mathbf{l} , in both Cartesian coordinates (according to (13.11)) and radial coordinates (according to (13.21) and (13.22)). In the former case, assume that the grid functions α and β are defined over the rectangular region $\mathbb{U}_{N_r, N_\theta}^2$, under any choice of clamped or free conditions for either of α or β . In the latter, assume that α and β are defined over $\mathbb{U}_{\circ, N_r, N_\theta}^2$, and that boundary conditions at the edge are of free or clamped type. Allow the user to specify a clamped or free center condition.

Programming Exercise 13.2 Program the difference scheme (13.10) for the von Kármán system, defined over the unit area rectangle \mathbb{U}_ϵ^2 . In order to do this, you will need to have generated a matrix form $D_{\Delta\boxplus, \Delta\boxplus}$ of the operator $\delta_{\Delta\boxplus, \Delta\boxplus}$, so as to perform the required linear system solution in (13.10b). (See Programming Exercise 12.2). Beyond allowing the specification of the plate parameters κ , ϵ , σ_0 and σ_1 , and readout locations x_o and y_o , allow an excitation function F_{exc} of the form (12.28), and assume that it is applied at a single point.

Programming Exercise 13.3 Program the difference scheme (13.10) for the spherical shell system, defined over the unit circle \mathbb{U}_\circ^2 . In order to do this, you will need to have generated a matrix form $D_{\Delta\circ,\Delta\circ}$ of the operator $\delta_{\Delta\circ,\Delta\circ}$, so as to perform the required linear system solutions. (See Programming Exercise 12.5). Assume that boundary conditions are of free type at the edge, and of either free or clamped type at the center. As above, allow an excitation function F_{exc} of the form (12.28), and assume that it is applied at a single point. You may wish to make use of the results of Programming Exercise 12.6 as a starting point.

